SINGLE BOUNDARY MEASUREMENTS IN FLOW ANALYSIS

by

Alan Edward DAVIES, MSc , CChem ., MRSC.

A Doctoral Thesis

Submitted in partial fulfilment of the requirements
for the award of

Doctor of Philosophy of the Loughborough University of Technology.

1st March 1994

'Far must thy researchers go
Wouldst thou learn the world to know;
Thou must temp the dark abyss
Wouldst thou prove what Being is;
Naught but firmness gains the prize,
Naught but fullness makes us wise,
Buried deep truth ever lies'

Schiller, *Proverbs of Confucius*

'Deep in the human unconsciousness is a pervasive need for a logical Universe that makes sense. But the real Universe is always one step beyond logic.'

Frank Herbert, *Dune*

'Science distinguishes a man of honour from one of those athletic brutes whom undeservedly we call heroes'

Dryden, *Fables*: Preface

Acknowledgements

I wish to acknowledge the support of my supervisor Dr. Arnold G. Fogg and to thank him for his critical appraisal of this thesis. I would also like to acknowledge the support of two my colleagues, first and foremost Dr. Ramin Pirzad, and Dr. Josino C. Moreira for their invaluable help with chemically modified electrodes. My work is partly a continuation of their studies on poly-L-lysine modified electrodes.

I wish to acknowledge the support given to me by the members of the *Photochemistry Coffee Club*, Dave Worrall, Dave McGarvey, Andy Goodwin, Jon Hobley, Phil Szekeres, Dave Mandley, Darren Greenhill, Gary Sturley and Siân Williams. I would especially like to acknowledge their friendship and support and especially the support and encouragement of Simon Cocks and Katrina Bell.

I would like to thank Dr. Roger J. Mortimer and Dr. Tony E. Edmonds for many useful discussions. I wish to acknowledge my 'Mac Guru' Peter Reid for his time and patience, and for assisting me in the layout of this thesis. I would also like to thank him for teaching me the more powerful aspects of the software used to produce this thesis. I would also like to thank his wife Helen for introducing me to EndNote a lifesaving bibliography database. I would like to thank Neil Pritchard for drawing the flow-cells shown in chapter 2.

I am indebted to the Agricultural and Food Research Council for the provision of a grant.

Finally I would like to acknowledge the support and encouragement of my family and this thesis is dedicated to them, especially to the memory of those who did not see its completion.

TABLE OF CONTENTS

Abstract

Single boundary measurements using a stream-switching valve in a single-channel manifold, where a large volume injection produces two discrete reaction zones at the extremities of the sample bolus, have been studied. When monitoring with both diode-array and double beam spectrophotometers, refractive index (RI) effects could be compensated for satisfactorily by subtracting measurements made at a second wavelength. This was less effective with a single beam spectrophotometer.

For larger volume flow-cells the indicated flow direction should be followed to obtain undistorted signals, but with an 8 µl flow-cell the direction of flow was immaterial. RI correction was possible with all three flow-cells studied, but the use of the 8 µl cell reduced the contribution of the flow-cell to the overall dispersion.

The use of single bead string reactors (SBSRs) with large volume injections offers an improvement in sample throughput by reducing dispersion in comparison with coiled reactors of similar dimensions. The peak appearance times are increased and the back pressure generated can be high. Coiled reactor lengths should not exceed 5 m if dual wavelength correction for RI is to be employed successfully with the single-channel manifold used and high back pressure is a limiting factor in the manifold design.

The first use of the sandwich technique in flow injection for an indirect determination (with a control and sample signal) is reported. RI correction was again successfully employed and any variation in the control signals were used to correct the signal obtained after the introduction of acidified sample/standards.

The rate of product formation and the degree of on-line analyte formation had no influence on the position of the peaks from on-line reactions when they were overlaid on the signals obtained for the injection of preformed analyte complexes. The peaks obtained from the on-line reactions were contained within the envelope that formed the response for the injection of the preformed complexes.

Polylysine adsorbs on glassy carbon and platinum electrodes, but the film lifetime is limited in a flowing stream. In a static system film adsorption improves the electrochemistry of ferricyanide and cobalt(III) oxalate reduction. Preliminary work on carbon ink electrodes indicates that the film adheres better to this type of electrode.

Publications and Presentations

Refereed papers

A. G. Fogg and A.E. Davies, "Reverse Flow Injection or Reagent Injections? Normal Flow Injection, Reverse Flow Injection and Single-boundary Measurements", *Analyst*, 1992, 117, 1055.

A. G. Fogg, J. C. Moreira, R. Pirzad, M. V. B. Zanoni and A. E. Davies, "Cathodic stripping voltammetry with anion accumulation on a poly-L-lysine modified hanging mercury drop electrode: determination of nitroprusside and sodium cromoglycate", *Analyst*, submitted.

R. Pirzad, J. C. Moreira, A. E. Davies and A. G. Fogg, "Differential pulse cathodic stripping voltammetric determination of nedocromil sodium at an unmodified and a poly-L-lysine modified hanging mercury drop electrode", *Analyst*, submitted.

Presentations

R&D Topics, Birmingham, July 92, "Aspects of Single Boundary Measurements in Flow Injection", A. E. Davies and A. G. Fogg.

SAC 92, Reading, September, "Single boundary Measurements and Sandwich Techniques in Flow Injection Analysis", A. E. Davies and A. G. Fogg.

CHAPTER 1

INTRODUCTION

1.1. Continuous flow techniques

1.1.1 Flow injection analysis: an historical perspective

The term "flow injection analysis" (FIA) was first used by *Ruzicka and Hansen*[1] in 1975 to describe the injection of samples into an unsegmented continuously flowing stream for rapid analysis. The workers demonstrated the feasibility of the technique by the spectrophotometric determination of methyl orange and phosphate; the phosphate was determined by the molybdenum yellow and molybdenum blue methods. The potentiometric determination of ammonia was also described in the paper. Even at the early stages of the technique a variety of detection methods was included. Independently and concurrently in the United States, *Stewart et al.*[2] described the same technique for the rapid determination of trypsin samples. The work of *Skeggs*[3], who in 1957 described the use of segmented streams in continuous flow analysis, formed the basis on which both groups of workers developed their ideas.

The technique of segmented flow analysis (SFA) was well established by this time, particularly in the field of clinical analysis. However, it suffers from a number of disadvantages. These disadvantages prompted both of the above groups of workers[1,2] to study the use of unsegmented streams for continuous flow analysis. The idea of unsegmented flow was not new as has been indicated in later publications by both *Stewart*[4] and *Mottola*[5]. Stewart cited the work of *Nagy et al.*[6] who in 1970 described the voltammetric determination of electroactive species after their injection into a continuously flowing stream. A great deal of interest was generated in FIA by a series of ten papers[1,7-15] published by *Ruzicka and Hansen* in the period 1975 to 1979. A review article by *Betteridge*[16] in 1978 describes the development of the theory, applications and apparatus of FIA and shows that a large number of workers entered the field at this time.

A review article by *Ruzicka and Hansen*[17] in 1980 lists nearly 80 papers covering several application areas, such as agricultural, clinical and environmental chemistry, and indicates the increase in the versatility of the technique. By 1986, as a later review article by *Ruzicka and Hansen*[18] containing over 800 references indicates, FIA was in use in 8 major application areas, and was used in the measurement of over 200 analytes. FIA uses 50 different analytical techniques and detection methods and is used for measurement of 10 different physical and

chemical values. Two text books[19,20] are of immense value as first sources of reference for any researcher new to the technique.

Review articles appear periodically in the scientific journals; that of *Miller*[21] covers the fundamental principles and recent developments of FIA, while *Pacey and Bubnis*[22] review industrial applications and techniques. *Masoom and Townshend*[23] have compared the advantages of FIA over SFA and cover the basic principles on which FIA is based. A more recent paper by *Ruzicka and Christian*[24] compares the basis of FIA with high performance liquid chromatography, and describes what the techniques have in common and where they may be used to aid each other. *Puchades et al.*[25] have comprehensively reviewed FIA methodology for on-line sample treatment and for on-line process monitoring, while *Chen et al.*[26] have reviewed anion determinations by FIA. *Ruzicka*[27] has reviewed the state of art of FIA and indicates that future developments will be in stopped-flow and sequential injection methodologies. He also recommends that flow injection (FI) and liquid chromatography (LC) would benefit from being unified as flow based impulse/response techniques. The large number of scientific papers published on FIA, indicates how active it has become as a modern analytical technique.

1.1.2. Genealogy of FIA

In the broadest definition of continuous flow techniques, the sample is introduced into a continuously flowing stream, which passes through some type of reactor/delay device before being detected downstream. Within this broadly defined group the techniques may be subdivided into those that separate the samples into their constituent components, such as gas-liquid chromatography (GLC) and high performance liquid chromatography (HPLC) and those that do not. The non-separation techniques may then be further divided between those using segmented flow, like SFA, and those using unsegmented flow, such as FIA. Within this broad framework of techniques the comparison of FIA, SFA and HPLC for their differences and similarities is of relevance.

Since FIA was initially developed from SFA, then it is appropriate to start by comparing the techniques. Common features of the two methods include the pumps, detectors and reaction/delay coils used in both types of manifold. It is also common for both types of manifold to have additional manifold elements incorporated, when various separation operations such as dialysis or solvent extraction are necessary. The main differences between the techniques are, the

absence of air bubbles in the FIA manifold. Air is introduced in SFA to separate the samples (aspiration) and to ensure mixing of the sample and reagents so that a steady state signal is obtained. In FIA a transient rather than a steady state signal is measured. Due to these differences another significant difference arises, and that is the simplicity in the design of the FIA manifold in comparison to the SFA manifold. The differing flow patterns that result and the detector signals that they produce are shown in Figure 1.1.

With both techniques the analyte concentration is related to the peak height, although peak width measurements can be made with a loss in precision[28]. In SFA mixing between the sample and reagent is obtained by the circulation that is induced in each liquid segment from the wall to the centre. The circulation is caused by the compressibility of the air segment which imparts an induced turbulence to the sample bolus. This homogenises the zone so that a steady state signal is obtained. In FIA mixing between the sample and the reagent is obtained by controlled dispersion, in which diffusive and convective mixing of the sample into the reagent flow occur. This process is not complete and so a transient signal is produced. Several workers have compared the advantages of FIA and SFA; *Snyder*[29] in 1980, *Ruzicka*[30] in 1981, *Patton and Crouch*[31]in 1986 and *Masoom and Townshend*[23] in 1988. The last authors considered there were three main advantages in FIA methodology in comparison to SFA; high sampling rate, low reagent consumption, and negligible reagent carry over. A disadvantage of the technique is its lack of sensitivity, because a transient signal is produced, while a steady state signal is obtained in SFA.

Initially FIA and HPLC would seem to have more in common than SFA and FIA. The concept of dispersion is common to both, although in HPLC dispersion is normally minimised to inhibit a detrimental effect on peak shape from increased band broadening. Factors that control dispersion in HPLC[32] are; (a) tortuous flow between particles of the stationary phase, (b) slow equilibration between mobile and stationary zones, and (c) axial diffusion. The design of HPLC systems is such that extra-column broadening is minimised by using the minimum length of < 0.2 mm diameter tubing to connect the manifold components. In FIA the dispersion (degree of mixing) is controlled and the manifold design is altered to change the degree of dispersion as required by each particular application.

A review by *Ranger*[33] compares FIA, HPLC and SFA; in Table 1. of that reference he lists a variety of operating characteristics which can be used to readily compare the merits of the three techniques. He highlights that both FIA and HPLC use

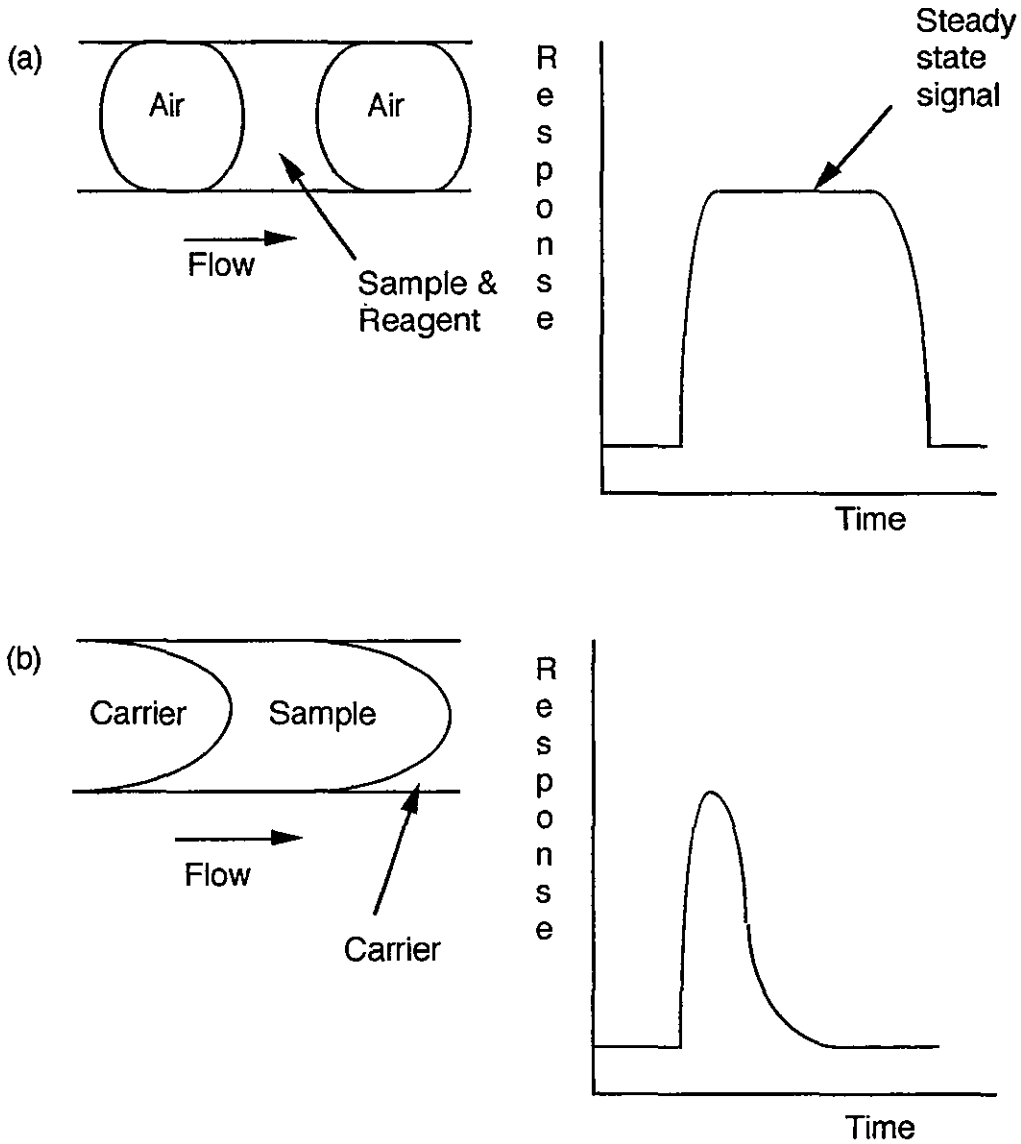

FIGURE 1.1. Flow patterns and their corresponding signals for (a) SFA and (b) FIA.

injection rather than aspiration for sample introduction, unsegmented rather than segmented flow, and tubes of < 1 mm internal diameter (i.d.) in comparison to 2 mm i.d. tubes used in SFA. *Burke et al.*[34] have compared the merits of ion chromatography (IC), SFA and FIA for the determination of nitrate in waters. IC was recommended if more than one analyte was to be simultaneously determined, and SFA or FIA were recommended if a large sample throughput was the controlling factor. If high sensitivity was critical, SFA was preferred over FIA, but FIA had the highest sample throughput rate.

Tyson[35] uses both an SFA and HPLC analogy to introduce the concept of dispersion in FIA, and explains why both analogies are not sufficient to give a true guide to dispersion in FIA. With increasing use of post column derivatisation in HPLC and micro-columns in FIA, the degree of overlap between the two techniques is increasing and this has been highlighted by *Ruzicka and Christian*[24], who also indicated an increase in coupling of the two techniques to overcome the shortfall in each. The above completes a brief review of the three techniques in which similarities and differences have been discussed. The next section will deal with factors that influence the signal shape in FIA.

1.2. Factors influencing the signal shape in FIA

1.2.1. Characterising the basic FIA signal

FIA is based on three principles which have been defined[15,36] as (a) sample injection; (b) controlled dispersion of the injected sample zone; and (c) reproducible timing of all events within an analysis cycle. The attainment of these three conditions produces a response at a detector that is shown in Figure 1.2. which illustrates a typical signal that is produced at a chart recorder by most detectors commonly used in FIA. The essential parameters that characterise the peak shape are shown and each is described more fully below.

- **i.p.** is the injection point where the sample is introduced into the carrier stream, in most cases using a rotary valve.
- $\mathbf{h_{max}}$ is the peak height at the maximum which is related to the concentration of analyte.
- $\mathbf{t_a}$ is the peak appearance time and this is the first significant deviation of the signal from the baseline.

- Δt is the baseline to baseline time, which is defined as the interval between the start of the signal and the return to the baseline ($\Delta t = t_w - t_a$).
- t_p is the residence time to the appearance of the peak maximum.
- t_w is the return time or wash out time, this is the period between the attainment of the peak maximum and the return to the baseline; the 'tail' portion of the peak.

As can be seen in Figure 1.2. the peak is not Gaussian and the above parameters do not fully define the peak profile, particularly the 'tail' which is characteristic of an FIA signal.

1.2.2. Controlled dispersion

To gain an understanding of how FIA works it is essential to review the mechanism that predominate in the dispersion of an injected sample bolus (zone) in a flowing stream. There are two main mechanisms occurring, (a) convective transport and (b) diffusional transport.

(a) Convective transport occurs under laminar flow conditions that are present in FIA. The convective transport mechanism produces a parabolic velocity profile, in which the sample molecules exhibit a distribution in linear velocity. This is close to zero at the tube walls and twice the average velocity at the tube centre.

(b) Diffusional transport occurs from the concentration gradients that are initiated by the convective transport processes. Radial diffusion is caused by concentration gradients that are perpendicular to the direction of flow, it has a significant effect on the overall dispersion. Axial diffusion which has a negligible effect on the overall dispersion, occurs at the leading and trailing edges of the sample bolus, is caused by the presence of concentration gradients that are horizontal to the direction of flow. The influence of each of the transport mechanisms (a) and (b), on dispersion and the resulting signals produced at the detector are shown in Figure 1.3.

Four different situations are represented in Figure 1.3., but situation (c) is the one that predominates in the vast majority of FIA manifolds. The dispersion of an FIA manifold can be measured experimentally, by injecting a non-reactive dye into an inert carrier stream[15]. The peak obtained will be affected by various factors of the manifold design such as injection volume, tube diameter and reactor length, but

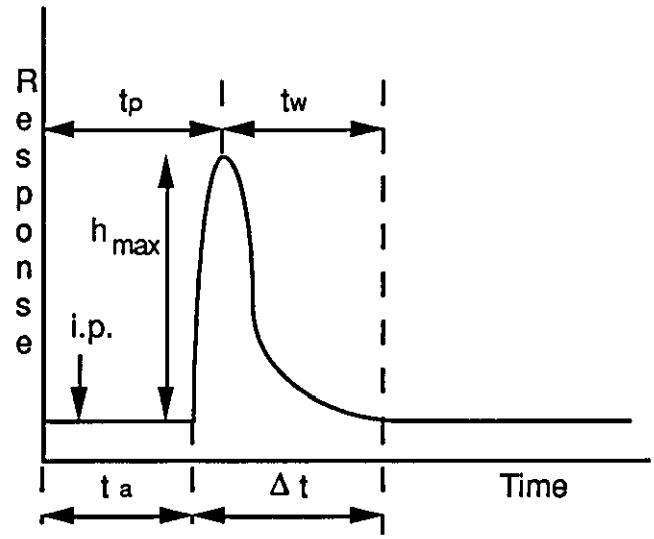

FIGURE 1.2. **Typical FIA signal and common peak defining parameters.**

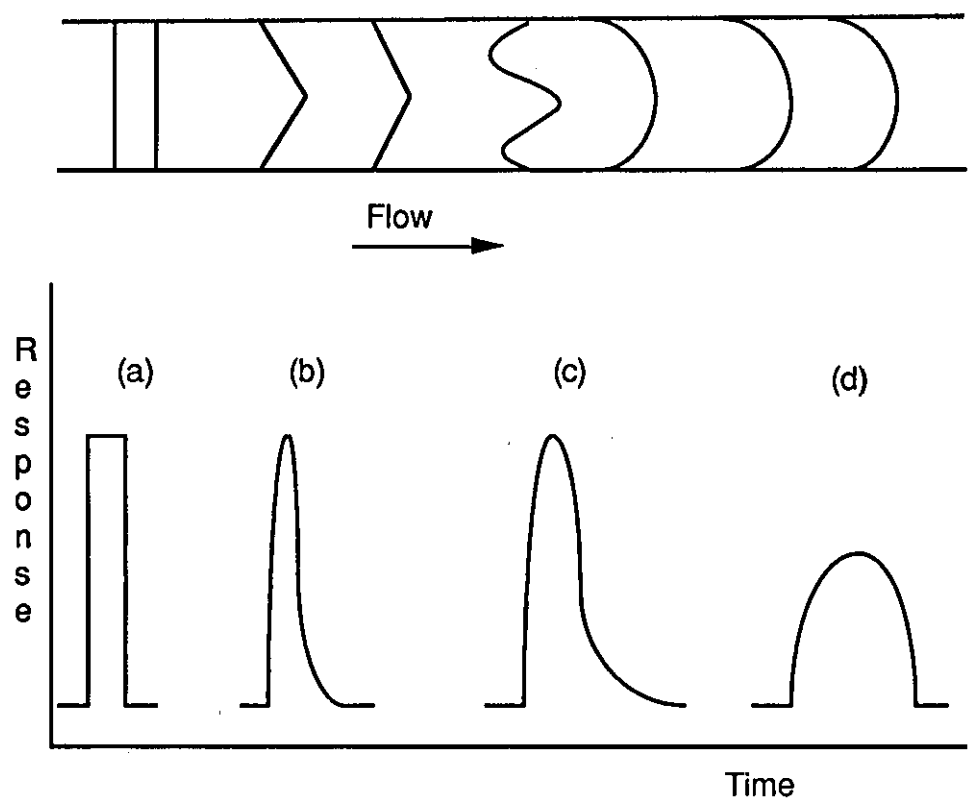

FIGURE 1.3. **Sample bolus dispersion and the resulting signal dispersion profiles. (a) no dispersion; (b) dispersion predominantly by convection; (c) dispersion by convection and diffusion; and (d) dispersion predominantly by diffusion.**

will be unaffected by chemical reaction (chemical diffusion). The procedure for evaluating the degree of dispersion in a manifold for fixed, flow rate, injection volume and reactor geometry is as follows:

(i) The transient signal is obtained by injecting a dye solution into a non-reactive carrier stream such as deionised water.

(ii) The steady state signal is obtained by continuously pumping the dye solution through the flow-cell.

The ratio of the transient signal over the steady state signal is a measurement of the manifold dispersion, the shape of the signal obtained also contains useful data on flow characteristics of the manifold.

1.2.3. The influence of various components on dispersion and signal shape

The influence of various experimentally variable manifold components on dispersion and hence signal shape have been studied extensively by several workers. This section will outline the influences of each experimentally variable parameter in turn.

(a) Flow rate:- Increasing the flow rate decreases the dispersion, t_p, t_a, and Δt, but increases h_{max}[15,37].

(b) Tube length and tube diameter:- Increasing the length[15,37] or diameter[15,20] of the reactor tubing produces the opposite effect to that of increasing the flow rate.

(c) Sample volume:- As the volume of the sample injected increases, there are four notable changes; dispersion decreases as the signal approaches the steady state and Δt increases. t_p increases until steady state is reached, after this point there is no increase in t_p, t_a is found to be independent of injected volume. The effect of the above observations have been reported by several workers[15-17,37], who have illustrated the changes diagrammatically.

(e) Reactors:- The experimental parameters discussed so far apply equally to straight and coiled unfilled reactors, but coiling introduces additional factors that affect the dispersion and signal shape, and these will be discussed here. *Tijssen*[38] noted that coiling the reactor introduces a secondary flow pattern that behaves

similarly to radial diffusion, in that the dispersion is reduced and this leads to a narrower peak. *van den Berg et al.*[39] reported that reducing the coiling diameter (the diameter of the coil in comparison to the diameter of the support around which the coil is wound) reduces the dispersion further. A disadvantage of having a very a high degree of coiling (diameter of the support approaching the diameter of the tubing) is that a high back pressure could be generated by the inclusion of a tightly wound coil in the manifold.

The behaviour of packed bed reactors (PBRs), which are typically short glass tubes (10 cm) of wide diameter (3 mm) packed with glass beads of a smaller diameter than the tube, is well known in chemical engineering and chromatography[39]. When used under the experimental conditions given by *van den Berg et al.*[39] they found the PBR's performance to be superior to the coiled reactor's, for the parameters evaluated. Unlike coiled reactors, it is the particle size of the glass beads filling the PBR that control the dispersion. The smaller the diameter of the bead the lower the dispersion. But decreasing the particle size of the beads cause an increase in the back pressure of the reactor as the beads become more tightly packed. *Brooks and Dorsey*[40] used four different designs of reactor in their manifold, coiled, knitted, single bead string reactor (SBSR) and Serpentine II reactors. They found that as the flow rate was increased the dispersion and reagent consumption decreased especially when the Serpentine II was used in the manifold. Their results were based on the second moment analysis of the peak shape (standard deviation of peak widths at various predetermined heights).

(f) Temperature:- The effect of changing the temperature on dispersion and the shape of the signal obtained in FIA has been reported by several workers[41-46]. As the temperature increases, radial mixing is promoted by a decrease in viscosity and axial dispersion is also decreased. h_{max} increases because the rate of product formation is increased because chemical kinetics are favoured by elevated temperatures. *Stults et al.*[43] have investigated the effects of temperature on dispersion with and without chemical reaction; they report that increasing the temperature decreased Δt in addition to the effects reported above. They indicated that for well-characterised reactions, the effects of temperature can readily be assessed and compensated for, without the need for rigorous temperature control.

(g) Multiline systems:- The factors that have been discussed so far apply equally to single and multiline manifolds; the specific effects of adding of one or more

line to the manifold, will be discussed here. The addition of another stream in a multiline manifold has the following effects on signal shape; h_{max} is reduced (dilution effect), dispersion, t_a, t_p and Δt are increased and additional secondary flow effects are encountered. The degree of these effects are governed by the relative flow rates of each line. This is sometimes advantageous as it permits the adjustment of an additional manifold parameter. *Tyson*[47-49] when comparing the merits of the two types of manifold showed, that in a single-line manifold one of the main methods of increasing sensitivity is to increase the volume of sample injected. A point is reached when double peaks are formed; this limits the sensitivity. In multiline manifolds the adjustment of the flow of the additional reagent/carrier streams, prevents the formation of double peaks and thereby increases the method's sensitivity.

Tyson[49] on comparing the sensitivity of three types of FIA manifold, concluded that the multiline configuration offered the best solution to refractive index (RI) and baseline absorbance problems. The multiline manifolds offer an approach to dealing with complex matrices, such as those where the viscosities of samples and reagents differ considerably[50], or where the sample can produce an undesirable effect on the monitored signal, such as adding an RI component[51]. The dilution of the sample before detection is more easily achieved in a multiline manifold and addition of reactors downstream from the confluence point (mixing point e.g. Y-piece or T-piece) enables mixing to occur before detection. *Clark et al.*[50] reported that the geometry of the confluence point the shape of the signal obtained and they optimised the angle of the confluence point to reduce the mixing time.

Finally *Wada et al.*[52] investigated the effects of pumps, reaction coils and mixing joints, on peak profile and report that pumps giving small pulsations used in combination with double coiled reactors gave well defined reproducible peaks.

1.2.4. Classification of dispersion

Ruzicka and Hansen[15] defined the dispersion coefficient 'D' as the ratio of the concentration of the sample before and after the dispersive process. If the bulk concentration of analyte is given the symbol C_o and the analyte concentration at the peak maximum is C_{max}, then dispersion is given by :-

$$D = \frac{C_o}{C_{max}} \qquad (1)$$

In FIA it is more common to measure the peak heights and the ratio of the steady state signal to the transient peak maximum is used to measure D experimentally :

$$D = \frac{h_o}{h_{max}} \qquad (2)$$

h_o is the response for the measurement of the bulk concentration, (usually obtained by pumping the preformed complex through the detection cell) and h_{max} has been defined previously (1.2.1.). For the sake of convenience dispersion has been divided into three categories[19,53];

(a) Limited dispersion (D = 1 - 3) is used where the flow system is merely a mechanism for transport and only limited sample dilution can be tolerated, as with atomic absorption detection[54] and some electrochemical detection systems[17].

(b) Medium dispersion (D = 3 - 10) allows sufficient time for a chemical reaction to take place and form a measurable species on-line. It is within this category that the vast majority of research on FIA has been focused.

(c) Large dispersion (D > 10) is used on three occasions, when on-line dilution is required, when the reaction is slow and needs a longer residence time to form a measurable species. Thirdly, when the sample matrix is complex and requires a process such as on-line dialysis in detection of the analyte.

1.2.5. Models for dispersion

Modelling dispersion of FI systems is an area of intense research interest and several approaches have been adopted over the years, these have recently been reviewed by *Hull et al.*[55] *Taylor*[56] first obtained a solution to the diffusion-convection equation (equation 3) by examining laminar flow in a straight tube of circular cross section for two extreme cases. The first case was for a region where dispersion was by pure convection, 'Taylor A' region and the second was for dispersion by axial diffusion alone, 'Taylor B' region (cases (b) and (d) in Figure 1.3. respectively). The general diffusion-convection equation is given below:

$$\frac{dC}{dt} + \left(\frac{u}{L}\right)\left(\frac{dC}{dx'}\right) = \left(\frac{D_m}{L^2}\right)\left(\frac{d^2C}{dx'^2}\right) \qquad (3)$$

C is the concentration (M), t is the time (s), u is the linear flow velocity (cms^{-1}), L is the length of the manifold (cm), x' is axial distance divided by manifold length (unitless) and Dm is the molecular diffusion coefficient (cm^2s^{-1}). The two extreme situations solved by Taylor are not normally encountered in FI and the regions where solutions for the diffusion-convection equations have been solved are shown schematically in Figure 1. of the paper by *Hull et al.*[55]

In a theoretical approach to modelling experimental manifolds, one way forward are models based on mixing tanks. *Ruzicka et al.*[15] proposed a tanks in series model, while *Tyson et al.*[28,57] favoured a single mixing tank mode. In a development from the single mixing tank mode, *Stone and Tyson*[37] evaluated the effects of flow rate, manifold length and injection method, with a well stirred tank and two tanks in series models. They found that the two tanks model gave a closer approximation to the experimental data than the well stirred tank model. Prediction of the inflection point, the rise curve and fall curve of a signal were possible with the two tanks model. The model of *Tyson and Idris*[57] could be used to predict parts of the rise and fall curves but missed the inflection points. *Stone and Tyson*[58] later extended the well stirred tank model to two tanks in parallel, but the predictive properties of this two tank model was limited to short (> 50 cm) manifold lengths.

The tanks in series model of *Ruzicka and Hansen*[15] is similar to the theoretical plates theory of LC. It relies on modelling fluid passing through a large number (n, the number of mixing tanks) of mixing chambers in sequence, with an assumption of instantaneous mixing occurring. *Stulik and Pacakova*[59] state that probability theory can be used to express the concentration distribution of a substance as a function of time. They also state that the concentration distribution is Poisson in nature, if an assumption of continuous solution flow is made. The equation for concentration distribution by the tanks in series model is given below:

$$\frac{C}{C_o} = \left(\frac{t}{\tau}\right)^n \frac{e^{-t/\tau}}{n!} \qquad (4)$$

Where τ is the mean residence time of the substance in one tank. As the number of tanks increase the peak obtained flattens and broadens and approaches a Gaussian distribution. This effect can be seen in Figure 2.12. of the book by *Stulik and Pacakova*[59] which shows the concentration distribution calculated for different numbers of tanks in series. The model does work well for a low value of n, as is

the case with short reactors but according to *Reijn et al.*[60] it is useful in predicting dispersion in SBSRs.

Other models have been used to predict dispersion in FI and they will be briefly mentioned here. The list is by no means exhaustive but will illustrate that no method has yet been found to accurately model the diffusion-convection process. *Brooks et al.*[40,61] used moment analysis to predict the dispersion coefficient in the manifold and the effect of various types of reactor on dispersion. *Betteridge et al.*[42] used a random walk simulation (stochastic, Markovian chain) to model dispersion in a single-channel manifold with and without a chemical reaction occurring. *van Nugteren-Osinga et al.*[62,63] used the convolution and deconvolution in the Fourier domain of the impulse/response function of individual components of an FI manifold to predict the dispersion. *Kolev and Pungor*[64] defined various sections of the manifold (as fore section, injection section, aft section, detector etc.) and derived mathematical equations for each section in the Laplace domain, to predict dispersion in a single-channel manifold without chemical reaction. Finally *Kolev*[65] derived equations for step and delta input functions to model the response obtained for both slug and time based injections. The most comprehensive review of dispersion models is that of *Hull et al.*[55] and the authors state that they are correlating and evaluating each of the models and theories and will report their results at a future date.

1.3. Terminology of injection processes

1.3.1. Normal flow injection

In normal flow injection analysis (nFIA) a small volume of sample is injected into a reagent/carrier stream travelling through narrow bore tubing where the product is monitored at a detector downstream. This is the most conventional mode of flow analysis and many innovations have been made to modify and apply the technique[19,20]. One innovation of FIA is where the roles of the sample and carrier solutions are reversed, a volume of reagent being injected into a sample carrier stream. This technique was introduced by *Johnson and Petty*[66] who named the technique reverse flow injection analysis (rFIA), to contrast it with the normal technique, normal flow injection analysis (nFIA). The term flow injection analysis (FIA) is frequently abbreviated to flow injection (FI), facilitating the use of terms such as flow injection amperometry. The abbreviated terms will be used here from now. The remainder of this section will deal with various aspects of modified FI and highlight the differences in comparison to nFI.

1.3.2. Reverse flow injection

In rFI only small volumes of reagents are used and, also, because the determinand concentration in the reagent bolus (injected plug) increases with increasing dispersion, the determination is carried out with only a small dilution[66,67]. Clearly, the sample must be plentiful and inexpensive. The shapes of the signals obtained for nFI and rFI are fundamentally different, double peaks, which are undesirable in most applications, being more prevalent in rFI[67-72]. Reverse FI is not the ideal name for the technique: perhaps inverse FI might have been better. In a development of rFI *Frenzel*[73], and *Israel and Barnes*[74] have used rFI to introduce standards into a flowing sample stream thereby giving a method for on-line standard addition. Another modified FI technique, termed flow reversal FI, has been proposed where the sample bolus is passed repeatedly (in the forward and reverse directions) through the detector (page 247 in *Ruzicka and Hansen*[19]), this method and the standard addition methods add to the uncertainty of what is meant by rFI. Some workers prefer the term 'reagent injection' to rFI, but the term only adequately describes simple systems.

A term is needed that describes whether the chemical species, the concentration of which limits the amount of product formed, is dispersing in or out of the bolus. Previously *Fogg et al.*[67-72] have indicated that a product is formed by rFI dispersion of species x, and x is dispersing in an rFI manner, giving the required information. In nFI using small volume injections, a finite amount of determinand is injected, all (usually) of this determinand is derivatized, and a good shaped peak is observed. In rFI an infinite amount of determinand is present (the carrier stream) ready to disperse into the injected reagent. Normal FI resembles classical manual methods in using a fixed amount of determinand with an excess of reagent. The amount of determinand in the reaction zone in nFI is constant; in rFI it increases continuously (with the reaction continuing until the reagent is exhausted). The fully formed nFI peak decreases in height as the fully formed derivative is diluted by further dispersion. For an infinitely concentrated reagent and fast derivatization, the rFI signal becomes rectangular with sufficient dispersion and, with increasing dispersion beyond this, the rectangle simply becomes broader. This has been discussed previously in more detail[67-72], and Figure 1. in the work of *Fogg et al.*[70] and Figure 3. in *Fogg and Zhao*[72], illustrate these points.

1.3.3. Multireagent systems and indirect methods

So far the use of a single-channel manifold, in which the solutions flow through a single tube, has been assumed. In most spectrophotometric applications, however, the use of multichannel systems is recommended in order to obtain more rapid mixing. Sample is injected into an inert carrier stream, which is then merged with one or more reagent stream. Reagents could equally well be injected into an inert carrier stream and merged with a sample stream. These situations present no difficulty in using the terms sample injection and reagent injection.

The terms begin to take on some ambiguity, however, if we return to using single-channel manifolds with several reagents, and one or more reagent is mixed with the sample solution prior to injecting it, or the carrier stream containing the other reagents. The term sample injection does not indicate that one or more reagents have been injected with the sample, and reagent injection does not indicate that some reagents are already in the sample stream.

A more serious problem arises in describing indirect methods in single-channel manifolds, when the determination is carried out by observing the decrease in the size of a monitorand signal. If the monitorand is preformed there is no problem: the monitorand is then the reagent. However, if the monitorand is being formed on-line, and it reacts as it is being formed with the determinand, then there is a problem with nomenclature. The on-line iodimetric determination of sulphite illustrates this[68,71]. If the carrier stream is a slightly alkaline solution containing iodate and excess iodide, into which either acid or acidified sulphite is injected, then the iodine is formed by reagent injection and the sulphite is determined by sample injection. At face value this seems fine; however, if the iodate/iodide solution is injected into an acid carrier stream, we can hardly say that iodine is formed by sample injection! (We could be determining iodate by sample injection however[75]). In any chemical reaction the species 'determined' is that at lowest equivalent concentration (that whose concentration limits the amount of product formed). In determining sulphite iodimetrically there are really two 'determinands', iodate and sulphite, but only one sample, the sulphite solution.

The advantage of the term nFI over sample injection, is that nFI only implies that the concentration-limited chemical is being injected, not necessarily the sample. Further, nFI can be used to express a direction of dispersion, into or out of the bolus. The terms into bolus dispersion (or out of carrier stream dispersion) and out of bolus dispersion, could be used, but are, perhaps, clumsy.

For the system in which acid or acid/sulphite is injected into iodate/iodide carrier, we can say that iodine is formed in the rFI manner (or iodine is formed by rFI dispersion of iodate) and sulphite is determined in the nFI manner. These expressions succinctly indicate that the reagent limiting the formation of iodine (the iodate) is in the carrier stream, and that the sulphite is in the injectate.

1.3.4. Single boundary measurements

When a sufficiently large volume injection is made with a single-channel manifold (this volume can be small if low dispersion occurs[76]) the carrier stream does not reach the centre of the bolus. If a derivative is being formed on-line then two distinct and independent reaction zones result[69,70,72]. Note the terms nFI and rFI lose their meaning in this situation.

Injecting a large volume is a convenient way of producing two complementary independent reaction zones for study (R<S and S<R, where S and R represent the sample and reagent solutions respectively, and R<S, for example indicates that S is flowing behind R), allowing the effect of reversing (if that word can be used) the order of flow to be observed[69,70,72]. Note also that if an injection loop is used, then the rear boundary travels further than the front boundary and is dispersed more. By using valve-switching techniques, or different valve configurations[69], boundaries can be formed at the same point at different times. These techniques also allow different boundaries to be formed[76-79]. By producing the flow sequence A<B<C, where A, B and C represent three different solutions flowing in the tube in the order indicated, double standardisation's can be made[77,78] (in this instance without reaction at the two boundaries), or two metals can be determined by the same reagent[76,79], present in solution B, in so-called sandwich techniques.

Refractive index effects can be appreciable when working with single boundaries[70], but even when this is corrected for, the order of flow of the two solutions often affects the signals formed[69]. Hence, for single boundary work, there appears to be a need for terminology to indicate whether a particular chemical species is dispersing forwards or backwards in the flow.

With small volume injections, in nFI and rFI the reagent and the sample solutions are in infinite supply, respectively. For single boundary measurements both sample and reagent solutions are in infinite supply, but clearly the equivalent reagent concentration in the reagent solution should be greater generally than the

determinand concentration in the sample solution. This latter statement assumes a simple derivatisation reaction is being used. When carrying out an indirect determination at a single boundary, clearly the two solutions at the boundary are in infinite supply, but also the concentration of reagent (e.g., iodate) limiting the formation of monitorand (e.g., iodine) needs to be sufficiently great to produce an excess of monitorand over determinand (e.g., sulphite) in the reaction zone at the boundary.

The terms sample injection and reagent injection are inadequate in describing FI systems in which a monitorand that is not the determinand is produced on-line, The term rFI may not be self-evident, but terms such as nFI and rFI can be used effectively to indicate whether a chemical species is in the injectate or carrier stream, and whether a product is being formed by a concentration-limited species dispersing into or out of the bolus. Any term replacing the term rFI must be equally versatile.

In direct FI methods the terms sample injection and nFI are synonymous, indicating that the concentration-limiting species (the determinand) is in the injectate. Similarly, the terms reagent injection and rFI indicate that the concentration-limiting species is in the carrier stream. However, the terms nFI and rFI are more versatile and can be used more widely to describe whether a particular species is dispersing out of or into the bolus (dispersing in the nFI manner), and whether the product is being produced by dispersion out of or into the bolus of the concentration-limited reactant (formed in the nFI or rFI manner, or formed by nFI or rFI dispersion of the concentration-limited species).

At single boundaries reactants can be described as backwards or forwards dispersing and products as being formed by the backwards or forwards dispersion of a concentration-limited reactant.

1.3.5. Peak width measurements

So far the techniques we have discussed are usually associated with peak height measurements, but techniques based on peak width measurements are also used in FI. The most common use of peak width measurements are the so-called FIA titration methods. The FIA titration methods, may be divided into two main groups, those that use an mixing chamber [33,80,81] and those that do not[82-86]. The mixing chamber approach produces signals that could not be classed as single

boundary measurements, because the sample and reagent can be completely mixed and doublet peaks are not produced.

The mixing chamber may be placed in a manifold before or after the sample and reagent are merged. If an exponential mixing chamber is placed before the sample and reagent streams are merged, then large dispersion of the sample occurs, before it is mixed with the titrant[33,80] and signals are obtained that may approach the steady state[33]. The second approach was used by *Turner et al.*[81] A mixing chamber was placed after the sample and carrier had been merged, before detecting the signal with an electrode. The signal they obtained did not approach the steady state and was in fact typical of those obtained in nFI. All of the workers using the mixing chamber approach measured the peak width at some predetermined height, close to half peak height in the case of *Ranger*[33] and *Turner et al.*[81] and nearer the baseline by *Stewart*[80]. A linear relationship between peak width and the logarithm of the sample concentration was obtained by all three workers.

Ruzicka and Hansen[87] describe a gradient FIA titration method in which a zone of an acid is injected into a basic carrier stream, the acid will be neutralised as the base penetrates the sample zone at the leading and trailing edges. If segments of the dispersed sample zone are identified with equal dispersion values (D) then the peak width Δt can be use to determine the concentration of the acid.

The second group of methods for FIA titrations are those that do not include a mixing chamber[82-86,88]; doublet peak are often obtained in these methods particularly if large volume injections are made and they may be classed as single boundary measurements. The exception to the above, is the work of *Clark et al.*[85] ; although no mixing chamber is used, a small volume sample injection is made (25 µl) and this means that the technique is not a single boundary measurement because there is complete penetration of the injected sample bolus. The signals produced by this method are flat topped, but the peak width is still proportional to the logarithm of the concentration of the injected sample species. FIA titrations using single boundary measurements produce doublet peak signals[82-84,86,88]. Δt measurements are made between a point on the rise curve of the front boundary peak and on a similar point on the fall curve of the rear peak (Δt at half h_{max} or Δt between t_a on the front boundary peak and t_w on the rear boundary peak have been used).

FIA titrations are best classed as peak width measurement techniques, but some workers have classed them as time-based methods[80,83,84,86]. The definition is strictly true because the width of the peak is measured in time units. However, the term can introduce some confusion, particularly when time-based injections[84,89,90] or timed pump operations[85,87] are also used to produce the signals.

1.4. Detection in FI

A detector in FI needs to meet certain performance characteristics; it should have a high signal to noise ratio (low noise, high signal) to enhance instrumental sensitivity, a linear response or linear related response to changes in analyte concentration and reproducibly give a stable signal. Various detectors have been employed in FI. A review of the applications of the differing detector types for the period 1975 to 1985[18] indicated that the largest group in use were spectrophotometric detectors, 46%; the next most used were electrochemical, 30%. The application and performance of various types of flow-through detectors have been reviewed by several workers[63,91-93]. *Poppe*[91] and *Krull*[92] evaluated the use of optical and electrochemical detectors for both FI and HPLC systems.

van Nugteren-Osinga et al.[63] modelled the impulse-response functions of spectrophotometers, ion-sensitive field effect transistors (ISFETs), potentiometric (glass pH electrode) and amperometric (wall-jet) detectors for use in FI systems. They concluded that the impulse-response function of an ideal detector is high and narrow. These conditions are met in spectrophotometry when the volume of the flow-cell used is small and for wall-jet electrodes and ISFETs, when the flow of solution is directly impinging on the electrode and not influenced by recirculation of analyte in the detector cell. *Kuban*[93] in a review of simultaneous determinations of several components by FI, considered the use of several detector types (optical and electrochemical either singly or as mixtures of all types). The detectors used were used in various manifold configurations, as a single detector (single or multichannel operation) or as multidetectors in series and in parallel configurations to obtain the multicomponent data.

1.4.1. Optical detectors

This class of detectors include, the atomic and molecular spectroscopy detectors and a wide range of wavelengths from the infrared through to the ultraviolet region of the spectrum may be detected. The use of atomic spectroscopy in flow

analysis is covered in a book by *Burguera*[94] and a paper by *Tyson*[95]. Its use with HPLC is covered briefly in a review by *Krull*[92] readers are referred to those texts for further information and the atomic spectroscopy techniques will not be considered here. *Valcarcel and Luque de Castro*[96] have reviewed the application of molecular spectroscopic detection to FI, and the techniques covered include, fluorimetry, infrared spectrometry, mass spectrometry, Raman spectrometry and spectrophotometry (visible and ultraviolet/visible). The review deals with approaches aimed at enhancing detector performance, improvements in the detection systems and coupling FI with unusual detectors. Readers are referred to this paper for information on the trends in the application of molecular spectroscopic detectors in FI systems.

Spectrophotometry is the technique in which we are mainly concerned for optical detection of the analyte species, and it is the area where most of our effort has been concentrated in achieving this objective. The detector types included within the category of spectrophotometric detectors are, colorimeters, ultraviolet/visible (UV/vis) spectrophotometers (single and double beam instruments) and more recently diode-array spectrophotometers. Also included in this category are solid-state photometers, which consist of light-emitting diodes (LEDs) as sources of visible light, and photodiodes or phototransistors as photometric detectors. The use of solid-state, flow-through photometers in FI manifolds have been reviewed by *Trojanowicz et al.*[97] and the workers claim that they are a viable, low cost alternative to commercial spectrophotometers as detectors of visible light.

Abbott and Kelderman[98] have assessed the effects of non-optical noise sources in optical detectors for use in HPLC systems and their observations are equally applicable to FI systems. They conclude that the best solution for the reduction of noise components in variable wavelength and diode-array detectors would be the development of higher power light sources which have geometries compatible with small volume flow-cell collection optics. The effect of non-optical noise is significant at very low absorbance values (0.0001 A, near the limit of detection) and its effect is not as detrimental at the higher absorbance values normally encountered. A critical review of UV/vis spectrophotometry has been made by *Lobinski and Marczenko*[99]: the developments that are covered in this paper may be utilised in FI. Any improvement in detector performance or use of new colour systems such as, macrocyclic and pyridylazo compounds, porphyrins, surfactants or basic dyes can be used to improve detection or develop new spectrophotometric determinations for FI.

Diode-array detectors (DADs) were first used as multiwavelength detectors in HPLC, where the possibility of monitoring components at their characteristic wavelengths represented a major improvement in mixture resolution. It was therefore a logical step to include DADs as fast scan detectors to aid in multicomponent determinations in FI. Several workers have used a DAD for simultaneous determinations in FI[100-106]. DADs have also been used to study chemical equilibria[107], manipulate FI signal sensitivity(amplification and dilution methods)[102], overcome problems of high background absorbance[108] and correct for refractive index differences[109]. There is a growing interest in the application of DADs in FI to overcome with the aid of chemometric data treatment the problems of multideterminations in FI systems. The advances in instrument design and data handling have been covered in the review by *Lobinski and Marczenko*[99] while the application of DADs, amongst other detector types, for simultaneous determinations have been reviewed by *Kuban*[93].

Valcarcel and Luque de Castro[110,111] report on detector developments for FI systems. In the second paper[111] several processes are combined, reaction and detection, or separation and detection, or reaction, separation and detection. The workers use the term sensors to describe these detectors where derivatisation or separation of the analyte species has been combined with the detection; optical and electrochemical applications of this sensor technology are described. In the case of combining reaction and detection the reagents can be immobilised in the detection cell, while for methods combining separation and detection, a phase separation (solid-liquid, liquid-liquid or gas-liquid) can occur in the cell, with or without previous derivatisation of the analyte species.

Krull[92] describes a two techniques where photolysis is used to produce species that have different electrochemical properties from the original compounds. The techniques are combinations of photochemistry and electrochemistry. In the first technique the sample passes a broad spectrum mercury discharge lamp immersed in a low temperature bath before entering the electrochemical cell. Species that have photolytic or hydrophotolytic properties are rapidly converted into new products. In the second technique a high intensity xenon discharge lamp is used to irradiate the sample in the electrochemical cell. This produces photolytic compounds that have different electrochemical properties than the unphotolysed compounds.

The above is a brief review of optical detectors in FI. Spectrophotometric detection is covered in more detail than any of the other atomic or molecular

spectroscopic techniques and the use of light sources to produce new compounds is also briefly reviewed.

1.4.2. Electrochemical detection

This category of detectors includes those that use coulometry, conductivity, potentiometry and amperometry to detect the analyte species. It is with the last category that our interest lies. Several types and geometries of electrode have been used to measure the amperometric response of an analyte species and these include, rotating disk electrodes (and ring disk), tubular electrodes, spherical electrodes, conical electrodes, dropping mercury electrodes, disk electrodes, microelectrodes and flat surfaced electrodes. The use of these electrode types in flowing solutions has been reviewed by *Pungor et al.*[112] , *Stulik and Pacakova*[59] and most recently by *Gunasingham and Fleet*[113]. The use of microelectrodes has been reviewed by *Fleischmann et al.*[114]

Pharmaceutical and biomedical applications of electroanalysis have recently been reviewed by *Kauffmann and Vire*[115]. The workers concluded that the electroanalytical techniques were still not widely used for drug analysis in hospitals and the pharmaceutical industry. Electroanalytical techniques offer highly sensitive and specific methods of analysis and are able to differentiate between enantiomers. The workers report[115] that the lack of popularity of electroanalytical methods for drug analysis is because the requirements for drug analysis are stringent, and if not well understood and applied, electroanalytical methods may only have limited success.

In FI amperometry solid electrodes are favoured over mercury electrodes, because they are more rugged and can be used over a wider anodic range of potentials. This alleviates the need to deoxygenate the solution, when the analytes are being detected in the oxidative mode. Glassy carbon electrodes are particularly suitable because they produce a low background noise level[116]. The selectivity and stability of the solid electrodes can be improved by chemically modifying the electrodes, as has been demonstrated by *Wang et al.*[117], who improved the permselectivity of their electrode by coating it with a polymer film. Mechanically or covalently bonding enzymes to platinum wires has also been shown by *Thomas et al.*[118,119] to improve selectivity.

Solid electrodes in FI amperometry can be used in several flow-through cells. Tubular and channel, thin-layer and wall-jet configurations are the most popular;

of the three types mentioned. Tubular (and channel) are the least popular in FI. They are more commonly used in HPLC[59], and one possible explanation for their lack of popularity in FI may be the difficulty encountered in preparing the electrode's surface (polishing).

The wall-jet configuration has been favoured by many workers and the commercially available Metrohm EA 1096 cell has been widely used. *Fogg* and co-workers have used a similar design of cell, to examine a variety of analytes using a glassy carbon working electrode. Nitrate was determined as the nitro-derivative of thiophene-2-carboxylic acid following nitration in an rFI method[120]. Bromine was used for a range of indirect analyses because its chemical reactivity and the fact that it can be reduced at positive potentials[68,121,122]. Iodine has also been used for indirect determinations[68,123]. Phosphate has been determined in an rFI method as phosphomolybdate[124], while nitoprusside[125], cyanide[126], sulphite[127], oxalate[128], nitrite[129] and EDTA[130] have been determined by direct anodic oxidation at glassy carbon.

1.4.3. Hydrodynamic voltammetry

Hydrodynamic voltammetry differs from static voltammetry because the mass transport of analyte to the electrode surface, has a convective term in addition to the molecular diffusion that is present in static voltammetry. The convective term occurs to account for the movement of the analyte species in the carrier solution. *Levich*[131] derived equations for the above combined processes (convective diffusion) that describe mass transport in both stirred and flowing solutions and derived equations for various electrode configurations. There are two main methods by which convective diffusion may be achieved, the solution may be moved past a stationary electrode, as is the case with flow-cells or the electrode may be moved in solution. The latter case occurs with rotating disk electrodes which stir the solution and their hydrodynamic behaviour and that of the flow-cell electrodes have been comprehensively reviewed by *Pungor et al.*[112] and by *Stulik and Pacakova*[59]. *Gunasingham and Fleet*[113] have comprehensively reviewed the hydrodynamic behaviour of various flow-through detectors including wall-jet and thin-layer detectors.

Yamada and Matsuda[132] studied the hydrodynamic behaviour of wall-jet cells and the workers derived the equation for the limiting current of a wall-jet cell that is given below:-

$$i_L = (1.60k)nFC_oD^{2/3}\upsilon^{-5/12}V^{3/4}a^{-1/2}r^{3/4} \quad (5)$$

i_L is the limiting current, k = 0.86, n is the number of electrons, F is Faradays constant, C_o is the concentration of the electroactive species, D is the diffusion coefficient of the species, υ is the kinematic viscosity, V is the volumetric flow rate, a is the diameter of the nozzle (in the wall-jet cell), and r is the radius of the electrode.

The workers[132] report that the value of k was calculated from a large number of experimental results. *Compton et al.*[133] have shown that a wall-jet electrode can be used to discriminate against various electrode reaction mechanisms. The workers[133] report that for a wide range of electrode processes, a wall-jet electrode offers a better mechanistic resolution (higher sensitivity) than a rotating disc electrode. In later work *Compton et al.*[134] have assessed the contribution of radial diffusion on the models for mass transport at a wall-jet electrode. They report that mass transport conditions can only accurately be described by a model that includes axial convection and normal diffusion, but specifically ignores radial diffusion.

The electrochemical response of the wall-jet cell used in this laboratory has been characterised for the limiting current region by *Powell and Fogg*[135]. They report that the response progressed from thin-layer to wall-jet behaviour as the flow rate was increased. In later work[136] FI signal transient were simulated using a resistance-capacitor (RC) circuit to test the validity of the time response of the amperometric system. They report that the RC circuit accurately models the rise curve of a signal except for residence times of 0.1 s or less. Finally *Powell and Fogg*[137] modelled the dynamic response of the wall-jet cell and indicated that the laminar flow initially encountered in the straight connecting tubing, is modified by the mixing stages in the electrode channel. The results obtained for the dispersion in the electrode channel defined an effective detector volume of 7 µl. Hence, it was concluded that the detector did not significantly contribute to the overall dispersion.

The above is a brief review of the hydrodynamic behaviour of wall-jet configuration detectors, the cited references give fuller descriptions. The other types of flow-through cells have been mentioned briefly and a more rigorous treatment of their hydrodynamic behaviour is given by *Compton and Unwin*[138], for channel and tubular electrodes and by *Weber*[139] for thin-layer electrodes. The hydrodynamic behaviour of thin-layer and tubular cells have also been studied

by *Matsuda*[140]. Finally *Wang and Chen*[141] report on a novel detector cell that is part of the injector. The cell is a hybrid of the a wall-jet and thin-layer configuration. When the detector was compared experimentally with a conventional thin-layer cell, the hybrid cell was found to be more sensitive, to have a higher sample throughput and to contribute negligibly to sample bolus dispersion. Hence its high sensitivity.

CHAPTER 2

INSTRUMENTATION, REAGENTS AND GENERAL PROCEDURES

2.1. Introduction

This section will detail the instrumentation, reagents and general procedures used to obtain the results given in the later chapters. General procedures are described to prevent any repetition in the later chapters, but any specific alterations to equipment or procedure will be given in the appropriate chapter.

2.2. Apparatus and Instrumentation

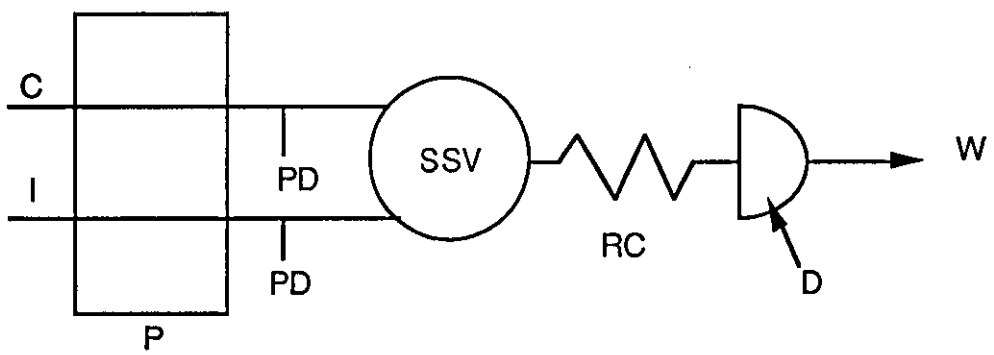

FIGURE 2.1. **Schematic diagram of the flow injection manifold. Where C = the carrier stream, I = the injectate stream, P = the peristaltic pump, PD = the pulse dampers, SSV = the stream switching valve, RC = the reaction coil, D = the detector and W = the waste outlet.**

The above diagram shows the general layout of the single-channel manifold used for most of the flow injection work carried out in the following chapters. The individual components of the manifold will be given below and any alteration will be covered in the relevant text.

Pump:- Gilson Minipuls 2 peristaltic pump

Tubing and connectors :- 0.8 mm internal diameter (i.d.) PTFE tubing, with tube ends and grippers supplied by Omnifit Ltd. The standard PVC pump tubing was 430 mm long with a 1.14 mm i.d. : coded red-red, supplied by Altec.

Pulse dampers :- The pulse dampers were manufactured in house and they consist of 30 mm long, 10 mm i.d., glass T-pieces with PTFE fittings, the 30 mm long side arm, which are stoppered and allowed to fill with air, they are used to reduce pump pulsation.

Stream switching valve (SSV):- This consists of a Rheodyne 5020 rotary injection valve under the control of an Apple IIe computer for the timed injections and valve switching sequences. The valve switching was achieved by sending pulses from the computer to a Philips 31104 stepper motor, which was connected to the valve by a Huco universal coupling and a 75:1 reduction gear drive from McLennan Servo Supplies. The advantage of using time based injections is that the valve loop volume can be ignored in the calculations made here because the front and rear reaction boundaries of a sample bolus travel the same distance, from the valve to the detection point.

Flow-cells :- The Hellma quartz flow-cells used were of 8 µl, 30 µl and 80 µl volume (reference numbers 178.713-QS, 178.720 and 178.710 respectively) : the optical path length in each case was 10 mm. The design of the flow of solution through the three flow-cells differs (see Figure 2.2.); with the 8 µl flow-cell the solution enters and leaves the cell from the top of its optical path and no recommended flow direction is indicated. The design of both the 30 µl and 80 µl flow-cells are identical to each other, in that the solution enters the cells at the bottom of their optical path and leaves through the top of the optical path: the recommended flow direction is clearly marked.

Reaction coil :- The vast majority of the flow injection work was carried out using a 3 m unfilled coiled reactor of 0.8 mm i.d. tubing coiled around a tube of 0.6 cm o.d.

Single bead string reactor (SBSR) :- 0.8 mm i.d. tubing was dry packed under vacuum with glass balitini (size range 0.490 - 0.700 mm) while vibrating the tubing to pack the balitini: the balitini were supplied by Jencons Ltd. of Nottingham. The initial length of the reactor was 3 m and it was reduced as required, the reactor was coiled to the same degree as that described above.

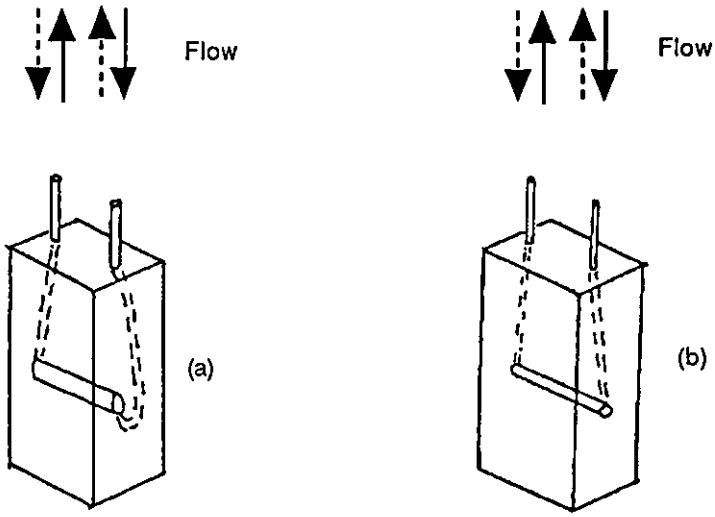

FIGURE 2.2. **Schematic diagram of the flow-cells used in the optical work, (a) 30 μl and 80 μl cells ; (b) 8 μl flow-cell. Solid arrows forward flow, dashed arrows reversed flow.**

2.2.1. Detectors

Both spectrophotometric and electrochemical detection were employed at different stages of this work; for the spectrophotometers the specification of each detector will be given. The electrochemical system will be described in its use with flow injection and for cyclic voltammetry with solid electrodes.

Pye Unicam SP6-250 visible spectrophotometer

This is a single beam instrument of older design that can only measure changes in the visible region of the spectrum. Its source is a tungsten halogen lamp and it covers the wavelength range 325 to 1000 nm.

Pye Unicam SP1750 Ultraviolet/visible spectrophotometer

The ultraviolet/visible (UV/vis) instrument is of a double beam design and it uses two sources to cover the wavelength range 190 to 850 nm. A tungsten filament lamp is used for the visible region of the spectrum while a deuterium arc lamp is employed for the UV region. Selection of the appropriate lamp and filter change is automatic and depends on the wavelength selected. Selection of the bandwidth is under manual control and the monochromator is an Ebert f/10 with a focal length of 254 mm.

The 10 mV output of both of the above spectrophotometers was recorded on a Linseis L650 (Y-t) chart recorder at a chart speed of 2 cm min^{-1}.

Hewlett-Packard HP 8451A Diode-array spectrophotometer

The diode-array is a single beam, microprocessor controlled, UV/vis instrument which operates at high speed. A deuterium lamp is use as the source and a wavelength range of 190 to 820 nm is available at a fixed bandwidth of 2 nm. A full absorbance spectrum can be obtained in 0.1 seconds (s) which can be repeated every 0.7 s. The output of the diode-array was monitored on its in-built cathode ray tube (CRT) and a hard copy of the spectrum was obtained from its in-built printer.

2.2.2. Electrochemical detection

The apparatus used for electrochemical detection with the flow injection manifold and for measurements with solid electrodes under static conditions will be described.

The detector cell

The construction of the cell has been described in detail by *Fogg and Summan*[142]. The cell was constructed in two parts machined from a PTFE rod of 2.5 cm diameter (see Figure 2.3.). The upper body was designed to accept a Metrohm glassy carbon electrode EA 286 which has an o.d. of 7 mm and a 3 mm diameter glassy carbon disk. The eluent inlet block (lower body) was drilled as follows ; the first 1 cm was drilled and threaded (1/4 inch x 28 threads per inch UNF) and flat bottomed to accept a threaded Omnifit tube end and gripper. The next 1 cm was drilled to a diameter of 1 mm and the remaining depth of about 1 mm was drilled to a diameter of 0.35 mm. The depth and width of the X-channel which separates the exit for the eluent into the bulk electrolyte and the glassy carbon working electrode were 0.25 and 2.5 mm respectively.

The detector cell was clamped in a beaker containing the supporting electrolyte so that the gap between the two halves of the cell body were covered by electrolyte and the eluent entered the cell body from below. The three electrode system for electrochemical detection was completed by the addition of a platinum flag counter electrode and a saturated calomel reference electrode. The counter and reference electrodes were placed in the beaker of electrolyte close to the working electrode housed in the PTFE body described above.

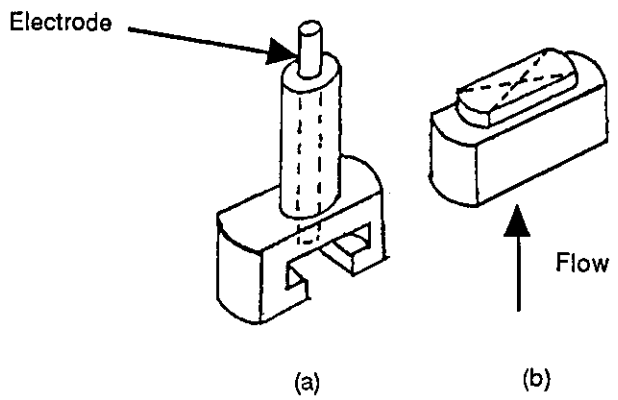

FIGURE 2.3. Schematic diagram of the wall-jet cell. (a) upper body part for holding the working electrode ; (b) lower body part, the solution enters from below and exits via the X-groves shown.

Princeton Applied Research (PAR) Polarographic Analyser Model 174A

The Model 174A was used for all electrochemical measurements with the flow injection manifold and for static cyclic voltammetry with a Metrohm glassy carbon working electrode (EA 286) and a platinum disk working electrode. The platinum electrode was housed in a PTFE body of 7 mm o.d. with a disk diameter of 3 mm. The electrode was of the rotating disk design but it was not used in this manner. The Polarographic Analyser is capable of performing the following modes of analysis:-

- DC polarography
- Sampled DC polarography
- Normal pulse polarography
- Differential pulse polarography
- Various voltammetric modes (linear sweep, pulse techniques)

The Polarographic Analyser was only used in the DC mode and a time constant of 0.3 s was used throughout to filter any spurious signal from the mains. The 1 V output from the Y axis (current) was recorded on the Linseis L650 chart recorder at 2 cm min^{-1} (a Y-t recorder) for the electrochemical signal from the flow injection manifold. A Gould HR2000 X-Y chart recorder or Princeton Applied Research Model RE 0073 X-Y chart recorder were used to record the cyclic voltammograms obtained using the solid electrodes. A 1.5 V full scale deflection (FSD) was obtained on the X axis while the FSD for the Y axis was 1 V as given

above. In all of the electrochemical experiments undertaken the potential and current ranges were varied to obtain an on scale signal and the values will be given in the relevant text or results as appropriate.

2.2.3. Voltammetric Measurements

Adsorptive stripping voltammetry was carried out using either (a) Metrohm VA scanner E612, with a VA detector E611, a 663 VA-stand and a Gould HR2000 X-Y chart recorder, or (b) Metrohm 647 VA stand and 647 VA processor. With both instruments the multimode electrode was used in the hanging mercury drop electrode (HMDE) mode only. The three electrode system was completed by the addition of a glassy carbon auxiliary electrode and a silver/silver chloride (Ag/AgCl) reference electrode immersed in a salt bridge of 3 M potassium chloride.

Cyclic voltammetry was carried out using the first of the two instrumental set ups described above. The pH measurements were made using a Corning combined pH/reference electrode connected to a Radiometer PHM 64 pH meter.

2.3. Reagents

In order to avoid repetition this section lists the reagents used and stock solutions prepared, and any dilution of the stock solutions to prepare working solutions will be given in the relevant text. The chemicals will be listed by manufacturer and purity where known and were used without further purification unless stated otherwise.

Fisons plc, Loughborough, Leics.

AnalaR reagents :- Potassium bromide, Potassium iodide, Potassium iodate, Concentrated Nitric acid, Concentrated Hydrochloric Acid, Sodium sulphite, Disodium ethylenediaminetetraacetic acid, Potassium chloride, Lead acetate, Potassium dihydrogen orthophosphate, Oxalic acid and Sodium hydrogen carbonate.

Reagent grade :- Sodium chloride, Sodium tetraborate, Cobalt carbonate, Potassium oxalate and Sodium hypochlorite solution (8% available chlorine).

BDH Ltd., Poole, Dorset

AnalaR reagents :- Potassium bromate, Sodium hydroxide, Glacial Acetic acid, Potassium hexacyanoferrate(III), Orthoboric acid, Orthophosphoric acid, Sodium acetate and Sodium nitrate.

Aldrich Chemical Co. Ltd., Gillingham, Dorset

SpectrosoL :- 980 mgl^{-1} Nickel standard solution and 10000 mgl^{-1} cobalt standard solution. Thiosemicarbazide (99%) and Salicylaldehyde (98%).

Sigma Chemical Company Ltd., Poole, Dorset

Poly-L-lysine hydrobromide (mw 9800), Diethylenetriaminepentaacetic acid (DTPA).

Absolute alcohol (100%) was supplied by Haymans and the following three reagents were prepared by synthesis as described below;
2-hydroxybenzaldehyde thiosemicarbazone (HBAT), Lead dioxide and Potassium cobalt(III) oxalatetrihydrate.

2.3.1. Synthesised reagents

Preparation of 2-hydroxybenzaldehyde thiosemicarbazone

The compound was prepared by the synthesis method given by *Sah and Daniels*[143]. 0.91 g of thiosemicarbazide was placed in the bottom of a 250 cm^3 round bottomed flask and 30 cm^3 of deionised water and 2 cm^3 of glacial acetic acid were added. The mixture was heated and refluxed for 15 minutes until a clear solution was obtained. 1.22 g of salicylaldehyde dissolved in 25 cm^3 of absolute alcohol was added to the hot thiosemicarbazide solution in the flask and the mixture was then refluxed for between 15 and 30 minutes. A yellow precipitate was obtained and this was filtered through a Whatman n° 1 filter paper under suction. The precipitate was purified by two recrystallisation from a mixture of 60:40 absolute alcohol: deionised water, and the resulting compound was dried at 110 °C under vacuum. (The solid is soluble in a hot mixture of alcohol and water and drops rapidly out of solution when cooled in an ice bath).

Preparation of lead dioxide

This compound was needed for the synthesis of the Co salt given below and the procedure described by *Newell and Maxson*[144] was followed. A solution of 5 g of sodium hydroxide in 45 cm^3 of deionised water and 10 g of lead acetate in 25 cm^3 of deionised water were mixed together. To the resultant white solution 40 cm^3 of Fisons sodium hypochlorite solution (8% available chlorine) was added while being thoroughly stirred and the reddish brown solution was then slowly brought to the boil and boiled for a few minutes. The precipitate was filtered through a Whatmans n° 540 filter paper under suction and washed with deionised water.

The precipitate was then thoroughly mixed with 25 cm^3 of 6 M nitric acid solution and again filtered through a Whatmans n° 540 filter paper under suction and washed five times with deionised water. The solid was then dried at 100 °C under vacuum.

Preparation of potassium cobalt(III) oxalate trihydrate

This compound was prepared using the lead dioxide synthesised as given above following the procedure given by *Bailar and Jones*[145]. To a hot solution of 5.04 g of oxalic acid and 14.74 g of potassium oxalate in 100 cm^3 of deionised water, 4.76 g of cobalt carbonate was added slowly. The solution was allowed to cool to approximately 40 °C and 4.78 g of lead dioxide was added slowly followed by the dropwise addition of 5 cm^3 glacial acetic acid while the solution was vigorously stirred. The solution was stirred for approximately 1 hour and turned a deep green colour. The solution was then filtered under suction through a Whatman n° 542 filter paper.

The Co salt was precipitated from solution by the addition of absolute alcohol and cooling in an ice bath and then filtered under suction through a Whatman n° 542 filter paper. The solid was purified by two recrystallisation steps from absolute alcohol. The final solid was dried under vacuum with a blacked out oven door because the compound is sensitive to heat and light. (The solid was dissolved in water and dropped out of solution on addition of alcohol and cooling; the volume of the aqueous solution should be kept as low as possible to prevent the use of an excessive amount of alcohol).

2.3.2. Stock solutions

- 1 M NaOH solution was prepared by dissolving 0.4 g of solid in deionised water and making up to the mark in a 100 cm^3 plastic volumetric flask.
- 4 M HNO_3 solution was prepared by diluting 63 cm^3 of concentrated acid to 250 cm^3 in a graduated flask with deionised water.
- 0.1 M $KBrO_3$ solution was prepared by dissolving 4.1751 g of solid in approximately 200 cm^3 of deionised water. The pH was adjusted to 11.0 by the dropwise addition of 1 M NaOH solution before it was made up to 250 cm^3 in a graduated volumetric flask with deionised water.
- 0.6 M KBr solution was prepared by dissolving 17.8509 g of solid in approximately 200 cm^3 of deionised water. The pH was adjusted to 11.0 by the dropwise addition of 1 M NaOH solution before it was made up to 250 cm^3 in a graduated volumetric flask with deionised water.
- $1x10^{-3}$ M KIO_3 solution was prepared by dissolving 0.0535 g of solid in approximately 200 cm^3 of deionised water. The pH was adjusted to 11.0 by the dropwise addition of 1 M NaOH solution before it was made up to 250 cm^3 in a graduated volumetric flask with deionised water.
- 2.3% m/v KI solution was prepared by dissolving 5.75 g of solid in approximately 200 cm^3 of deionised water. The pH was adjusted to 11.0 by the dropwise addition of 1 M NaOH solution before it was made up to 250 cm^3 in a graduated volumetric flask with deionised water.
- The pH of the solutions above were adjusted to prevent the premature formation of Br_2 and I_2 when $KBrO_3$ and KBr were mixed together and KIO3 and KI were mixed together respectively.
- 0.1 M EDTA solution was prepared by 7.4448 g of solid in 200 cm^3 of deionised water in a graduated volumetric flask.
- $1x10^{-2}$ M $NaSO_3.7H_2O$ solution was prepared by dissolving 0.2521 g of solid in 10 cm^3 of 0.1 M EDTA before it was made up to 100 cm^3 in a graduated volumetric flask. The EDTA was added to stabilise the sulphite solution.
- 0.1 M KCl solution was prepared by dissolving 1.864 g of solid in 250 cm^3 in a graduated volumetric flask.

- 0.05% m/v HBAT solution was prepared by dissolving 0.05 g of solid in 100 cm^3 of absolute alcohol in a graduated volumetric flask.

2.3.3. Buffer solutions

- 0.2 M sodium acetate buffers were prepared by dissolving 6.804 g of solid in approximately 200 cm^3 of deionised water, the pH was then adjusted to the desired value by the dropwise addition of 1 M NaOH or 50% v/v acetic acid. The pH adjusted solution was then made up to 250 cm^3 in a graduated volumetric flask; acetate buffers used were pH 5.2, 5.4, 5.8 and 6.2.

- Britton-Robinson buffer pH 1.7 was prepared by dissolving 2.50 g of boric acid, 2.70 cm^3 of orthophosphoric acid and 2.30 cm^3 of glacial acetic acid in 500 cm^3 of deionised water in a graduated volumetric flask.

- 0.2 M KH_2PO_4 buffer pH 7.0 was prepared by dissolving 6.8045 g of solid in approximately 200 cm^3 of deionised water the pH was adjusted by the dropwise addition of 1 M NaOH before the solution was made up to 250 cm^3 in a graduated volumetric flask.

- 0.05 M $NaHCO_3$ buffer pH 8.5 was prepared by dissolving 1.0501 g of solid in 250 cm^3 of deionised water in a graduated volumetric flask.

Deionised water of Milli-Q standard (18 MΩ cm^{-1}) was used in throughout.

2.4. General procedures

2.4.1. Flow injection

The following procedure was used with the single-channel manifold when both UV/vis and electrochemical detection were used. A large volume injection of 3 cm^3 was used throughout and this was achieved by means of time based injection. This negated sample loop effects since both the front and rear of the sample bolus travelled the same distance from the injection point to the detector. The computer controlled SSV was sent a signal which caused it to change the flow from the carrier line to the injectate line and a second signal was sent after 90 s to return the flow to the carrier line. Since a flow of 2 cm^3min^{-1} was maintained in both carrier and injectate lines by means of a peristaltic pump, the volume injected was 3 cm^3. The large volume of injectate was then allowed to react with the carrier as it passed down the manifold and the results were monitored at a detector.

The spectrophotometric detectors were all given at least 20 minutes time to stabilise before attempting to record any signals. The wavelength for detection were manually selected on the SP6-250 and SP1750 spectrophotometers and their response were recorded on a Linseis L650 Y-t chart recorder. Data was recorded by the diode-array spectrophotometer after the wavelength, absorbance range and time scale were entered into a microprocessor program. The signals were recorded on the CRT and data points were integrated for 0.1 s repeated every 0.5 s from the start of the run to the end, a hard copy of the results were printed out on the instruments printer. An 8 µl flow-cell was used with the three detectors for most of the signals recorded.

The electrochemical detector was given a 20 minute warm up time and signals were recorded on a Linseis L650 Y-t chart recorder. As part of the initial set up of the instrument a hydrodynamic voltammogram was recorded to decide the best potential for measurement of the analyte. The PAR 174A was used in the DC mode and each potential was manually selected and held (HOLD button depressed) and the current time signal at each potential recorded. The best potential for measurement was then used for the rest of the analyses.

Three replicate readings were obtained at each wavelength used and five replicate readings were obtained at each potential used.

2.4.2. Cyclic voltammetry with solid electrodes

The PAR 174A and the X-Y recorder were switched on and given 20 minutes to stabilise, then a 50 cm^3 aliquot of the analyte dissolved in the buffer was placed in a voltammetric cell and the solution was purged with nitrogen for 10 minutes. The cyclic voltammograms were recorded after allowing the initial current to stabilise for 10 s. The working electrodes (glassy carbon and Pt) were used after polishing with alumina (0.3 µm) and removing any adhering particles with washing and drying on a clean soft tissue. Both electrodes were also used with a coating of poly-L-lysine on the surface.

2.4.3. Adsorptive stripping and cyclic voltammetry at a HMDE

The instruments were allowed 10 minutes to warm up, then a 20 cm^3 aliquot of buffer was placed in a voltammetric cell and the stirrer was switched on and the solution was purged with nitrogen for 10 minutes. After forming a new HMDE, accumulation was effected for the required time while stirring the solution. The maximum drop size were used on both the 663 VA stand and the 647 VA stand

and these were 0.40 mm^2 and 0.60 mm^2 respectively. At the end of the accumulation period the stirrer was switched off and after 10 s delay to allow the solution to become quiescent, a negative potential scan was obtained between the accumulation potential and a final potential of - 1.2 V. Both the accumulation and final potential were varied as the analyte being studied was changed. Differential pulse scans were obtained at 10 mVs^{-1} on both instruments.

Cyclic voltammetry was carried out after applying the accumulation potential or immediately after forming a new HMDE. The scan rate was varied but most voltammograms were obtained at 20 mVs^{-1}.

2.5. Statistical treatment of results

The following procedure was used when recording the results given in the later chapters. Three replicate readings were recorded at each of the two wavelengths used when studying refractive index correction, and five replicate readings were recorded when single wavelength or single potential settings were used. The errors for the replicate readings were calculated as confidence intervals at the 95% confidence level, following the procedure given in *Miller and Miller*[146] using equation (6).

$$\mu = \bar{x} \pm t\left(\frac{s}{\sqrt{n}}\right) \qquad (6)$$

Where μ is the true result, $\bar{x}$ is the mean, t is the quantity used in calculating the confidence limits (given in statistical tables), s is the standard deviation of the sample and n is the sample size. Confidence intervals are calculated at n - 1 degrees of freedom and the value of t at the 95% confidence interval is 4.30 for three replicates and 2.78 for five replicate readings.

CHAPTER 3

DUAL WAVELENGTH REFRACTIVE INDEX COMPENSATION OF UV/VISIBLE SPECTROPHOTOMETRIC SIGNALS OBTAINED USING A SINGLE-CHANNEL MANIFOLD

3.1 Introduction

Absorbance detectors used in both flow injection analysis and liquid chromatography often exhibit an anomalous absorbance signal when a sample is injected into a carrier stream. Ideally the detectors should respond only to substances which absorb the source radiation at a given wavelength. However, an anomalous response occurs due to a change in the refractive index (RI) between the carrier and the injectate solutions and from the RI gradient that results from the injection process (the initial mixing of the two streams). This response can occur even when non-absorbing species are introduced. A change in RI within the flow-cell causes reflection and refraction of the source radiation and this results in a change in the light intensity at the detector. When this response occurs at the measurement wavelength it seriously limits the sensitivity of the technique. This effect has been observed in flow injection[147] and is far more pronounced in a single-line manifold with limited dispersion[19], where there is less mixing than with a dual-line (merging) manifold.

The effect is also more pronounced in systems that rely on the formation of a concentration gradient because an RI gradient is formed at the same time as the concentration gradient. According to *Zagatto et al*[109] the effect is more pronounced at the front and tail portion of a sample zone where both gradients are higher. *Krug et al.*[148] first reported this effect when developing a method for the determination of sulphate using turbidimetric detection. When they removed the cell from the detector and visually observed a sample or blank injection "a mixing boundary (Schlieren pattern) could be seen very clearly".

The changes in RI that occur in flow injection were discussed by *Betteridge et al.*[147] Under the laminar flow conditions that exist in flow injection isolines of different RI acting as liquid lenses are established. Isolines are points of equal RI that occur within a sample bolus when a gradient is established. These liquid lenses will either focus light to the detector or scatter it, as the sample passes through the cell. When the flow-cell was removed from the detector and the passage of the sample was visually observed the image was initially magnified then diminished. This produces a reproducible peak followed by a smaller negative peak as

reported by both *Betteridge*[147] and *Ruzicka*[19]. The heights of both of these peaks are proportional to the concentration injected.

Several workers[109,147-152] have reported RI effects in flow injection analysis. As stated above *Krug et al.* [148]reported the effect when turbidimetrically determining sulphate, while *Betteridge et al.* [147]and later *Fields* [149] report using a light emitting diode and phototransducer as a sensitive detector for refractometry in a flow injection manifold. *Ham* [150]considers the effects of both modifying the design of the flow-cell and the addition of confluence points as a means of reducing the effect of RI on the analytical signal. He states that to improve sensitivity the path length of the flow-cell may be increased but this also increases the contribution of the flow-cell to the dispersion of the manifold.

In later work *Betteridge et al.* [151]compare several detectors including a refractometer for the measurement of viscosity in a high precision flow injection manifold. *Leach et al.* [152]report on RI effects in a manifold using serial differential detectors where both the absorbance peaks and RI response were distinguishable by their peak shapes. *Zagatto et al.* [109]report on the use of dual wavelength spectrophotometry to compensate for the Schlieren effect (RI) in flow injection. Two monochromatic beams were measured simultaneously by two separate detectors and real-time correction of non-specific absorbance was achieved.

RI effects in liquid chromatography (LC) have also been reported by several workers[153-160] and some of their ideas are equally applicable to flow injection. Most of the workers report on the design and contribution of the flow-cell to RI changes in LC. *Little and Fallick* [153] proposed a new design of flow-cell with a tapered bore to overcome the shortfalls of RI effect encountered with the conventional design of flow-cell. On the other hand *Stewart* [154,155] indicates how the optics of the detector may be designed so as to minimise the contribution of RI to the absorbance signal. In a later paper[156] the design of the optics and the effect of RI on temperature jump kinetics and stopped flow LC are reported. *Lyons et al.* [157] discuss the optimisation of flow-cell design for fluorescence detection in LC.

Most of the papers discussed above have dealt with designing the flow-cell to minimise the contribution of RI to the signal. *Synovec* [158] optimises the design of a cylindrical flow-cell using a ray tracing algorithm to improve RI detection of alkylbenzenes in LC, while *Evans et al.* [159,160] adopt a completely different approach. Instead of trying to modify the design of the flow-cell the RI effects are

modelled using a ray tracing algorithm. The first paper[159] deals with the dynamic lens response of a Z-pattern flow-cell to the injection of water-methanol and water-tetrahydrofuran mixtures. The second paper[160] extends the model obtained from the ray tracing algorithm to non-ideal injection methods and gradient elution. They report that their model may be useful in designing future types of flow-cell.

The main exploitation of the RI effect in LC has been with thermal lens calorimetry and concentration gradient sensors. Conventional RI detectors used in LC systems only cover a limited range of RI values and cannot be used with gradient elution. To overcome these shortfalls *Leach and Harris* [161] and other workers[162,163] use the thermal lens effect (perturbation of the light beam) induced by a laser as a method of detecting changes in RI. On the other hand *Pawliszyn* [164,165] uses a concentration gradient sensor which exploits both the concentration gradient and RI gradient that occur when the sample is injected to distort a laser probe beam and detect changes in RI. The method uses a sheath flow cuvette to control peak broadening and a very low detector volume (in the nanolitre range) and was used with both an LC and flow injection system.

Cheng and Dovichi [166] used picolitre probe volumes with their sheath flow cuvette to detect RI changes caused by the injection of dilute methanol samples into a water carrier stream. Finally *Hancock and Synovec* [167] have detected femtomole quantities of polymers with a RI gradient detector coupled to a size-exclusion chromatography instrument. In further work *Lima and Synovec*[168] have shown that dispersion and convection affect the radial concentration profile (and hence the radial RI gradient) of the volume of sample probed by a laser beam in an RI gradient detector. The effects of flow rate and temperature, on the diffusion and convection were evaluated by observing the results obtained from the injection of different molecular mass polyethylene glycol polymers . The workers report that the contribution of diffusion and convection could be separated and assessed independently, and convection was not affected by flow rate because it is a systematic phenomena that is only affected by the design of the flow-cell.

3.2. Preliminary Experiments

3.2.1. Introduction

The shape of the signal obtained from a single-channel manifold in flow injection (FI), has been the subject of a series of studies in this laboratory[68-72,124] The

studies started with the application of both normal and reverse flow injection (rFI) to systems using amperometric detection and conventional injection volumes (< 100 µl)[68,121,124,169]. Later work involved larger volume injections (> 2 cm^3)[69,70,72] in which two reaction boundaries were formed. The boundaries were formed at the extremities of the injected sample bolus, with the dispersions at the boundaries being completely separate from each other. A stream switching valve was used to ensure that both boundaries were formed at the same place and travelled the same distance to the detector, thus eliminating differences in dispersion which would otherwise occur because of this.

In the work of *Fogg et al.*[70] on the on-line formation of bromine, there were six possible combinations of the reagents that could be used. All of the signals that they obtained, except those from one combination (5 in reference[70]), exhibited RI components that resulted in peaks of unequal heights being obtained at the reaction boundaries. *Fogg et al.*[70] adopted the approach of matching the RI of the carrier and injectate streams by making each stream 7% m/v in sodium nitrate. This present work is a continuation of previous studies. In particular a diode-array spectrophotometer has been used in an attempt to compensate for RI effects. The results have been compared with those obtained on a conventional visible spectrophotometer.

3.2.2. Experimental

The single-channel manifold described in chapter 2 was used with an 8 µl flow-cell, a 3 m coiled reactor a Hewlett-Packard HP 8451A diode-array spectrophotometer and a Pye Unicam SP6-250 visible spectrophotometer. The spectrophotometers were use to monitor the RI affected bromine signal at 393 nm and the absorbance signal from the RI component alone at 550 nm, where bromine did not absorb.

Three solution combinations used by *Fogg et al.*[70] for the on-line formation of bromine were chosen for this study. These were combination 1, which exhibited the worst interference in signal shape from the RI component, combination 4 which exhibited negligible interference and combination 5 which was an intermediate case. No attempt was made to match the RI of the carrier and injectate streams. The carrier and injectate solutions were prepared by dilution of the stock solutions (see section 2.3.2. in chapter 2) with the following concentration of bromate, bromide and acid in each solution as appropriate.

- $5x10^{-4}$ M potassium bromate $KBrO_3$

- $3x10^{-2}$ M potassium bromide KBr
- 1 M nitric acid HNO_3

The solution combinations used as carrier and injectate are given below in Table 3.1.

Solution A	Solution B	Combination n° *
H^+, BrO_3^-	H^+, Br^-	(4)
BrO_3^-, Br^-	H^+	(1)
BrO_3^-, Br^-	H^+, Br^-	(5)

TABLE 3.1. Flow injection solution combinations used

*see text above for the relevant information on combination n°.

3.2.3. Results and Discussion

Signal sizes (absorbances and apparent absorbances from RI components) for the three solution combinations studied with solution A as the carrier and solution B as the injectate and vice versa are presented in Tables 3.2. and 3.3. Table 3.2. gives the results obtained with the diode-array spectrophotometer and Table 3.3. gives the results obtained with the visible spectrophotometer.

A comparison of Tables 3.2. and 3.3. suggest that it is more usual to obtain peaks of equal height using compensation of the RI effects with the diode-array spectrophotometer, than with the visible spectrophotometer. The peak heights at both the front and rear reaction boundaries are equal when the absorbance from the RI component at 550 nm is subtracted from the Br_2 signal at 393 nm. This is not the case with the results from the visible spectrophotometer (see Table 3.3.): these results agree with those obtained by *Fogg et al.*[70] on a visible spectrophotometer. The results to date are encouraging but certain other factors such as physical dispersion and flow-cell volume must be investigated before any conclusions can be made.

		Forward Flow					
		Front boundary			Rear boundary		
Carrier	Injectate	h_{max} 393 nm (A)	h_{max} 550 nm (A)	Diff* (A)	h_{max} 393 nm (A)	h_{max} 550 nm (A)	Diff* (A)
H^+, BrO_3^-	H^+, Br^-	0.128	0.003	**0.125** ± 0.0030	0.130	0.003	**0.127** ± 0.0000
H^+, Br^-	H^+, BrO_3^-	0.128	0.003	**0.125** ± 0.0015	0.126	0.003	**0.123** ± 0.0030
BrO_3^-, Br^-	H^+	0.076	0.017	**0.059** ± 0.0000	0.076	0.013	**0.063** ± 0.0042
H^+	BrO_3^-, Br^-	0.072	0.014	**0.058** ± 0.0045	0.113	0.047	**0.066** ± 0.0042
BrO_3^-, Br^-	H^+, Br^-	0.187	0.054	**0.133** ± 0.0030	0.141	0.013	**0.128** ± 0.0042
H^+, Br^-	BrO_3^-, Br^-	0.146	0.013	**0.133** ± 0.0030	0.180	0.046	**0.134** ± 0.0030

* Diff is the RI corrected signal, absorbance 393 nm - absorbance 550 nm. The errors given are the sum of the errors of the two values used to calculate the value given in the Diff column (n = 3).

TABLE 3.2. **Peak heights for the bromine and RI signals, using forward flow through an 8 µl flow-cell in the diode-array spectrophotometer.**

		Forward Flow					
		Front boundary			Rear boundary		
Carrier	Injectate	h_{max} 393 nm (A)	h_{max} 550 nm (A)	Diff* (A)	h_{max} 393 nm (A)	h_{max} 550 nm (A)	Diff* (A)
H^+, BrO_3^-	H^+, Br^-	0.112	0.000	**0.112** ± 0.0030	0.108	0.004	**0.104** ± 0.0027
H^+, Br^-	H^+, BrO_3^-	0.110	0.004	**0.106** ± 0.0030	0.106	0.000	**0.106** ± 0.0015
BrO_3^-, Br^-	H^+	0.060	- 0.016	**0.076** ± 0.0057	0.056	0.040	**0.016** ± 0.0030
H^+	BrO_3^-, Br^-	0.054	0.042	**0.012** ± 0.0057	0.054	- 0.018	**0.072** ± 0.0060
BrO_3^-, Br^-	H^+, Br^-	0.134	- 0.020	**0.154** ± 0.0060	0.140	0.044	**0.096** ± 0.0072
H^+, Br^-	BrO_3^-, Br^-	0.140	0.060	**0.080** ± 0.0057	0.120	- 0.030	**0.150** ± 0.0072

* definition as given with Table 3.2.

TABLE 3.3. Peak heights for the bromine and RI signals, using forward flow through an 8 µl flow-cell in the visible spectrophotometer.

3.3. Effect of flow-cell volume and the direction of flow on the signal obtained in a single-channel manifold

3.3.1. Introduction

The results obtained from the preliminary experiments were encouraging, but other factors needed to be studied and their effect on the signal recorded before any conclusions could be reached. The effect of flow-cell geometry has been studied previously and several workers have proposed new cell designs including improvements in the optical layout of the detector to overcome these effects. Some workers have also modelled the effect of RI in the flow-cell using ray tracing algorithms (see section 3.1. for the relevant information and references).

Several workers[170-173] have investigated the effect of flow-cell volume on dispersion (peak broadening) in LC. *Ishii et al.*[170] and *Tsuda et al.*[171] have prepared micro flow-cells to reduce the contribution of the cell volume to the overall dispersion of the peaks. On the other hand *Yang*[172] comments on the decrease in sensitivity when the cell volume is reduced and *Larkins and Westcott*[173] in addition to studying the effect of flow-cell volume, also consider the influence of flow-cell geometry on peak dispersion.

In FI *Reijn et al.*[174] has investigated the effect of both the type of detector used and the injection process on dispersion of the analytical peak, while *Poppe*[175] reports on the effects of cell volume on peak dispersion and on its influence on the sensitivity of detection (sensitivity decreases with decreasing cell volume). The influence of cell volume on dispersion of the analytical peak has also been reported by *Stone and Tyson*[176,177].

Here effects of cell volume and the direction of flow through the cell have been studied and the effectiveness of using a diode-array spectrophotometer in compensating for the RI component of the signal has again been evaluated. The results obtained were compared with those obtained using a conventional visible spectrophotometer.

3.3.1. Experimental

The experimental procedure given 3.2.2. was followed, but additionally three different flow-cells of 8 µl, 30 µl and 80 µl volumes were used with two flow directions, forward and reversed flow. The design of the three flow-cells were given in section 2.2. (chapter 2), with the design of the 8 µl flow-cell being

different from both the 30 µl and 80 µl flow-cells. Additionally there was no flow direction arrow on the 8 µl flow-cell, but the recommended flow direction was clearly marked on the other two cells. When the solutions were pumped through the cells in the recommended direction, we have adopted the term *forward flow* and conversely flow against the recommended direction has been termed *reversed flow*.

Since the flow direction is not indicated on the 8 µl flow-cell, forward flow was when the solutions were pumped in through the cell at the face marked QS 1.000 and reversed flow was in the opposite direction. (This mark was present on all three cells and was the face where the direction arrow was placed on the lager volume cells). The face marked QS 1.000 was placed furthest away from the light source in both spectrophotometers during all of the measurements undertaken.

In addition to the three solutions listed in Table 3.1. physical dispersion measurements were recorded by injecting a solution of preformed bromine (all three reagent mixed together in the same concentration as those used for on–line bromine formation) into a carrier stream of deionised water. The signals obtained for the bromine formed on-line, its RI component and the physical dispersion measurements on both spectrophotometers are given in the following Tables and Figures.

3.3.3. Results and discussion

Signals obtained from the three solution combinations studied with solution A as the carrier and solution B as the injectate and vice versa, for the 8 µl flow-cell with reversed flow are given in Tables 3.4. and 3.5., for the diode-array and visible spectrophotometers respectively. It can be seen that as with the earlier results for forward flow (Tables 3.2. and 3.3.), obtaining peaks of equal height at each reaction boundary is possible, when using the diode-array spectrophotometer. Manual correction of absorbances was employed with both spectrophotometers (subtraction of the absorbance due to RI at 550 nm) and for one solution combination only peaks of equal height were obtained at both boundaries when using the visible spectrophotometer. This was the solution combination that had acid in both carrier and injectate and consistently gave the lowest apparent absorbance values at the wavelength used to measure the RI component.

The physical dispersion of the sample bolus was measured for both flow directions using preformed bromine and the results for all three sizes of flow-cell

are given in Table 3.6. and 3.7. for the diode-array and visible spectrophotometers respectively. Figures 3.1. and 3.2. show the signals obtained on the diode-array spectrophotometer for the 8 µl flow-cell, for both flow directions. With the results in Table 3.6., these show that no major difference in the sample bolus dispersion is obtained on altering the direction of flow. The results in Table 3.7. show a similar outcome when the visible spectrophotometer is used. Thus differences in the peak shapes when the flow direction is altered cannot be explained in terms of differences in physical dispersion.

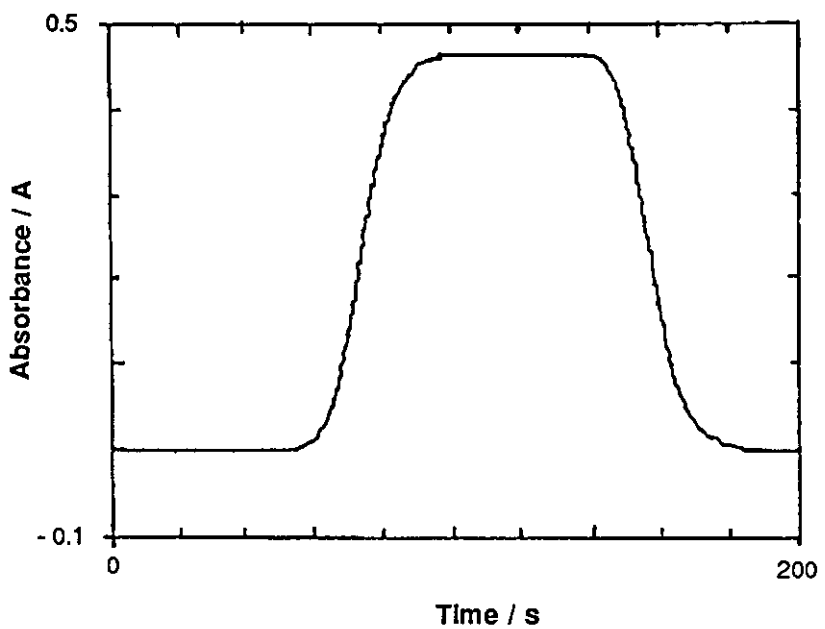

FIGURE 3.1. **Signal obtained at 393 nm using the diode-array spectrophotometer from the injection of a preformed bromine solution, using forward flow through an 8 µl flow-cell. Carrier deionised water; injectate 1 M H^+ and $5x10^{-4}$ M BrO_3^- and 0.03 M Br^-.**

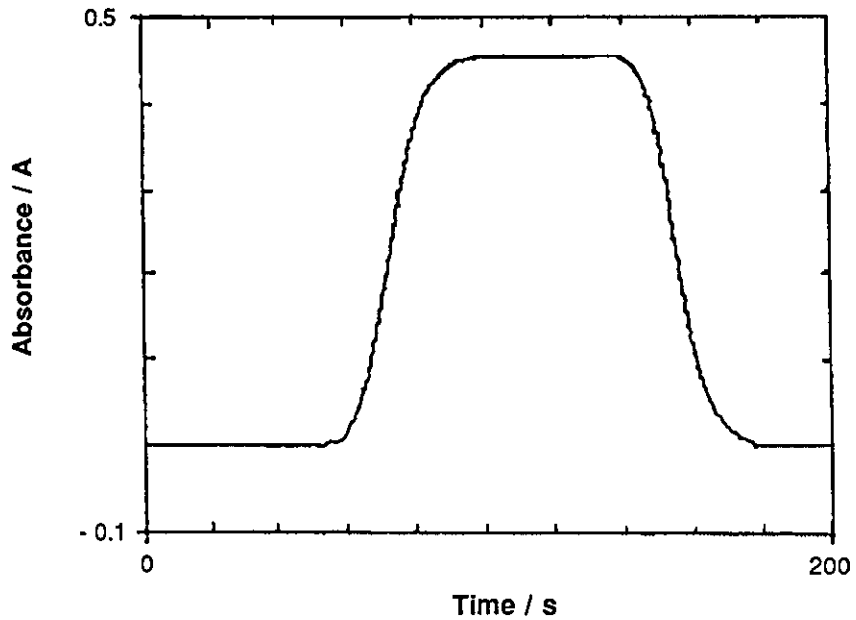

FIGURE 3.2. **Signal obtained at 393 nm using the diode-array spectrophotometer from the injection of a preformed bromine solution, using reverse flow through an 8 µl flow-cell. Carrier deionised water; injectate 1 M H^+ and $5x10^{-4}$ M BrO_3^- and 0.03 M Br^-.**

With the two larger volume flow-cells used the flow direction was clearly marked: physical dispersion measurements were recorded for the recommended flow direction (forward) and signals were also obtained for the reversed flow direction. The results in Tables 3.6. and 3.7. show that when the flow direction is reversed through the 80 µl flow-cell, the pattern of flow becomes highly disrupted. With the 30 µl flow-cell the disruption of the flow pattern seems to be negligible with reversed flow.

Figures 3.3 to 3.6. show the signals that were obtained on the diode-array spectrophotometer. These illustrate the flow patterns more clearly. An increase in washout time for the 80 µl flow-cell using the forward flow direction is seen by the amount of "tailing" present (see figure 3.5.). The present results on dispersion in different volume flow-cells agree with the earlier work of *Stone and Tyson*[176,177]. They concluded that there was no significant difference in the signal shapes obtained when the flow-cell volume was changed from 8 µl to 25 µl. When the flow-cell volume is altered to 80 µl differences in physical dispersion become apparent and the results of this study are again in agreement with those of *Stone and Tyson* [176,177] on this point. Our results also concur with other workers[170,171,173,175] as the volume of the flow-cell is increased then the contribution it makes to the dispersion of the peak increases.

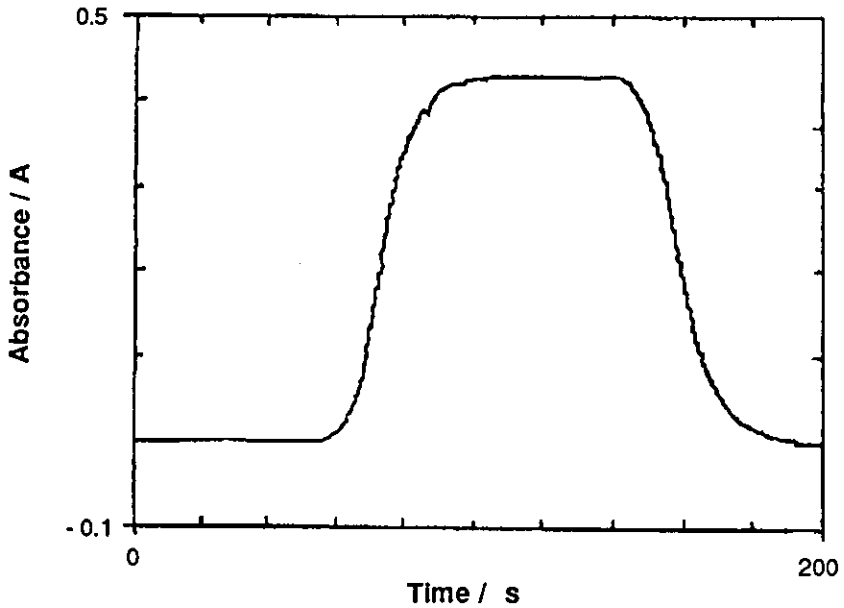

FIGURE 3.3. Signal obtained at 393 nm using the diode-array spectrophotometer from the injection of a preformed bromine solution, using forward flow through a 30 µl flow-cell. Carrier deionised water; injectate 1 M H^+ and $5x10^{-4}$ M BrO_3^- and 0.03 M Br^-.

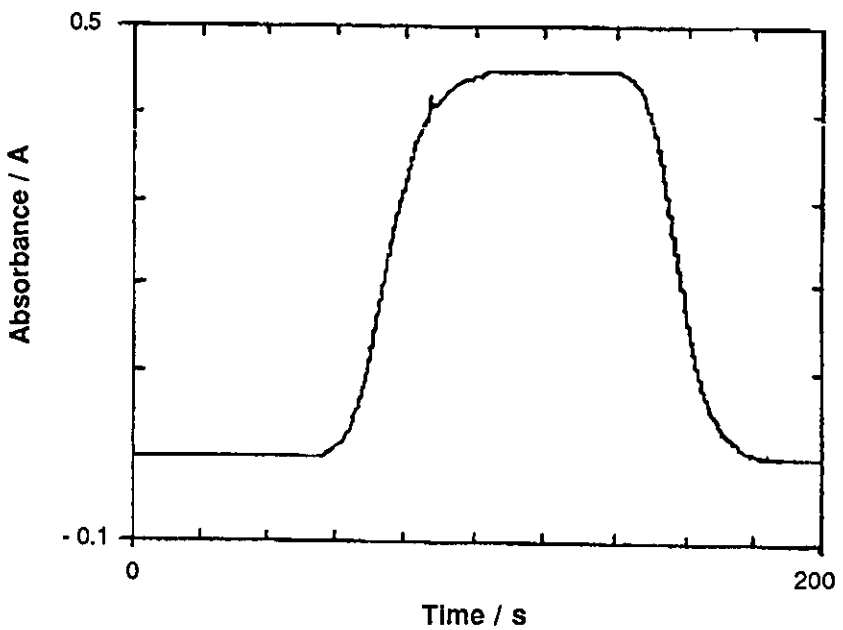

FIGURE 3.4. Signal obtained at 393 nm using the diode-array spectrophotometer from the injection of a preformed bromine solution, using reverse flow through a 30 µl flow-cell. Carrier deionised water; injectate 1 M H^+ and $5x10^{-4}$ M BrO_3^- and 0.03 M Br^-.

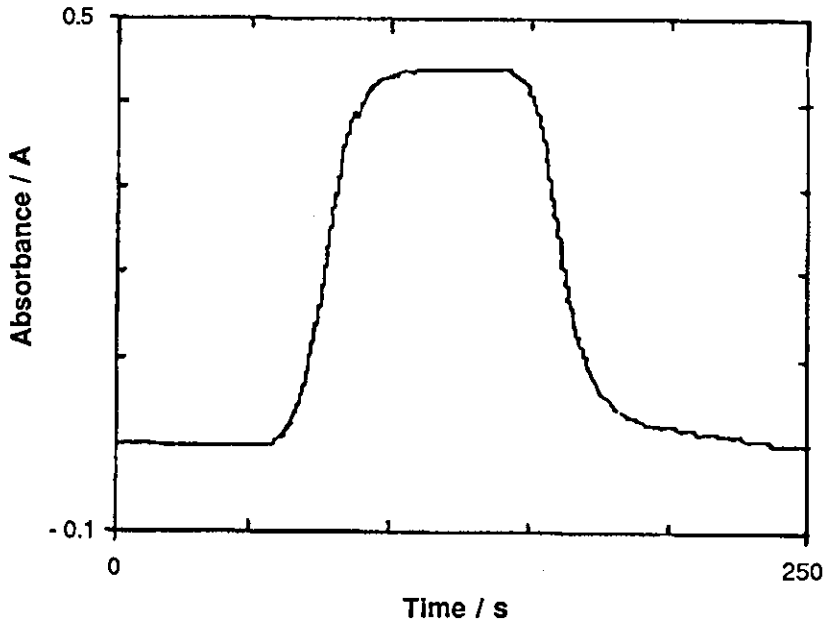

FIGURE 3.5. **Signal obtained at 393 nm using the diode-array spectrophotometer from the injection of a preformed bromine solution, using forward flow through an 80 µl flow-cell. Carrier deionised water; injectate 1 M H^+ and $5x10^{-4}$ M BrO_3^- and 0.03 M Br^-.**

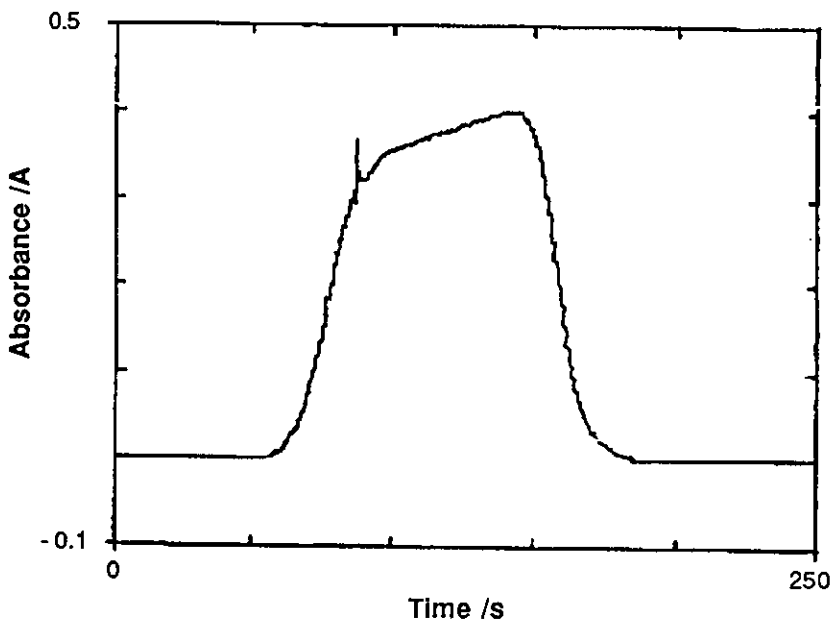

FIGURE 3.6. **Signals obtained at 393 nm using the diode-array spectrophotometer from the injection of a preformed bromine solution, using reverse flow through an 80 µl flow-cell. Carrier deionised water; injectate 1 M H^+ and $5x10^{-4}$ M BrO_3^- and 0.03 M Br^-.**

The three solution combinations studied using the 8 µl flow-cell were again studied using the larger volume flow-cells. Results are reported with forward and reversed flow for the 30 µl flow-cell, but numerical results for the 80 µl flow-cell are given for forward flow alone. Figures 3.7. and 3.8. show the distortion of the peak shape on using reversed flow through the 80 µl flow-cell: the rear peak becomes superimposed on the "tail" of the front peak, when solution A is the carrier and solution B the injectate (third solution pair in Table 3.1.). When the roles of carrier and injectate are reversed, the "tailing" is seen as a second flatter peak at the rear reaction boundary. With this type of signal there is no possibility of correcting for RI effects, because flow pattern distortions must also be accounted for. The results for the three solution combinations studied using the two larger volume flow-cells are given in Tables 3.8., 3.10. and 3.11. for the diode-array, and in Tables 3.9., 3.12. and 3.13. for the visible spectrophotometer respectively.

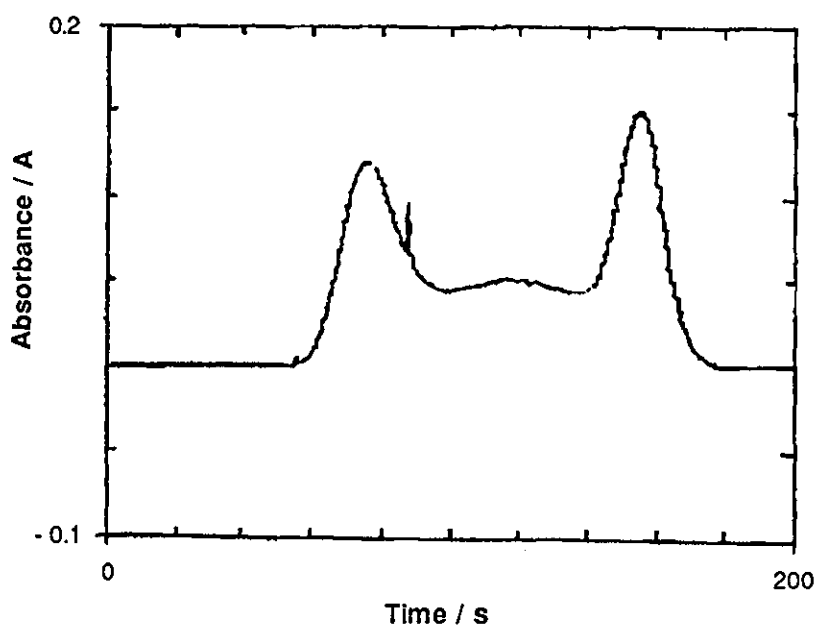

FIGURE 3.7. **Signal obtained at 393 nm using the diode-array spectrophotometer from the on-line formation of bromine, using reverse flow through an 80 µl flow-cell. Carrier $5x10^{-4}$ M BrO_3^- and 0.03 M Br^-; Injectate 1 M H^+ and 0.03 M Br^-.**

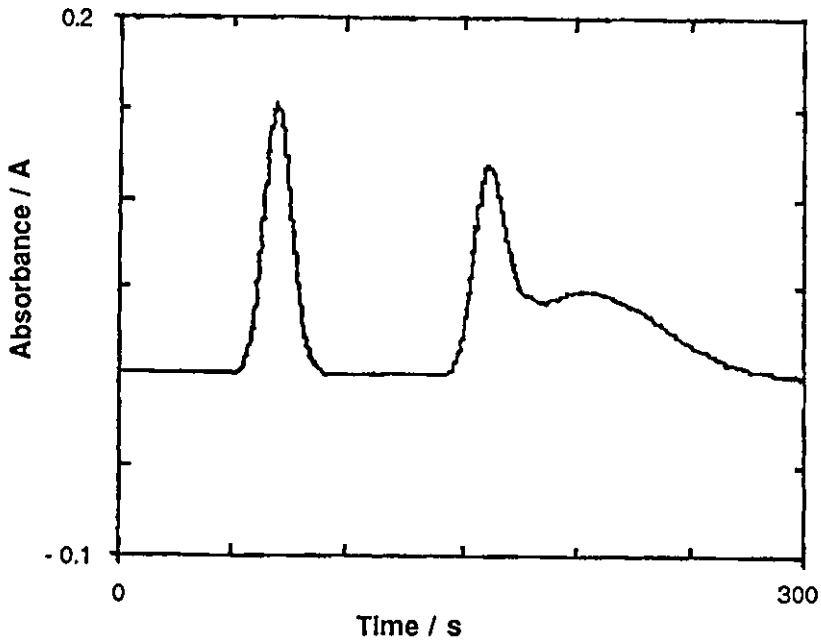

FIGURE 3.8. **Signal obtained at 393 nm using the diode-array spectrophotometer from the on-line formation of bromine, using reverse flow through an 80 µl flow-cell. Carrier 1 M H^+ and 0.03 M Br^-; injectate $5x10^{-4}$ M BrO_3^- and 0.03 M Br^-.**

The results for the 80 µl flow-cell (Tables 3.8. and 3.9.) again demonstrate that it is easier to compensate for RI effects to obtain peaks of equal height using the diode-array than with the visible spectrophotometer. Some double peaks, however, were obtained and these occurred within the peak width of the bromine signal (compare Figure 3.9. with 3.10.). The value that appears in the Diff column (absorbance at 393 nm - absorbance at 550 nm) was corrected for RI only if the signal at 550 nm had at the same peak maximum time (t_p) as the bromine signal. If the RI signal occurred before or after the bromine signal then its value was not deducted from the bromine signal, because a value of 0.000 A was obtained in the RI signal at the same temporal position as the bromine h_{max}. This is shown in Figure 3.9.: the valley between the two RI peaks is at 0.000 A, but in this instance one of RI peaks occurs at the same t_p value as the bromine h_{max}.

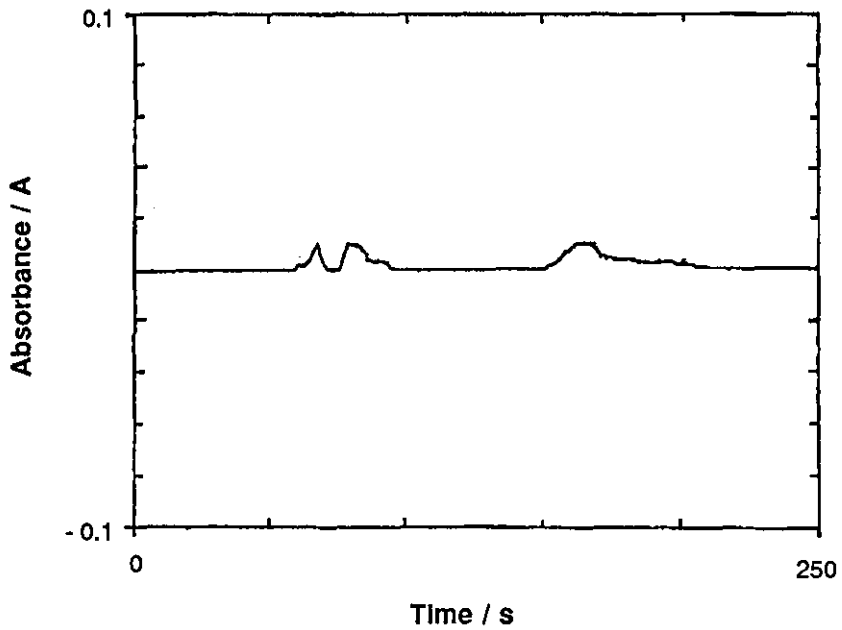

FIGURE 3.9. Signals obtained at 550 nm (RI component) using the diode-array spectrophotometer from the on-line formation of bromine, using forward flow through an 80 µl flow-cell. Carrier $5x10^{-4}$ M BrO_3^- and 0.03 M Br^-; injectate 1 M H^+.

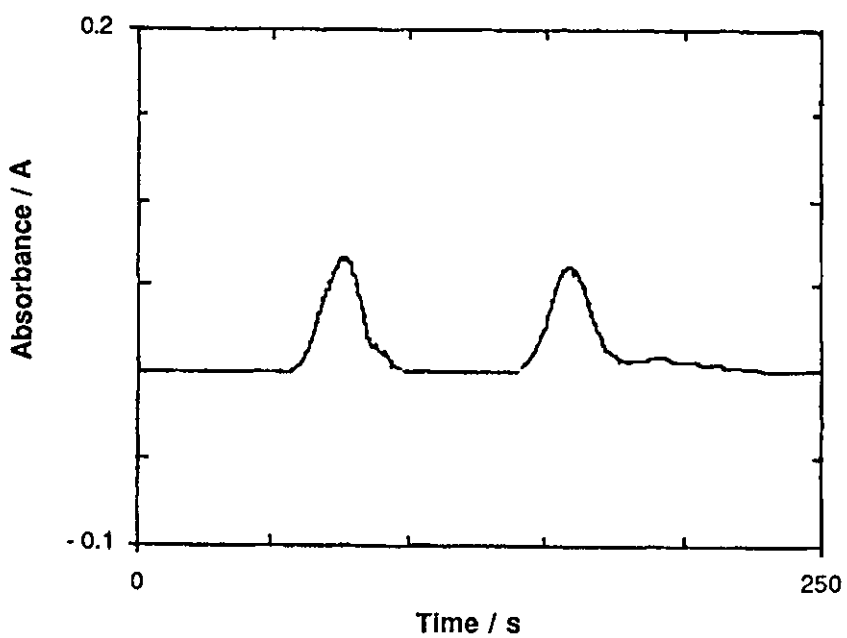

FIGURE 3.10. Signals obtained at 393 nm using the diode-array spectrophotometer from the on-line formation of bromine, using forward flow through an 80 µl flow-cell. Carrier $5x10^{-4}$ M BrO_3^- and 0.03 M Br^-; injectate 1 M H^+.

The results obtained with the 30 µl flow-cell indicate that here again it is possible to compensate for RI effects to obtain peaks of equal height for either flow direction, when a diode-array spectrophotometer is used. In most cases the height of the peaks at each boundary are equal, when the RI component is subtracted (see Tables 3.10. and 3.11.). The results in Table 3.10. are the first indication that significant negative RI peaks can be obtained using the diode-array spectrophotometer. They again occur within the peak width of the bromine signal and have only been subtracted from the bromine signal when they occur at the same temporal position as the bromine h_{max}. Their positions are reversed when the roles of carrier and injectate reversed (see Tables 3.10. and 3.11.).

		Reversed Flow					
		Front boundary			Rear boundary		
Carrier	Injectate	h_{max} 393 nm (A)	h_{max} 550 nm (A)	Diff* (A)	h_{max} 393 nm (A)	h_{max} 550 nm (A)	Diff* (A)
H^+, BrO_3^-	H^+, Br^-	0.126	0.004	**0.122** ± 0.0030	0.126	0.004	**0.122** ± 0.0015
H^+, Br^-	H^+, BrO_3^-	0.126	0.003	**0.123** ± 0.0000	0.126	0.004	**0.122** ± 0.0015
BrO_3^-, Br^-	H^+	0.076	0.014	**0.062** ± 0.0030	0.063	- 0.003	**0.066** ± 0.0045
H^+	BrO_3^-, Br^-	0.063	- 0.003	**0.066** ± 0.0000	0.080	0.016	**0.064** ± 0.0060
BrO_3^-, Br^-	H^+, Br^-	0.146	0.016	**0.130** ± 0.0045	0.129	-0.004	**0.133** ± 0.0042
H^+, Br^-	BrO_3^-, Br^-	0.128	- 0.003	**0.132** ± 0.0057	0.150	0.020	**0.130** ± 0.0030

* for definition see Table 3.2.

TABLE 3.4. Peak heights for the bromine and RI signals, using reversed flow through an 8 µl flow-cell in the diode-array spectrophotometer.

Negative RI peaks were much more commonly obtained when the visible spectrophotometer was used, with all volume of flow-cells studied. The results in Table 3.12. for the visible spectrophotometer, seem to indicate that in certain instances RI correction is possible for the signal obtained with forward flow through the 30 µl flow-cell. In Table 3.13.: however, results indicate that peaks of equal height are not obtained even after correcting for RI effects. The results for the different volume flow-cells with both flow directions indicate that for successful RI correction the diode-array is the detector that should be used.

		Reversed Flow					
		Front boundary			Rear boundary		
Carrier	Injectate	h_{max} 393 nm (A)	h_{max} 550 nm (A)	Diff* (A)	h_{max} 393 nm (A)	h_{max} 550 nm (A)	Diff* (A)
H^+, BrO_3^-	H^+, Br^-	0.112	0.002	**0.110** ± 0.0057	0.116	0.004	**0.112** ± 0.0042
H^+, Br^-	H^+, BrO_3^-	0.120	0.004	**0.116** ± 0.0030	0.116	0.002	**0.114** ± 0.0057
BrO_3^-, Br^-	H^+	0.022	-0.024	**0.046** ± 0.0000	0.056	0.034	**0.022** ± 0.0057
H^+	BrO_3^-, Br^-	0.052	0.034	**0.018** ± 0.0060	0.020	- 0.024	**0.044** ± 0.0042
BrO_3^-, Br^-	H^+, Br^-	0.133	- 0.031	**0.164** ± 0.0072	0.197	0.049	**0.148** ± 0.0060
H^+, Br^-	BrO_3^-, Br^-	0.161	0.051	**0.110** ± 0.0087	0.125	- 0.034	**0.159** ± 0.0077

* for definition see Table 3.2.

TABLE 3.5. Peak height for the bromine and RI signals, with reversed flow through an 8 µl flow-cell in the visible spectrophotometer.

Cell Volume (µl)	Flow Direction	*t_a (s)	*t_w (s)	* Δt (s)	*Absorbance maximum (A)
8	Forward	55 ± 1.5	181 ± 0.0	126 ± 1.5	0.452 ± 0.0057
8	Reversed	56 ± 0.0	177 ± 1.5	121 ± 1.5	0.447 ± 0.0072
30	Forward	57 ± 0.0	191 ± 1.5	134 ± 1.5	0.446 ± 0.0099
30	Reversed	57 ± 0.0	180 ± 1.5	123 ± 1.5	0.449 ± 0.0114
80	Forward	60 ± 1.5	243 ± 0.0	183 ± 1.5	0.453 ± 0.0072
80	Reversed	59 ± 0.0	189 ± 3.0	130 ± 3.0	** 0.388 ±0.0114

* t_a and t_w are the peak appearance and washout times respectively, Δt is the peak width (t_a - t_w) and the absorbance maximum is the steady state signal, (n = 3).

** no plateau was obtained, this is the maximum reading (see Figure 3.6.)

TABLE 3.6. Physical dispersion in the flow-cells with forward and reversed flow using the diode-array spectrophotometer.

Cell Volume (µl)	Flow Direction	*t_a (s)	*t_w (s)	* Δt (s)	*Absorbance maximum (A)
8	Forward	51 ± 0.0	184 ± 3.0	133 ± 3.0	0.455 ± 0.0114
8	Reversed	51 ± 0.0	187 ± 3.0	136 ± 3.0	0.458 ± 0.0228
30	Forward	51 ± 0.0	203 ± 3.0	152 ± 3.0	0.452 ± 0.0228
30	Reversed	51 ± 0.0	193 ± 4.2	142 ± 4.2	0.454 ± 0.0256
80	Forward	52 ± 0.0	252 ± 4.2	200 ± 4.2	0.457 ± 0.0228
80	Reversed	53 ± 3.0	199 ± 4.2	146 ± 7.2	0.422 ± 0.0256

* for definitions see Table 3.6. above.

TABLE 3.7. Physical dispersion in the flow-cells with forward and reversed flow using the visible spectrophotometer.

		Forward Flow					
		Front boundary			Rear boundary		
Carrier	Injectate	h_{max} 393 nm (A)	h_{max} 550 nm (A)	Diff* (A)	h_{max} 393 nm (A)	h_{max} 550 nm (A)	Diff* (A)
H^+, BrO_3^-	H^+, Br^-	0.139	0.004	**0.135** ± 0.0030	0.135	0.004	**0.131** ± 0.0030
H^+, Br^-	H^+, BrO_3^-	0.143	0.006	**0.137** ± 0.0030	0.139	0.004	**0.135** ± 0.0030
BrO_3^-, Br^-	H^+	0.065	° 0.009 ° 0.010	**0.065** ± 0.0045	0.061	0.009	**0.061** ± 0.0030
H^+	BrO_3^-, Br^-	0.070	° 0.009 ° 0.011	**0.061** ± 0.0057	0.074	° 0.009 ° 0.010	**0.064** ± 0.0045
BrO_3^-, Br^-	H^+, Br^-	0.161	° 0.009 ° 0.009	**0.152** ± 0.0042	0.158	0.013	**0.145** ± 0.0057
H^+, Br^-	BrO_3^-, Br^-	0.157	° 0.013 ° 0.013	**0.144** ± 0.0060	0.177	0.026	**0.150** ± 0.0077

* definition as given with Table 3.2.

° this indicates that a double peak was obtained (see text for details).

TABLE 3.8. Peak heights for the bromine and RI signals, with forward flow through an 80 µl flow-cell in the diode-array spectrophotometer.

		Forward Flow					
		Front boundary			Rear boundary		
Carrier	Injectate	h_{max} 393 nm (A)	h_{max} 550 nm (A)	Diff* (A)	h_{max} 393 nm (A)	h_{max} 550 nm (A)	Diff* (A)
H^+, BrO_3^-	H^+, Br^-	0.117	0.003	**0.114** ± 0.0106	0.120	0.003	**0.117** ± 0.0080
H^+, Br^-	H^+, BrO_3^-	0.121	0.002	**0.119** ± 0.0030	0.125	0.002	**0.123** ± 0.0030
BrO_3^-, Br^-	H^+	0.074	- 0.010	**0.084** ± 0.0000	0.072	0.005	**0.067** ± 0.0030
H^+	BrO_3^-, Br^-	0.073 ° 0.022	0.006 ° 0.002	**0.067** ± 0.0030	0.080	- 0.012	**0.092** ± 0.0000
BrO_3^-, Br^-	H^+, Br^-	0.136	- 0.009	**0.145** ± 0.0080	0.125	0.006	**0.119** ± 0.0030
H^+, Br^-	BrO_3^-, Br^-	0.133 ° 0.023	0.006 ° 0.002	**0.127** ± 0.0030	0.151	- 0.010	**0.161** ± 0.0030

* definition as given with Table 3.2.

° A slight "tail" was observed on the bromine peak and this was mimicked by the RI peak, the value shown in the maximum value of the "tail".

TABLE 3.9. Peak heights for the bromine and RI signals, with forward flow through an 80 µl flow-cell in the visible spectrophotometer.

		Forward Flow					
		Front boundary			Rear boundary		
Carrier	Injectate	h_{max} 393 nm (A)	h_{max} 550 nm (A)	Diff* (A)	h_{max} 393 nm (A)	h_{max} 550 nm (A)	Diff* (A)
H^+, BrO_3^-	H^+, Br^-	0.140	0.003	**0.137** ± 0.0030	0.140	0.004	**0.136** ± 0.0030
H^+, Br^-	H^+, BrO_3^-	0.143	0.004	**0.139** ± 0.0030	0.143	0.003	**0.140** ± 0.0015
BrO_3^-, Br^-	H^+	0.074	- 0.010° - 0.006°	**0.074** ± 0.0045	0.078	0.007	**0.071** ± 0.0057
H^+	BrO_3^-, Br^-	0.089	0.019	**0.080** ± 0.0030	0.076	- 0.011° - 0.006°	**0.076** ± 0.0042
BrO_3^-, Br^-	H^+, Br^-	0.174	0.023	**0.151** ± 0.0060	0.157	0.008	**0.149** ± 0.0071
H^+, Br^-	BrO_3^-, Br^-	0.150	0.009	**0.141** ± 0.0045	0.143	- 0.010° - 0.006°	**0.143** ± 0.0030

* definition as given in Table 3.2.

°This indicates that a double peak was obtained (see text for details).

TABLE 3.10. Peak heights for the bromine and RI signals, with forward flow through a 30 µl flow-cell in the diode-array spectrophotometer.

		Reversed Flow					
		Front boundary			Rear boundary		
Carrier	Injectate	h_{max} 393 nm (A)	h_{max} 550 nm (A)	Diff* (A)	h_{max} 393 nm (A)	h_{max} 550 nm (A)	Diff* (A)
H^+, BrO_3^-	H^+, Br^-	0.126	0.003	**0.123** ± 0.0030	0.123	0.004	**0.119** ± 0.0030
H^+, Br^-	H^+, BrO_3^-	0.130	0.004	**0.126** ± 0.0030	0.126	0.003	**0.123** ± 0.0015
BrO_3^-, Br^-	H^+	0.074	0.011	**0.063** ± 0.0030	0.061	0.000	**0.061** ± 0.0060
H^+	BrO_3^-, Br^-	0.063	0.000	**0.063** ± 0.0045	0.072	0.010	**0.062** ± 0.0057
BrO_3^-, Br^-	H^+, Br^-	0.128	0.006	**0.122** ± 0.0045	0.124	0.005	**0.119** ± 0.0060
H^+, Br^-	BrO_3^-, Br^-	0.138	0.010	**0.128** ± 0.0060	0.130	0.006	**0.124** ±0.0057

* definition as given in Table 3.2.

TABLE 3.11. **Peak heights for the bromine and RI signals, with reversed flow through a 30 µl flow-cell in the diode-array spectrophotometer.**

		Forward Flow					
		Front boundary			Rear boundary		
Carrier	Injectate	h_{max} 393 nm (A)	h_{max} 550 nm (A)	Diff* (A)	h_{max} 393 nm (A)	h_{max} 550 nm (A)	Diff* (A)
H^+, BrO_3^-	H^+, Br^-	0.126	0.003	**0.123** ± 0.0080	0.129	0.004	**0.125** ± 0.0027
H^+, Br^-	H^+, BrO_3^-	0.130	0.004	**0.126** ± 0.0000	0.132	0.003	**0.129** ± 0.0030
BrO_3^-, Br^-	H^+	0.052	- 0.010	**0.062** ± 0.0000	0.083	0.011	**0.072** ± 0.0060
H^+	BrO_3^-, Br^-	0.081	0.014	0.067 ± 0.0030	0.055	- 0.012	**0.067** ± 0.0030
BrO_3^-, Br^-	H^+, Br^-	0.124	- 0.011	**0.135** ± 0.0030	0.154	0.015	**0.139** ± 0.0030
H^+, Br^-	BrO_3^-, Br^-	0.145	0.019	**0.126** ± 0.0060	0.124	- 0.015	**0.139** ± 0.0057

* definition as given in Table 3.2.

TABLE 3.12. **Peak heights for the bromine and RI signals, with forward flow through a 30 µl flow-cell in the visible spectrophotometer.**

		Reversed Flow					
		Front boundary			Rear boundary		
Carrier	Injectate	h_{max} 393 nm (A)	h_{max} 550 nm (A)	Diff* (A)	h_{max} 393 nm (A)	h_{max} 550 nm (A)	Diff* (A)
H^+, BrO_3^-	H^+, Br^-	0.117	0.000	**0.117** ± 0.0077	0.125	0.006	**0.119** ± 0.0057
H^+, Br^-	H^+, BrO_3^-	0.129	0.005	**0.124** ± 0.0060	0.129	0.003	**0.126** ± 0.0030
BrO_3^-, Br^-	H^+	0.052	- 0.022	**0.074** ± 0.0000	0.105	0.081	**0.024** ± 0.0060
H^+	BrO_3^-, Br^-	0.104	0.079	**0.025** ± 0.0077	0.057	- 0.022	**0.079** ± 0.0030
BrO_3^-, Br^-	H^+, Br^-	0.124	- 0.022	**0.146** ± 0.0000	0.176	0.086	**0.090** ± 0.0000
H^+, Br^-	BrO_3^-, Br^-	0.169	0.087	**0.082** ± 0.0087	0.125	- 0.022	**0.147** ± 0.0057

* definition as given in Table 3.2.

TABLE 3.13. Peak heights for the bromine and RI signals, with reversed flow through a 30 µl flow-cell in the visible spectrophotometer.

The ability to compensate effectively for the absorbance due to the RI effect, to obtain signals of equal height at each boundary is clearly easier with the diode-array spectrophotometer. *Zagatto et al.*[109] recently reported that a diode-array spectrophotometer was used to compensate for RI effects (Schlieren effects). They injected various samples (such as sucrose) with RI's differing greatly from the carrier stream (bromocresol green) and were successful in compensating for non-specific absorbances associated with the RI effect on the signal. They also concluded that a diode-array would not be necessary for the compensation. Instead they suggest the use of a modified spectrophotometer with two detectors set at different wavelengths. Our results (so far) with the visible spectrophotometer indicate that the second approach suggested by *Zagatto et al.*[109] would not be successful. But their experimental manifold would need to be evaluated to ensure that this is the case.

It has been shown that there are advantages in using a diode-array in comparison with both conventional visible and UV/vis spectrophotometers[178,179]. The diode-array does not suffer from a movement of its absorption bands, because the whole spectrum is captured at once on a linear array of photodiodes after dispersion by a prism, and not by a stepper motor driven grating which brings each individual wavelength to bear on the detector in turn in a visible and UV/vis spectrophotometer. This leads to an improvement in spectrum reproducibility, but the precision is dependant on the response of the individual diode to each wavelength[179].

The explanation for the improvement in the ability to compensate for RI effects with a diode-array spectrophotometer may lie with a difference in optical layouts between the two spectrophotometers. Alternatively it may have to do with different photomultiplier tube sensitivities between the two instruments: some further experimental work will be needed before any conclusions can be reached.

The signals obtained in this study, for all three flow-cell sizes studied, exhibit the same behaviour that was noted by *Fogg et al.*[70] When the roles of carrier and injectate are reversed, the position of the front and rear boundary peaks are also reversed. This was equally true for the bromine and RI signals. When the RI of the two solutions were relatively closely matched, as was the case when acid was present in both reagents, the cell volume had relatively little effect on the shape of the signal obtained. Indeed no significant "tailing" from increased washout time was observed for this combination of reagents, when an 80 µl flow-cell was used.

3.4. Variation of the bandwidth and its influence on RI correction of signals obtained in single boundary measurements

3.4.1. Introduction

It was observed in the work described in the preceding section on RI correction in flow injection, that when a visible spectrophotometer of conventional design was used, peaks of equal height at each reaction boundary were not obtained. But when the detector was changed to a diode-array spectrophotometer peaks of equal height were obtained at each reaction boundary after correcting for the absorbance from the RI component of the signal. The improvement in response or more specifically, the ability to correct for RI effects on the signal, may be due to differences in the optical layout of the two instruments. In order to evaluate differences in instrumental parameters between the spectrophotometers a third detector was used in the extension of this study. The instrument is a UV/vis spectrophotometer of older design operated in the double beam mode; it is possible with this instrument to vary the bandwidth and thereby observe its influence on the signals obtained and on RI correction.

3.4.2. Experimental

The experimental procedure given 3.2.2. was followed, again using the manifold described. The detector was changed to a Pye Unicam SP1750 UV/vis spectrophotometer fitted with an 8 µl flow-cell used with forward flow. The three solution combinations given in Table 3.1. were again used but in this instance the roles of the carrier and injectate streams were not reversed. The bandwidth of the spectrophotometer was varied from 0.1 nm to 3.0 nm and three replicate signals were recorded at both 393 nm and 550 nm. The results are given in the following Tables.

3.4.3. Results and discussions

The minimum bandwidth that gave a sufficiently steady response at the detector was 0.5 nm: at 0.1 nm the energy reaching the detector from the lamp was too low (an off-scale reading was obtained). When the bandwidth was increased to 0.2 nm the energy throughput improved but a very noisy baseline was obtained making interpretation of the resulting signals difficult. As stated in the experimental section the three solution combinations given in Table 3.1. were used but no additional information would be gained by reversing the roles of carrier and injectate streams.

	Front boundary			Rear boundary		
Bandwidth (nm)	h_{max} 393 nm (A)	h_{max} 550 nm (A)	Diff* (A)	h_{max} 393 nm (A)	h_{max} 550 nm (A)	Diff* (A)
0.5	0.072	0.029	**0.043** ± 0.0030	0.050	- 0.006° 0.011 - 0.004°	**0.039** ± 0.0015
1.0	0.076	0.029	**0.047** ± 0.0015	0.051	- 0.006° 0.010 - 0.004°	**0.041** ± 0.0057
1.5	0.064	0.023	**0.041** ± 0.0015	0.044	- 0.008° 0.006 - 0.004°	**0.038** ± 0.0072
2.0	0.073	0.029	0.044 ± 0.0060	0.042	- 0.008° 0.002 - 0.008°	**0.040** ± 0.0052
2.5	0.071	0.027	**0.044** ± 0.0045	0.048	- 0.008° 0.008 - 0.008°	**0.040** ± 0.0037
3.0	0.072	0.028	0.044 ± 0.0030	0.047	- 0.008° 0.007 - 0.004°	**0.040** ± 0.0030

*for definition see Table 3.2.

° w-shaped peaks obtained (see text for details).

TABLE 3.14. Peak heights for the bromine and RI signals, with various bandwidths on the SP1750 UV/vis spectrophotometer. Carrier 1M H^+; Injectate $5x10^{-4}$ M BrO_3^- and 0.03 M Br^-.

	Front boundary			Rear boundary		
Bandwidth (nm)	h_{max} 393 nm (A)	h_{max} 550 nm (A)	Diff* (A)	h_{max} 393 nm (A)	h_{max} 550 nm (A)	Diff* (A)
0.5	0.127	0.035	**0.092** ± 0.0037	0.104	- 0.006° 0.016 - 0.004°	**0.088** ± 0.0000
1.0	0.131	0.035	0.096 ± 0.0037	0.108	- 0.006° 0.016 - 0.004°	**0.092** ± 0.0052
1.5	0.116	0.024	**0.092** ± 0.0030	0.098	- 0.004° 0.009 - 0.004°	**0.089** ± 0.0015
2.0	0.117	0.024	0.093 ± 0.0057	0.096	- 0.008° 0.007 - 0.008°	**0.089** ± 0.0052
2.5	0.123	0.027	0.096 ± 0.0045	0.094	- 0.008° 0.009 - 0.008°	**0.090** ± 0.0042
3.0	0.132	0.033	**0.099** ± 0.0015	0.104	- 0.008° 0.010 - 0.004°	**0.094** ± 0.0045

*for definition see Table 3.2.

° w-shaped peaks obtained (see text for details).

TABLE 3.15. Peak heights for the bromine and RI signals, with various bandwidths on the SP1750 UV/vis spectrophotometer. Carrier 1M H^+ and 0.03 M Br^- ; Injectate $5x10^{-4}$ M BrO_3^- and 0.03 M Br^-.

	Front boundary			Rear boundary		
Bandwidth (nm)	h_{max} 393 nm (A)	h_{max} 550 nm (A)	Diff* (A)	h_{max} 393 nm (A)	h_{max} 550 nm (A)	Diff* (A)
0.5	0.092	0.004	0.088 ± 0.0015	0.085	0.000	**0.085** ± 0.0000
1.0	0.096	0.004	**0.092** ± 0.0000	0.092	0.000	**0.092** ± 0.0000
1.5	0.094	0.004	**0.090** ± 0.0025	0.088	0.000	**0.088** ± 0.0000
2.0	0.092	0.004	0.088 ± 0.0025	0.086	0.000	**0.086** ± 0.0000
2.5	0.094	0.004	**0.090** ± 0.0015	0.088	0.000	**0.088** ± 0.0000
3.0	0.096	0.004	**0.092** ± 0.0015	0.089	0.000	**0.089** ± 0.0015

*for definition see Table 3.2.

TABLE 3.16. **Peak heights for the bromine and RI signals, with various bandwidths on the SP1750 UV/vis spectrophotometer. Carrier 1M H^+ and 0.03 M Br^- ; Injectate 1 M H^+ and $5x10^{-4}$ M BrO_3^-.**

The previous experimental work has already shown that the positions of the front and rear reaction boundary peaks reverse when the roles of carrier and injectate streams are reversed.

The results obtained from all three Tables (3.14. to 3.16.), indicate that peaks of equal height will be obtained at both reaction boundaries when the absorbance from the RI component is subtracted from the bromine signal. Altering the bandwidth over the range 0.5 to 3.0 nm exhibited very little influence on RI correction. The effect of altering the bandwidth on the absorbance signal of the RI component is complex. W-shaped or distorted w-shaped peaks were obtained at the rear reaction boundary, with a high central point in the 'w' and this value was subtracted from the bromine signal. At the front reaction boundary only a single peak was obtained.

The trend observed with the RI signals were as follows: high initial values at 0.5 nm, then a minimum was attained at 1.5 to 2.0 nm followed by an increase as the bandwidth was increased to 2.5 to 3.0 nm. For this spectrophotometer the results suggest that a bandwidth of 2.0 nm should be used to minimise the influence of RI on the signal without decreasing the sensitivity to the bromine signal. It was also interesting to note that no signal from the RI component was attained at the rear reaction boundary **for solution combination n° 4.**

The influence of the spectrophotometer bandwidth on the signal and on RI correction seems to be negligible as long as sufficient number of photons from the lamp reach the detector. At all bandwidths used correction for the effect of RI on the bromine signal was possible, although as stated above larger bandwidths are preferred because of the increase in light reaching the detector. *Stewart*[180] investigated the influence of spectral bandwidths on the signal obtained by variable wavelength detectors in LC. He recommends the use of large bandwidths to improve sensitivity to most analyte components except those that absorb close to the monochromator settings. A trade off between sensitivity and linearity will occur because increasing the bandwidth will decrease the linear range for calibration purposes but increases the sensitivity to certain analyte components (a larger photon flux).

This series of experiments has shown that the influence of the spectrophotometer bandwidth on RI correction is small. No information on the bandwidth of the visible (SP6-250) spectrophotometer is available, while the bandwidth of the diode-array is 2.0 nm. The different sensitivities of the three spectrophotometers

to changes in RI will need further investigation. We believe that optical geometry and photomultiplier tube sensitivities are the critical factors that determine whether a spectrophotometer can be successfully used to correct for RI effects.

3.5. RI changes from non-absorbing species

3.5.1. Introduction

The previous section dealt with the influence of spectrophotometer bandwidth on the signals obtained in single boundary measurements and with its effect on correcting those signals for RI effects. In this section the influence of the optical layout of the spectrophotometer and photomultiplier tube sensitivities will be evaluated. *Betteridge et al.*[147] designed a flow injection manifold that had a high sensitivity to detecting changes in RI and their work with certain modifications, forms the basis of our experimental section. All three spectrophotometers were evaluated for sensitivity to changes in RI.

3.5.2. Experimental

The experimental procedure given 3.2.2. was followed, again using the manifold described, with one modification the injection volume was reduced to 1 cm^3. Three detectors the Pye Unicam SP1750 UV/vis, the Pye Unicam SP6-250 visible and Hewlett Packard HP 8451A diode-array spectrophotometers were used fitted with an 8 µl flow-cell using forward flow. 10% m/v solutions of sodium chloride, potassium chloride and sodium tetraborate were prepared by dissolving the appropriate amount of solid in 100 cm^3 of deionised water in a graduated volumetric flask. The concentration of the solutions were increased in comparison to those used by *Betteridge et al.*[147] because their detector was far more sensitive to changes in RI. In their manifold the light source was placed directly on one side of the flow-cell (transmission tubing) and the photodetector on the other. In all three spectrophotometers used the light sources and photodetectors are placed further away from the flow-cell.

The signals produced from five replicate injections of the three solutions into a carrier stream of deionised water were recorded at 550 nm on all of the spectrophotometers. A spectral scan of all three solutions over the wavelength range 200 to 800 nm showed that none of the solutions exhibited any significant absorbance above 240 nm.

3.5.3. Results and discussion

In the manuals supplied with two of the spectrophotometers (HP 8451A and SP6-250), wavelengths were specified for obtaining maximum precision, 512 nm for the HP 8451A and 535 nm for the SP6-250 respectively. When these wavelengths were selected to monitor the response to the injection of the NaCl solution, there was a negligible difference between the readings and those obtained at 550 nm. 550 nm was therefore used for all measurements on all three spectrophotometers. The injection volume was reduced to 1 cm^3 to decrease sample dispersion while still maintaining the independent integrity of both the front and rear reaction boundaries.

The spectrophotometers response to the injection of all three solutions are given in Table 3.17. The results for the diode-array show that a similar response was obtained for each solution injected, although the magnitude of the signals were dependant on the composition of the injected solution. The peak at the front reaction boundary was always larger than that at the rear reaction boundary and at no stage did the value of the signal decrease below 0.000 A. The broadest peaks were obtained from the injection of the sodium tetraborate solution.

The results for the double beam instrument (SP1750) were the exact opposite to those obtained above: a large peak was obtained at the rear reaction boundary and negative responses were obtained for all three solutions. For the injection of NaCl at the front reaction boundary a negative peak was followed by a small positive peak and at the rear boundary a small negative peak was followed by a larger positive peak. With the sodium tetraborate solution a broad negative peak was obtained at the front reaction boundary and a small positive spike followed by the main peak was obtained at the rear boundary.

The response of the visible spectrophotometer (SP6-250) was the least consistent of all three instruments. Its response was similar to that of both of the other instruments and was very dependant on the composition of the injected solution. The baseline was also less stable than that obtained with the other spectrophotometers: it drifted downwards as the duration of the analysis increased. The response for the injection of NaCl was similar to that obtained on the SP1750: a negative peak was followed by positive peak at the front reaction boundary and this response was repeated at the rear reaction boundary. The magnitude of the peak at the front reaction boundary was larger than that obtained with the SP1750.

		Front boundary		Rear boundary	
Detector*	Solution	h_{max} (A)	t_p (s)	h_{max} (A)	tp (s)
HP 8451A	NaCl	0.151	59	0.051	90
HP 8451A	KCl	0.072	59	0.032	88
HP 8451A	$Na_2B_4O_7$	0.048	57	0.024	91
SP1750	NaCl	- 0.010 0.021	51 61	- 0.004 0.072	75 91
SP1750	KCl	- 0.019	57	- 0.012 0.031	74 93
SP1750	$Na_2B_4O_7$	- 0.024	59	0.012 0.056	78 94
SP6-250	NaCl	- 0.010 0.054	46 56	- 0.005 0.082	70 89
SP6-250	KCl	0.098	56	0.024	87
SP6-250	$Na_2B_4O_7$	- 0.011 - 0.015	48 66	0.047	88

* for convenience the detectors are referred to by their model n°, HP 8551A is the diode-array, SP1750 is the double beam UV/vis and SP6-250 is the visible spectrophotometer respectively.

TABLE 3.17. Peak heights and peak maximum times obtained on the spectrophotometers for the three solutions injected.

When KCl was injected the response was similar to that obtained using the diode-array, one peak was obtained at each reaction boundary with the larger signal at the front and no negative peaks were recorded. For the injection of sodium tetraborate the response followed that of the SP1750, but instead of a flat broad negative peak at the front reaction boundary a negative w-shaped peak was obtained.

The inconsistency in response to the injection of the three solutions when using the visible spectrophotometer explains why it cannot be successfully used for RI correction. Although the response of the other two spectrophotometers differ from each other they are consistent for the injection of all three solutions and this consistent response explains why they can successfully be used for RI correction. While this experiment does not answer the initial question of the influence of instrument layout and photomultiplier tube sensitivity on RI correction, it does provide a simple diagnostic test to determine whether an instrument can be used for RI correction. To evaluate the instrumental parameters referred to above an instrument would need to be constructed so that several parameters could be varied. These would include several optical parameters such as focal length, acceptance angle , aperture and field stops and easy access to the photodetector compartment, so that different designs could be mounted and evaluated without losing the light tight integrity of the compartment.

3.6. Conclusions

In this chapter we have demonstrated that to limit the contribution of the flow-cell to dispersion smaller volume cells are preferred. The direction of flow used with a flow-cell should follow that recommended by the manufacturer or the flow will become highly distorted: this is particularly true for the largest volume flow-cell used. With the 8 µl flow-cell no flow direction was recommended and either flow direction may be used with no detrimental effect on the signal recorded.

It has been shown that the use of a diode-array spectrophotometer to monitor an analytical signal and its RI component at two different wavelengths, enables RI compensation of the signal to be carried out. This was achieved without the need for RI matching previously employed and offers an improvement in contamination control by removing the need to add another reagent and the inherent risks that are associated with this. A flow-cell of up to 30 µl may be used without significant degradation in the performance of the diode-array

spectrophotometer as a FI detector. However, as stated above smaller volume flow-cells are recommended to limit the effect of the cell on the dispersion of the sample bolus. It would be possible to programme more recent versions of the diode-array spectrophotometer to make the RI corrections automatically.

When employing RI correction the visible spectrophotometer should not be used because it does not respond in a consistent manner to the injection of solutions with various refractive indices. This problem was best illustrated with the final experiment, which can also be used as a simple diagnostic tool for determining the suitability of various designs of spectrophotometer for RI correction. With the other two design of spectrophotometer the diode-array is preferred because less complex signals are obtained (the occurrence of double negative peaks were less).

CHAPTER 4

USE OF REACTORS IN SINGLE-CHANNEL MANIFOLDS FOR SINGLE BOUNDARY MEASUREMENTS WITH SPECTROPHOTOMETRIC DETECTION

4.1 Introduction

The effect of two types of reactor on the signals obtained in single boundary measurements was studied. The first section deals with the inclusion of single bead string reactors (SBSRs) in the single-channel manifolds and compares the benefits in reduced peak width with those obtained using coiled reactors of similar dimensions. In the latter section the shape of the signal obtained by incorporating various lengths of coiled reactor in the manifold is reported, reduction in peak widths, peak appearance times and peak heights at each of the two reaction boundaries are recorded as the length of the coiled reactor is reduced. The influence of coiled reactor length on RI correction is also reported.

4.2. Signals obtained in single boundary measurements using a single bead string reactor in the manifold

4.2.1. Introduction

Single bead string reactors (SBSRs) were first described by *Reijn et al.*[60,181] who proposed the name. They consist of PTFE tubes (0.5 to 1.0 mm i.d.) packed with glass beads which have diameters that are between 60 to 80 % of the tube's diameter. According to *Reijn et al.*[60,181] the main advantage obtained from beads in the reactor was their effect of increasing radial diffusion which in turn decreases dispersion. They also reported that in comparison to unfilled straight and coiled reactors, increasing the sample residence time does not degrade the sampling frequency, because the SBSR has a lower sample dispersion. This implies that for a fixed residence time, the SBSR will have a higher sampling frequency than the other two types of reactor.

Reijn et al.[182] have within certain experimental constraints (pressure drop of 1 bar) developed an approach to the optimisation of four types of reactor used in FI. The unfilled straight and coiled reactors along with an SBSR and packed bed reactor (PBR) were optimised for high sampling frequency and low reagent consumption. This enabled a ready comparison of the reactor's performance and highlighted the shortfall of each design. *Brooks and Dorsey*[40] used moment

analysis on the signals from an unfilled coiled, knitted and Serpentine II reactors and an SBSR to evaluate the merits of each design. The last two designs were reported as having lower reagent consumption even when the flow rate was increased. While dispersion of the sample bolus was less in both the Serpentine II and knitted reactor than in the other two designs. *van Veen et al.*[183] have derived optimisation criteria for the utilisation of an SBSR in the determination of analytes using consecutive kinetic reactions.

Patton and Crouch[31] when comparing the merits of FI and air segmented continuous flow analysis (CFA), report that the inclusion of an SBSR in their FI manifold led to an increase in sample throughput, because the sample washout time was decreased. This meant that a faster return to the baseline signal after the passage of a sample bolus was achieved with an SBSR in the manifold. The sensitivity attained with the FI manifold was lower than with the air segmented CFA because only transient signals and not steady state signals were obtained from the FI manifold.

Reijn et al.[184] and *Yoshizawa et al.*[185] have noted that over a limited flow rate of 0.5 to 1.5 cm^3min^{-1}, h_{max} is independent of flow rate when an SBSR is used. For *Yoshizawa et al.*[185] the inclusion of an SBSR in the manifold and the use of rapid scan square wave voltammetry enabled the simultaneous determination of caffeic and vanillic acids to be made. *Fogg et al.*[186] report an increase in sensitivity (h_{max}) when a short SBSR was used in their manifold. They also report that gas bubbles were redissolved into the solution by including an SBSR in the manifold, but they could not use a longer SBSR because of high back pressure problems.

Finally *van Nugteren-Osinga et al.*[62] used two SBSRs in their manifolds to ensure adequate radial mixing before the solution entered the manifold component under investigation. The impulse/response function of each component was then obtained and this could be used in a predictive manner to help improve manifold design.

The influence of a SBSR on the shape of the signal obtained in a single-channel manifold has been studied by several workers[40,60,181-186]. They reported that the main advantage of the SBSR was an increase in sample throughput due to the reduced dispersion created by the reactor; this is normally seen as a decrease in Δt, the baseline peak width. All of the above authors worked with conventional injection volumes (< 200 µl). It is the intention of this study to investigate if the

improvement in sample throughput is also observed with the larger injection volumes used (3 cm^3).

4.2.2. Experimental

The experimental procedure given in 2.4.1. was again followed, but the manifold was modified from that shown in Figure 2.1. by including various lengths of unfilled coiled reactors and coiled SBSRs. The 8 µl flow-cell was used with forward flow and the signals (at 393 nm) were recorded on the diode-array spectrophotometer. The SBSR was prepared as detailed in 2.2. and the length of the reactor was varied over the range 1.00 to 0.25 m in 0.25 m increments. An unfilled coiled reactor was also used for signal comparison and its length was varied over the same range: it was also varied in volume to match the volume of each length of SBSR used. The volume of each SBSR was calculated by timing the passage of a bubble of air through the reactor and since the flow rate was known, the volume of each reactor could be calculated. All three solution combinations given in Table 3.1. at the concentrations given in 3.2.2. were again studied and preformed bromine solutions (see 3.3.2.) were again used to obtain physical dispersion measurements.

4.2.3. Results and discussion

The results of the physical dispersion measurements are shown graphically in Figures 4.1. and 4.2. for reactors of equal volume and equal length respectively. In the case of both matched length and matched volume, the SBSRs have lower dispersion values than the coiled reactors, and this manifests itself as smaller Δt values. The improvement in Δt with the SBSRs is much larger when the two types of reactor are matched in length rather than volume. This suggests that the more appropriate comparison is on the basis of matched volume. When the two types of reactor were compared for their effect on peak appearance time t_a, in the case of both matched volume and matched reactor length the t_a values were smaller for the coiled reactor than for the SBSRs. The effect of the type of reactor on t_a is shown graphically in Figures 4.3. and 4.4. for equal volume and equal length reactors respectively. This delay in peak appearance time has not been reported for the smaller injection volumes investigated so far[31,40,60,62,181-186].

The type of reactor used did not affect the magnitude of the steady state signal: this remained at 0.45 A. The first SBSR constructed was 3 m in length. When this was placed in the manifold and a flow rate of 2 cm^3min^{-1} was used, severe back

pressure problems were encountered in the form of leaking joints. The problem was not alleviated until the reactor length was reduced to 1 m: this size was used as the starting point of the study of the effect of reactor type on the signal shape obtained. The findings on decreased dispersion when using an SBSR are in agreement with those of earlier workers in the field[31,40,60,62,181-186]. The increase in peak appearance time would cause a decrease in the sample throughput, unless a series of samples were placed concurrently in the manifold. This would involve injecting the next sample before the rear boundary peak of the preceding sample appears and calculating a sufficient delay between the injections so that there is no cross contamination between samples. If this type of approach is not adopted, then any time saving that occurs because of the decreased dispersion must be offset against the increase in run time because of the longer peak appearance times.

When the three solution combinations were injected through both types of reactor the magnitude of the signal was reduced in comparison to those obtained with the 3 m coiled reactor. For solution combination n° 4 in Table 3.1. the magnitude of the signal obtained at each reaction boundary was reduced from 0.128 A at 3 m, to 0.081 A using a 1 m SBSR and using a 0.25 m SBSR the signal was only 0.049 A (0.079 A and 0.046 A in 1 m and 0.25 m coiled reactors respectively). The decrease in the magnitude of the signals can be explained by a reduction in the degree of on-line formation of bromine as the reactor length is decreased. The most important design criteria for single-channel manifolds with two reaction zones at the extremities of the sample bolus is the amount of time allowed for the on-line formation of the analyte. In comparison to coiled reactors, SBSRs do not offer any appreciable improvement in sample mixing: there is no significant increase in the magnitude of the signals obtained when SBSRs are used instead of coiled reactors.

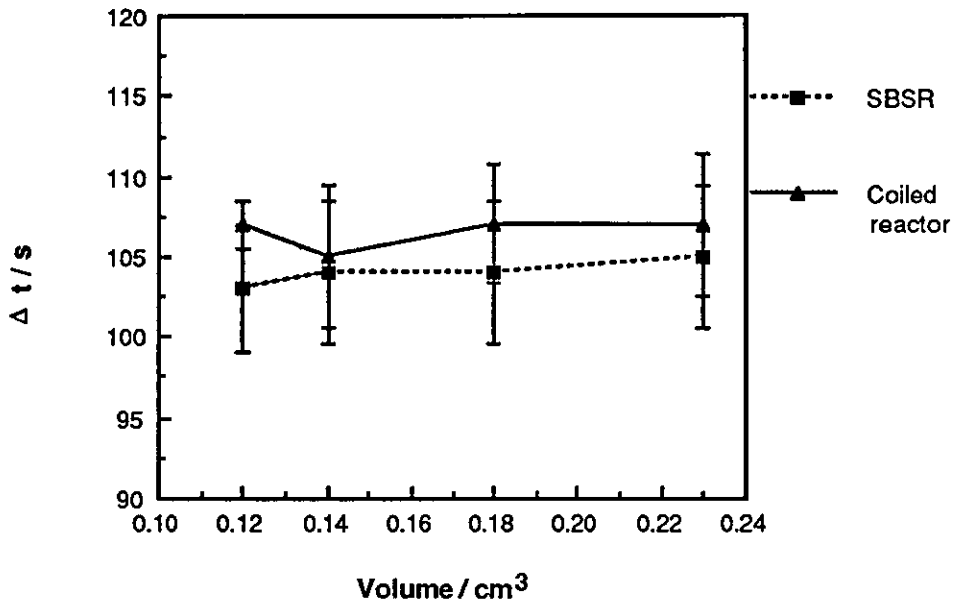

FIGURE 4.1. **A comparison of the effect of SBSRs and coiled reactors of equal volume on peak width Δt.**

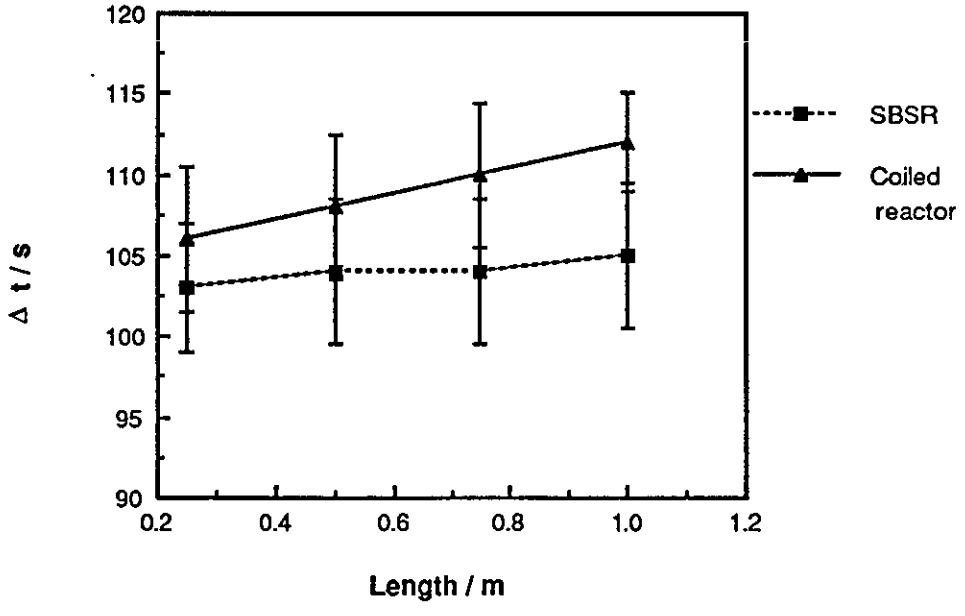

FIGURE 4.2. **A comparison of the effects of SBSRs and coiled reactors of equal lengths on peak width Δt.**

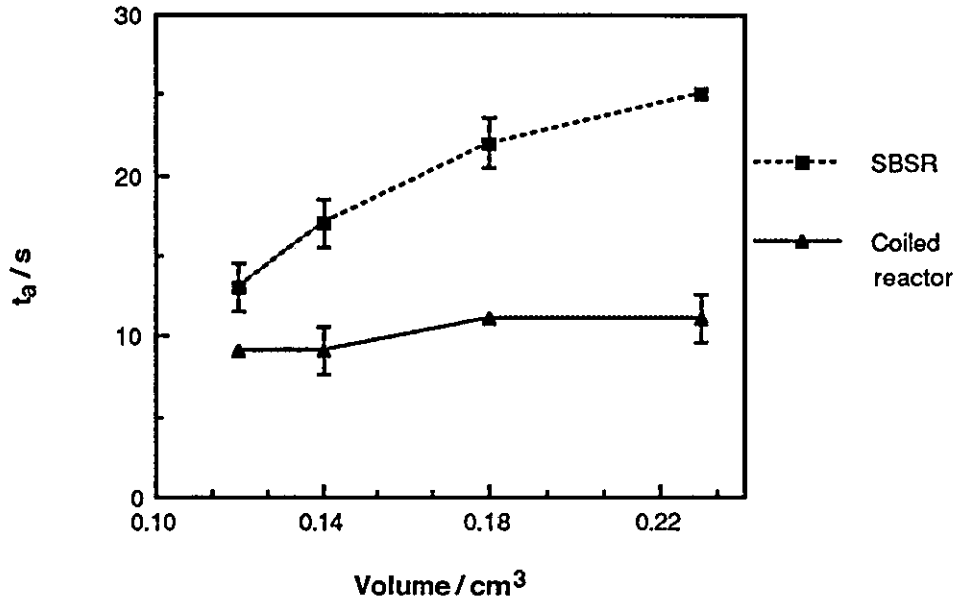

FIGURE 4.3. **A comparison of the effect of SBSRs and coiled reactors of equal volume on peak appearance times t_a.**

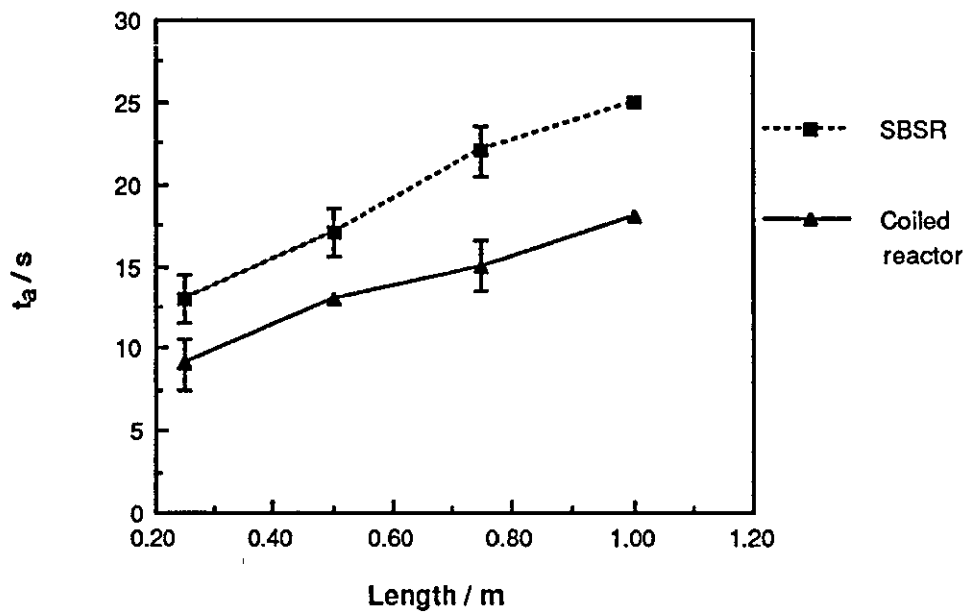

FIGURE 4.4. **A comparison of the effect of SBSRs and coiled reactors of equal lengths on peak appearance times t_a.**

4.3. Influence of varying the size of a coiled reactor on RI correction in single boundary measurements using visible spectrophotometric detection

4.3.1. Introduction

In a paper on the shapes of normal and reverse flow injection signals *Fogg et al.*[69] have introduced a large sample bolus using both slug injection and time based injection. In the time based injection mode the two reaction boundaries that were formed, took the same time and travelled the same distance from the injection valve to the detector. With the slug injection mode the two reaction boundaries formed took different times and travelled different distances from the injection valve to the detector: the front boundary had to travel distance L while the rear boundary travelled an additional distance L + l (l being the distance of the sample loop). This additional distance l also meant that the rear junction was dispersed more than the front junction.

In a continuation of this work the influence of various length of coiled reactor on signals obtained at both reaction boundaries was studied rather than again comparing slug and time based injections, so that both boundaries would encounter the same degree of dispersion. In our earlier work with SBSRs we observed that as the length of the reactor decreased, t_a, Δt and h_{max} decreased as the dispersion decreased and the time given for the degree of on-line analyte formation decreased. The effect of reducing the coil length on these parameters will be reported and the effect of RI correction on the signals obtained at each coil length will also be reported.

4.3.2. Experimental

The experimental procedure given in 2.4.1. was again followed but the manifold was modified from that shown in Figure 2.1. by including various lengths of unfilled coiled rector. The 8 µl flow-cell was used with forward flow and the signals (at 393 and 550 nm) were recorded on the diode-array spectrophotometer. The length of the coiled reactor in the manifold was reduced from 10.0 m to 0.5 m in 0.5 m increments. One solution combination n° 1 in Table 3.1. was studied, with solution B as the carrier and solution A as the injectate, at the component concentrations given in 3.2.2. Additionally to increase the magnitude of the signal obtained from the on-line formation of bromine a second injectate solution of $5x10^{-3}$ M BrO_3^- and 0.03 M Br^- was used. Preformed bromine solutions (see 3.2.2.) were again used to obtain physical dispersion measurements. Three replicate

readings were recorded for each solution at each of the wavelengths used (393 and 550 nm for bromine formed the on-line and 393 nm for the preformed bromine solutions).

4.3.3. Results and discussion

The results for both peak width times Δt, and for peak appearance times t_a are shown in Figures 4.5. and 4.6. respectively. The results for both parameters follow the expected trends i.e. both Δt an t_a decrease as the length of the coiled reactor decreases. Results from the injection of the preformed bromine solution and for the bromine formed on-line (both reaction boundary peaks) show a decrease in both peak parameters occurring, whether an on-line chemical reaction is occurring or not. In Figure 4.5. Δt values were plotted for the preformed bromine solution and for both reaction boundary peaks for the bromine formed on-line, at the higher bromate concentration. The results cover a much wider range of reactor lengths than were shown in Figure 4.2. and emphasise the decrease in Δt values. The value of the errors for both Figures 4.2. and 4.5. are similar (largest error 4.5 s) and error bars are plotted on the Y axis in Figure 4.5., but do not show up as clearly because the range of Δt values plotted are larger than those plotted in Figure 4.2.

Similarly in Figure 4.6. t_a values were plotted for the preformed bromine solution and for both reaction boundary peaks for the bromine formed on-line at the higher bromate concentration. A larger range of values was again plotted in Figure 4.6. than in Figure 4.4. and the Y error bars do not appear to be as wide in Figure 4.6., for the reasons given above. In most cases the error associated with t_a values are less than those of the Δt values because Δt is the difference between t_a and t_w (peak washout time) and the error occurring in the measurement of t_w values has to be added to that of the t_a value when Δt values are plotted.

For the solutions with the lower bromate concentration, Figure 4.7. shows $\Delta t_{1/2}$ values rather than Δt values ($\Delta t_{1/2}$ peak width measurements at half peak height). At the longer coiled reactor lengths the peaks exhibited severe "tailing" and the signal was not baseline resolved between the two peaks, which made measurement of t_w values impossible for the front boundary peaks and so Δt values could not be obtained. $\Delta t_{1/2}$ values follow the same trend as Δt values, they decrease as the length of the coiled reactor decreases. The error bars appear wider in Figure 4.7. than in either Figure 4.5. or 4.6. because a smaller range of value are plotted on the Y axis although the magnitude of the error are similar to

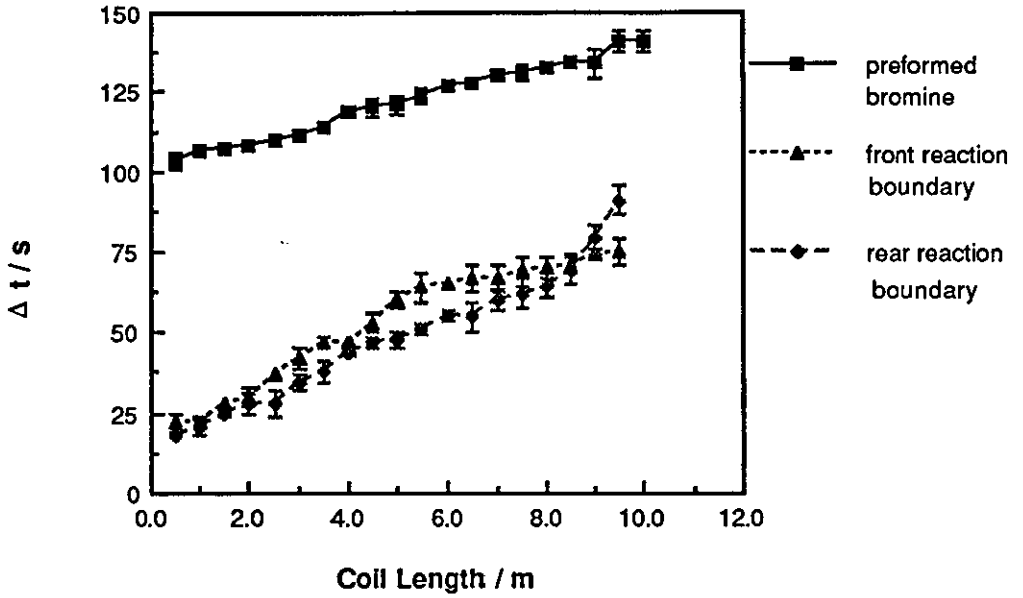

FIGURE 4.5. **Variation of peak width values with reaction coil length for the injection of a preformed bromine solution, and both reaction boundary peaks of bromine formed on-line from 1 M H^+, $5x10^{-3}$ M BrO_3^- and 0.03 M Br^-.**

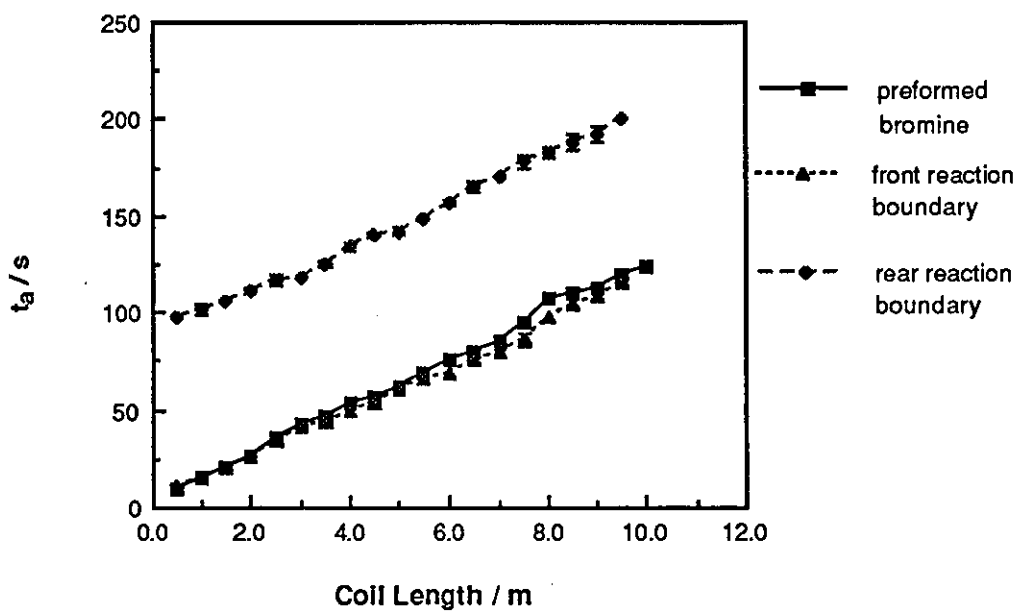

FIGURE 4.6. **Variation of peak appearance values with reaction coil length for the injection of a preformed bromine solution, and both reaction boundary peaks of bromine formed on-line from 1 M H^+, $5x10^{-3}$ M BrO_3^- and 0.03 M Br^-.**

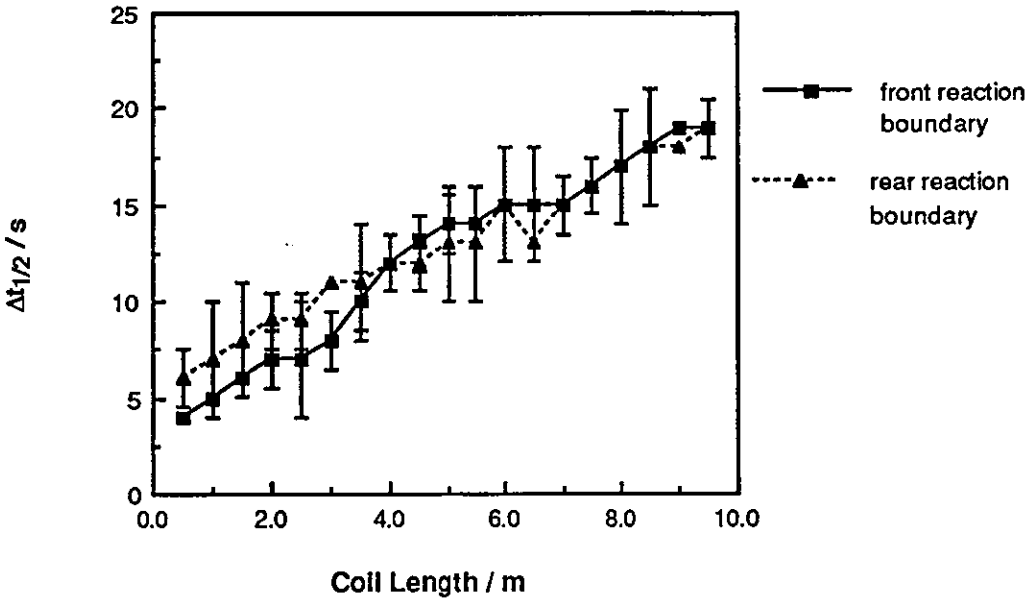

FIGURE 4.7. **Variation of half peak width values with reaction coil length for both reaction boundary peaks of bromine formed on-line from 1 M H^+, $5x10^{-3}$ M BrO_3^- and 0.03 M Br^-.**

those for the other two Figures. No t_a values were plotted for the bromine formed on-line at the lower bromate level because the t_a value could not be measured accurately at either reaction boundaries, with most of the coiled reactor lengths used (baseline resolution problems, an offset of 0.005 A was present between the two peaks).

Tables 4.1. and 4.2. give the peak heights for both the bromine and RI peaks at both reaction boundaries for the injectate solutions containing the low and high concentration of bromate respectively. In both cases the value of h_{max} decreases as the length of the coiled reactor decreases and this is as expected because the time for reaction is decreasing and so the amount of product formed on-line is less. This is in agreement with the work of *Fogg et al.*[69], who compared the signals obtained when a large volume injection were made using both slug and time based injection processes. In the slug injection process the height of the rear boundary peak obtained was higher than that obtained at the front reaction boundary. The rear reaction boundary was given a longer reaction time by travelling through the injection loop in addition to travelling the same distance through the manifold as the front reaction boundary and so the magnitude of the signal was greater.

The results in Table 4.1. for the injectate solution with the lower bromate level show that it is possible to obtain peaks of equal height at each reaction boundary when the RI component is subtracted, at most of the coiled reactor lengths used. This was not the case with the injectate solutions containing the higher level of bromate (see Table 4.2.). Peaks of equal height were not obtained at each reaction boundary even after correcting for RI effects until the length of the reaction coiled reactor was reduced to 4.5 m. At the longer reaction coil lengths differences in the heights of the peaks at reaction boundary of 0.03 A or greater were recorded.

The differences in the peak height at each reaction boundary suggests that, as the degree of analyte formation increases the contribution of RI to the differences in peak heights at the reaction boundaries decreases. Other processes such as diffusion of the analyte must therefore be considered as the cause for the differences in the peak heights observed. These effects are more apparent at higher on-line bromine levels (compare the results in Table 4.2. with those in Table 4.1.).*Zagatto et al.*[109] have also suggested that increasing the coil length improves the signal to noise ratio because the contribution from the Schlieren effect (RI) to the signal obtained is decreased and our results agree with this.

	Front boundary			Rear boundary		
Coil Length (m)	h_{max} 393 nm (A)	$\bullet h_{max}$ 550 nm (A)	Diff* (A)	h_{max} 393 nm (A)	h_{max} 550 nm (A)	Diff* (A)
9.5	0.113	0.002	**0.111** ± 0.0052	0.132	0.010	**0.122** ± 0.0104
9.0	0.102	- 0.010	**0.112** ± 0.0030	0.124	0.018	**0.106** ± 0.0000
8.5	0.095	- 0.008	**0.103** ± 0.0042	0.105	0.011	**0.094** ± 0.0045
8.0	0.092	- 0.006	**0.098** ± 0.0057	0.113	0.019	**0.094** ± 0.0057
7.5	0.083	- 0.010	**0.094** ± 0.0030	0.108	0.020	**0.088** ± 0.0030
7.0	0.079	- 0.009 - 0.010	**0.089** ± 0.0062	0.109	0.023	**0.086** ± 0.0067
6.5	0.078	- 0.009 - 0.010	**0.087** ± 0.0037	0.102	0.020	**0.082** ± 0.0015
6.0	0.078	- 0.012 - 0.011	**0.089** ± 0.0052	0.104	0.018	**0.086** ± 0.0045
5.5	0.077	- 0.009	**0.086** ± 0.0057	0.102	0.022	**0.080** ± 0.0030
5.0	0.071	- 0.006	**0.077** ± 0.0000	0.089	0.012	**0.077** ± 0.0015
4.5	0.072	- 0.004	**0.076** ± 0.0030	0.092	0.017	**0.075** ± 0.0045
4.0	0.067	- 0.005	**0.072** ± 0.0045	0.086	0.013	**0.073** ± 0.0050

	Front boundary			Rear boundary		
Coil Length (m)	h_{max} 393 nm (A)	•h_{max} 550 nm (A)	Diff* (A)	h_{max} 393 nm (A)	h_{max} 550 nm (A)	Diff* (A)
3.5	0.061	- 0.010 0.000 - 0.009	**0.061** ± 0.0045	0.079	0.017	**0.062** ± 0.0045
3.0	0.052	- 0.012 0.000 - 0.013	**0.052** ± 0.0030	0.072	0.023	**0.049** ± 0.0037
2.5	0.052	- 0.008 - 0.001 - 0.010	**0.053** ± 0.0045	0.073	0.025	**0.048** ± 0.0030
2.0	0.037	- 0.015 0.002 - 0.012	**0.035** ± 0.0040	0.071	0.038	**0.033** ± 0.0042
1.5	0.031	- 0.014 0.003 - 0.010	**0.028** ± 0.0000	0.070	0.044	**0.026** ± 0.0030
1.0	0.035	- 0.013 0.006 - 0.010	**0.029** ± 0.0042	0.089	0.062	**0.027** ± 0.0015
0.5	0.037	- 0.012 0.013 - 0.009	**0.024** ± 0.0030	0.096	0.076	**0.020** ± 0.0077

* see Table 3.2. for details.

• see text for information on the change in the RI signal with reaction coil length.

TABLE 4.1. **Peak height signals for bromine and RI peaks at both reaction boundaries for various lengths of coiled reactor. Carrier 1 M H^+, injectate $5x10^{-4}$ M BrO_3^- and 0.03 M Br^-.**

	Front boundary			Rear boundary		
Coil Length (m)	h_{max} 393 nm (A)	$\bullet h_{max}$ 550 nm (A)	Diff* (A)	h_{max} 393 nm (A)	h_{max} 550 nm (A)	Diff* (A)
10.0	0.871	0.016	**0.855** ± 0.0114	0.879	0.042	**0.837** ± 0.0156
9.5	0.843	0.013	**0.830** ± 0.0166	0.853	0.039	**0.814** ± 0.0057
9.0	0.776	0.008	**0.768** ± 0.0181	0.771	0.033	**0.738** ± 0.0206
8.5	0.773	0.015	**0.758** ± 0.0000	0.751	0.020	**0.731** ± 0.0015
8.0	0.708	0.004	**0.704** ± 0.0214	0.719	0.033	**0.686** ± 0.0156
7.5	0.679	0.006	**0.673** ± 0.0015	0.692	0.036	**0.656** ± 0.0151
7.0	0.675	0.005	**0.670** ± 0.0099	0.675	0.035	**0.640** ± 0.0181
6.5	0.671	0.006	**0.665** ± 0.0129	0.675	0.034	**0.641** ± 0.0030
6.0	0.656	0.004	**0.652** ± 0.0099	0.659	0.030	**0.629** ± 0.0072
5.5	0.627	0.005 0.006	**0.621** ± 0.0015	0.622	0.034	**0.588** ± 0.0144
5.0	0.552	0.002 - 0.005	**0.550** ± 0.0087	0.568	0.030	**0.538** ± 0.0072
4.5	0.515	0.006	**0.509** ± 0.0072	0.512	0.017	**0.495** ± 0.0099

	Front boundary			Rear boundary		
Coil Length (m)	h_{max} 393 nm (A)	•h_{max} 550 nm (A)	Diff* (A)	h_{max} 393 nm (A)	h_{max} 550 nm (A)	Diff* (A)
4.0	0.449	0.003	**0.446** ± 0.0015	0.465	0.025	**0.440** ± 0.0087
3.5	0.418	0.006 - 0.006	**0.412** ± 0.0000	0.437	0.030	**0.407** ± 0.0072
3.0	0.389	- 0.005 0.000 - 0.008	**0.389** ± 0.0057	0.417	0.032	**0.385** ± 0.0057
2.5	0.390	- 0.003 0.006 - 0.008	**0.384** ± 0.0057	0.408	0.028	**0.380** ± 0.0087
2.0	0.256	- 0.006 0.008 - 0.010	**0.248** ± 0.0087	0.285	0.037	**0.248** ± 0.0060
1.5	0.209	- 0.011 0.006 - 0.009	**0.203** ± 0.0000	0.252	0.045	**0.207** ± 0.0057
1.0	0.194	- 0.009 0.011 - 0.008	**0.183** ± 0.0057	0.243	0.062	**0.181** ± 0.0070
0.5	0.154	- 0.010 0.015 - 0.007	**0.139** ± 0.0057	0.203	0.067	**0.136** ± 0.0000

* see Table 3.2. for details.

• see text for information on the change in the RI signal with reaction coil length.

TABLE 4.2. **Peak height signals for bromine and RI peaks at both reaction boundaries for various lengths of coiled reactor. Carrier 1 M H^+, injectate $5x10^{-3}$ M BrO_3^- and 0.03 M Br^-.**

The decrease in the magnitude of the RI signals as the length of the coiled reactor is increased are shown in Tables 4.1. and 4.2. and the decrease is of a similar magnitude for both bromate levels. The difference in the peak heights at each reaction boundary was in the degree of on-line bromine formation which was higher for the solutions used to give the results in Table 4.2. In both Tables the results in the *Diff column are the differences in the peak heights when the value of the absorbance at 550 nm is subtracted from that at 393 nm. As explained earlier in chapter 3 the absorbance value at 550 nm was only subtracted if it occurred at the same t_p value as the h_{max} at 393 nm.

The shape of the RI peak varies with the length of the coiled reactor used, for the solution containing the lower level of bromate the following was observed. At 9.5 m the RI peak at the front boundary was slightly positive (0.002 A): then a negative peak was obtained between 9.0 and 7.5 m (- 0.011 A). At 7.0 m the negative peak broadens until the coil length is reduced to 5.5 m, where its appearance follows that of the 9.0 to 7.5 m coiled reactors. When the coiled reactor's length is reduced further to 3.5 m and below, negative w-shaped peaks are obtained. At the rear reaction boundary a much simpler situation was encountered; a positive peak that varied in magnitude only was obtained.

When the concentration of the bromate in the injectate solution was increased a similar trend to that reported above was seen for the RI peaks. At the front reaction boundary a positive RI peak was obtained which decreased in magnitude and broadened slightly until the length of the reactor was reduced to 5.5 m. At this length a double positive peak was obtained: from 5.0 to 3.5 m the positive peak was followed by a small negative peak. At 3.0 m and below a negative w-shaped peak was obtained. The arch of the 'w' was sometimes significantly positive: again the rear boundary peak was a simple positive hump that varied in magnitude only.

The separation between the peaks formed at both reaction boundaries remained fairly consistent at the lengths of coiled reactor used (approximately an 83 s separation between the front and rear reaction boundary peaks). Decreasing the length of the coiled reactor reduces the amount of tailing that occurs at each peak and decreases the height of the peaks formed at each reaction boundary but does not alter the separation between the reaction boundary peaks. This value would only be altered by changing the volume of the injectate. Decreasing the length of the coiled reactor decreased the amount of back pressure generated by the inclusion of the reactor in the manifold. The back pressure was monitored

visually by observing the height of solution that entered the side arm of the pulse dampers, the higher the level of solution in the side arm the higher the back pressure. By placing the pulse dampers between the pump and the injection valve any back pressure problems caused by the restriction of the flow of solution, could be observed, including the injection valve not fully opening. This gave a fast diagnostic tool for overcoming problems with restricted flow in the manifold.

4.4. Conclusions

It has been shown that using a SBSR in single boundary measurements leads to a decrease in dispersion that manifests itself as a decrease in the width of the peaks obtained. In single boundary measurements this is shown as a decrease in the width between the start of the front boundary peak and the tail of the rear boundary peak. SBSRs should be employed in single boundary measurements as mixing devices before and after the main reaction coil, to impart the improvement in dispersion while still permitting sufficient time for a larger degree of analyte conversion in the main reaction coil. They would be more usefully employed at lower flow rates than used in this study, because this would lead to a decrease in the amount of back pressure that is generated when they are included in the manifold. Further work would include assessing their effect on the signals obtained as the sample volume is decreased in direct comparison to other reactors of various designs but all having the same volume.

The results of the experiments with the coiled reactors are similar to those with the SBSRs, peak width, peak appearance time and peak height decrease as the length of the coiled reactor is decreased. It was also shown that increasing the length of the coiled reactor was beneficial in reducing the contribution of RI to the analytical signal. Reactors over 5.0 m however, are not recommended because correction for RI becomes difficult as the contribution of other factors such as analyte diffusion need to be considered. The reason for the differences in the heights of the peaks at each reaction boundary at higher levels of on-line analyte formation (higher component concentrations and longer coil lengths) are as yet unknown. Nor can we explain why each reaction boundary apparently encounters a different set of conditions, even when the distance and time taken for each reaction boundary to travel from the injection valve to the detector are identical.

CHAPTER 5

THE FLOW INJECTION SANDWICH TECHNIQUE APPLIED TO INDIRECT VISIBLE SPECTROPHOTOMETRIC DETERMINATIONS

5.1. Introduction

When a sufficiently large volume injection is made into a carrier stream of a single-channel flow injection manifold, signals from on-line reactions at each of the two boundaries formed are observed. This situation can be represented by B>A>B, where B is the carrier stream and A is the injectate, and the direction of flow is as indicated. A slug of injectate (A) is introduced into carrier B, and the reaction products are formed at the two interfaces between A and B. This situation has been used by *Fernandez et al.*[187] for the kinetic determination of cobalt and nickel in the same sample, by exploiting the difference in the rate of metal complex formation using 2-hydroxybenzaldehyde thiosemicarbazone as the complexing agent. Peaks of different height were obtained at the two boundaries, because by using loop injection the junctions were formed at different places. Therefore the junctions travelled different distances to the detector from the injection valve and took different times to get there. *Fogg et al.* have also exploited the above situation for the on-line formation of both iodine[69,71,72] and bromine[70,72], in two separate reaction zones prior to using them as monitorand species for the indirect determination of sulphite[70-72].

The methods described above lead to the formation of more than one peak per injection when using conventional six-port rotary valves, but the versatility of this technique is limited. If stream switching or a combination of valve and valve types are used, situations represented by C>B>A> can be produced, where C and A are either different samples/standards or reagents and B is either a reagent or sample. This situation and others have been used to produce the so-called sandwich techniques. Sandwich techniques are techniques in which more than one analyte or species is determined per injection, or in which a single analyte is determined in two solutions. The final category would include situations in which more than one calibration curve is produced from the injection by causing a dilution to occur at one of the reaction boundaries. Two arrangements of valve design have been used commonly to produce the sandwich methods in flow injection. Two internally coupled six-port rotary valves (nested loop) were favoured by *Rios* and co-workers[78,188-190] and an eight-port rotary valve has been used by *Alonso* and co-workers[77,79,191].

Dasgupta and Hwang[192] introduced the concept of a coupled valve configuration (nested loop) where one six-port rotary valve is connected into the sampling loop of the other for the simultaneous determination of aqueous and organic peroxides. Two peaks were produced the first being due to both aqueous and organic peroxides and the second peak being due to organic peroxides alone. The aqueous peroxides had been removed by passing the sample through a MnO_2 reactor in the sample loop of the second (nested) valve.

Rios et al.[189] used their coupled valve configuration to produce a pH gradient by sandwiching their sample between two buffer solutions of different pH. This enabled them to determine lead(II) and vanadium(V) simultaneously in the same sample; the same workers also used the pH gradient formed by the sandwich method to determine simultaneously ammonia and hydrazine fluorimetrically[188]. The formation of pH gradients in flow injection manifolds was proposed in earlier work by *Betteridge et al.*[16,193,194] but the sandwich technique is a refinement of their work because it ensures that the appropriate concentration of reagent is present in the centre of the sample zone[188,189].

The coupled six-port valve configuration has also been used by *Bermudez et al.*[190] to determine nitrite and nitrate simultaneously in the same sample. A redox column was included in the sample loop of the second valve so that the first peak obtained was due to nitrite alone, while the second peak was due to nitrite and nitrite formed by the reduction of nitrate. A similar arrangement was used by *Perez Pavon et al.*[195] for the simultaneous determination of thorium and uranium.

Another application of the coupled valve configuration used by *Rios et al.*[78] was to determine a single component in two solutions, a sample and a standard. They determined formaldehyde in samples and standards using UV/vis spectrophotometry. The shape of the peaks produced by introducing a sample between two standards was unusual: two peaks were not always obtained by this method. When the concentration of the sample and standards were equivalent a large flat topped peak was produced. If however, the concentration of the standard was higher than the sample, the sample was shown as a valley between the two standard peaks. When the concentration of the sample exceeded that of the standards, the standard peaks appeared as shoulders on either side of the sample peak. The authors used derivative absorbance signals to improve the interpretation of the data by emphasising the difference or lack of difference between the sample and the standards.

The idea of adding sample to standards is a refinement of the work of *Frenzel*[73] who, using a rFI method, added standards to a carrier stream of sample to monitor chloride, fluoride and phosphate continuously in tap water. The signals produced by this method differed from those above because the signal of the sample alone gave the baseline and if the concentration of standard added exceeded that of the sample a positive peak was obtained. Conversely if the concentration of the added standard was less than that of the sample negative peaks were obtained and if the concentrations were equal then no deflection of the baseline signal would be observed. The advantages of the method of *Rios et al.*[78] above is that more than one peak is produced per injection and both the sample and the standards are injected which lowers the volume of sample required if this is a limiting factor.

Erickson et al.[196] describe a modified twelve-port rotary valve that may be configured to produce a large variety of sandwich arrangements, including a pH gradient system, a sample/standard/sample system and a double injection system (with two sample slugs in the manifold at one time). The valve was constructed in-house and does not seem to be commercially available. It has, in common with an eight-port rotary valve, an advantage over the coupled valve system because only one valve is needed to produce the resultant sandwich. *Alonso et al.*[77] first used the eight-port rotary valve for a sandwich technique involving continuous recalibration in process control. Two manifolds were described, one using an ion-selective electrode and the other using a photometer as the detector. In a second paper *Alonso et al.*[79] determined total iron and iron(II) in the same sample simultaneously. The signals produce by this method consisted of an Fe(II) peak that appeared as a shoulder before the main total Fe peak. The authors demonstrated that injection volumes in excess of 1 cm^3 were needed to produce a well defined shoulder.

Araujo et al.[191] ,using the expertise developed by *Alonso* and co-workers, applied the sandwich technique to the simultaneous determination of chromium(VI) and total iron in waste water. In this instance two distinct peaks were obtained that were almost baseline resolved, but the complexity of the manifold design had to be increased to achieve these results. Three reagent lines with two confluence points led to a mixing chamber situated before the injection valve, and the mixed reagents for the total iron determination then travelled through a single line into one port of the injection valve. Similarly a two reagent lines with one confluence point led to a separate mixing chamber which was again situated before the injection valve, and these mixed reagents for the Cr(VI) determination then

travelled through a single line to another port on the injection valve. The mixed reagents were then introduced either side of the sample slug.

More recently *Montesinos et al.*[197] have presented results of mathematically modelling sequential determinations using an eight-port rotary valve in a flow injection manifold configured for the sandwich technique. The effects of various manifold parameters (injection volume, reactor length and flow rate) and chemical kinetics were evaluated and results from the simulations using the model were compared with experimental data for the enzymatic determination of glucose. The front and rear peaks were produced separately using the eight-port rotary valve. Three solutions were pumped into the valve; the reagents, the sample and deionised water. By altering the lines used to introduce the reagents and water two boluses of the following composition were produced, water>sample>reagent and reagent>sample>water producing a response for the front and rear boundary peaks respectively. Manipulation of the valve in this manner enabled the authors to model the processes occurring at each peak, and they claim some success with their model in optimising the manifold for the sandwich technique.

The sandwich technique has also been used to produce more than one calibration curve by effectively having two ranges of analyte present per injection. *Araujo et al.*[198], when determining chlorine in natural and residual waters, followed a similar method to that above but two peaks were produced per injection. The lower calibration curve was obtained by monitoring the response at the front peak which was diluted by including a plug of deionised water between the reagent and the sample. At the rear boundary a higher degree of sample reagent mixing occurred by allowing them to mix directly and this enabled a calibration curve for higher concentrations of analyte to be constructed. A similar approach was adopted by *Alonso-Chamarro et al.*[199] This time, however, the sample was sandwiched between the same reagent but the reagents were at different concentrations. The lower concentration of reagent preceded the sample and the higher concentration of reagents followed. The lower range calibration curve was again produced from the response at the front boundary peak and the higher range from the rear boundary peak.

Two review papers also cover sandwich techniques in flow injection. In the first *Luque de Castro*[200] considers using a coupled valve system for both simultaneous determinations and for the introduction of calibration standards with the sample. The manifold is one of several considered for continuous monitoring of process

streams to give real time feedback on the status of the process. In a comprehensive review by *Kuban*[93] on simultaneous determination of several components by flow injection, several approaches to multidetection are discussed including manifolds containing both sixteen and eight-port rotary valves. The sandwich technique is only one of several considered for use in multidetection and several special modules are also covered.

Indirect amperometric and spectrophotometric methods in which a reagent (monitorand) is formed on-line and reacted with the determinand have previously been reported by *Fogg et al.*[70-72] When both large and small volume injections are made into a carrier stream, two separate injections are needed to obtain the full monitorand signal and the reduced signal in the presence of the determinand. In this present study the C>B>A> sandwich configuration has been used to obtain two signals, the full (control) monitorand signal at the front reaction boundary and the reduced signal in the presence of the determinand at the rear boundary from a single injection.

5.2. Experimental

The flow injection manifold was modified as shown in Figure 5.1. by including a three-way valve in the carrier line. The experimental procedure given in 2.4.1. was followed, but was modified so that an acidified sulphite sample could be introduced through the three-way valve. For the sandwich technique, the three-way valve was turned from the carrier to sample when the stream-switching valve was turned from the carrier to the injectate line. The process was reversed when the stream-switching valve returned from the injectate line to the carrier line. At present the stream-switching valve is under computer control while the three-way valve is manually operated. The composition of the sandwich bolus that is produced by the above procedure is shown in Figure 5.2. An 8 µl flow-cell was used with forward flow and the signals were recorded on the diode-array spectrophotometer.

The bromine formed on-line was monitored at 393 nm and the absorbance signal from the RI component was monitored at 550 nm. Similarly iodine formed on-line was monitored at 352 nm and its RI component was monitored at 500 nm. Three replicate signals were recorded for each sample at both the monitorand and RI wavelengths. Carrier and injectate solutions were prepared by diluting the stock solutions given in section 2.3.

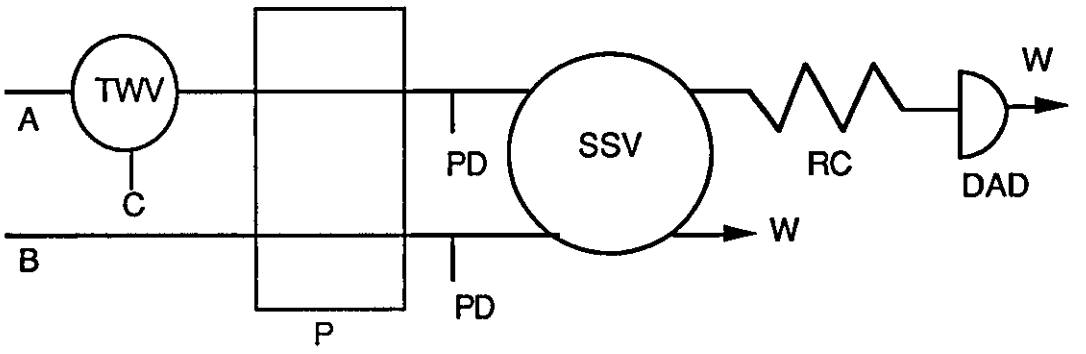

FIGURE 5.1. **Flow injection manifold for the indirect determination of sulphite using the sandwich technique. A is the carrier, B is the injectate, C are the acidified sulphite standards, TWV is the three-way valve, P is the peristaltic pump, PD are pulse dampers, SSV is the stream-switching valve, RC is the 3 m reaction coil, DAD is the diode-array detector and W is the waste.**

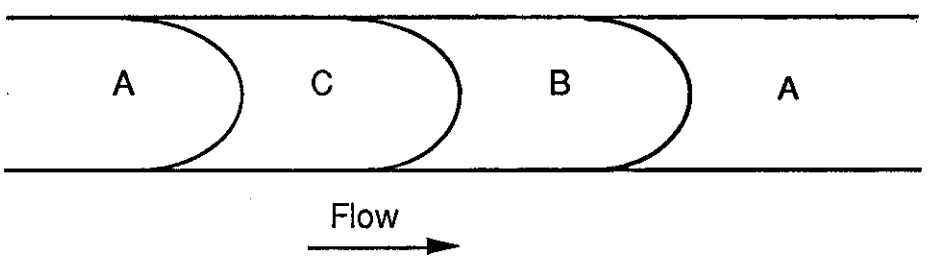

FIGURE 5.2. **Composition of the sandwich bolus flowing through the manifold. A, B, and C are as given above in figure 5.1.**

The composition of the carrier and injectate solutions used for both on-line bromine and iodine formation are given below in Table 5.1.

For on-line bromine formation

- (1) Carrier, 1 M H^+ (blank solution providing in combination with (3) the fully formed monitorand signal).
- (2) Samples, 1 M HNO_3 acidified sulphite solutions (introduced as discrete slugs into the carrier line).
- (3) Injectate, 0.03 M Br^- and $5x10^{-3}$ M BrO_3^-.

For on-line iodine formation

- (4) Carrier, 0.1 M H^+ (the blank solution providing in combination with (5) the fully formed monitorand signal).
- (5) Samples, 0.1 M HNO_3 acidified sulphite solutions (as for (2) above).
- (6) Injectate, 0.23 % m/v I^- and $2x10^{-5}$ M IO_3^-.

TABLE 5.1. Carrier and injectate solution compositions

5.3. Results and discussion

The operation of the two valve configuration of the manifold gave a sandwich bolus which had a composition of A>C>B>A, where A, B and C are as given in Figures 5.1. and 5.2. The sandwich composition is shown diagramatically in Figure 5.2. and the simultaneous valve operation resulted in a 3 cm^3 slug of B followed by a slug of C (fixed but unknown volume) being injected into carrier stream A. The large volume injections ensured that the signals obtained at the front reaction boundary were not affected by dispersion at the rear reaction boundary and vice-versa. The solution compositions used were chosen after a series of preliminary experiments. Addition of sulphite to an acid bromate solution lead to the premature formation of bromine, and addition of acid to iodide leads to premature iodine formation. These considerations were therefore taken into account when deciding on the solution compositions and for continuity a similar composition of solutions were used for both bromine and iodine formation.

The results for the sandwich technique are shown in Figures 5.3. and 5.4. using bromine and iodine as the monitorands respectively. In both cases the fully formed monitorand signal appeared at the first reaction boundary between A and B, and the reduced (determinand) signal appeared at the rear reaction boundary between B and C. No signals above the baseline were obtained for the boundary between C and A at any of the wavelengths used (393 nm and 352 nm for the monitorands, and 550 nm and 500 nm for the RI components). When iodine was used as the monitorand various wavelengths other than 500 nm were used for RI correction, but no difference in the signals at 500, 550 and 600 nm were observed, and so 500 nm was used. *Monks et al.*[201] have reported that iodine as I_2 absorbs at 460 nm and triiodide (I_3^-) absorbs at 285 and 350 nm: therefore triiodide was the species monitored in the work here. Triiodide has a far higher molar absorptivity than iodine and it can be formed from the disproportionation of iodine[201]. In the solutions used the equilibrium is strongly biased to I_3^- formation and the contribution of I_2 is negligible. 500 nm could therefore be used for RI correction without any appreciable effect from I_2 formation.

The results for the sulphite determination using bromine as the monitorand are shown in Figure 5.3., both with and without correction for the absorbance from the RI components. The range of sulphite standards used were between $1x10^{-5}$ M and $2.5x10^{-2}$ M; there was no significant decrease in the height of the rear boundary monitorand peak until a $1x10^{-4}$ M SO_3^{2-} solution was injected, at which point a slight decrease in signal was observed. A rectilinear response to sulphite was obtained between $1x10^{-4}$ M and $5x10^{-3}$ M SO_3^{2-}.The RI corrected signals were lower than the uncorrected signals and at $2.5x10^{-2}$ M SO_3^{2-} the signal was due to the absorbance from the RI component alone (a residual signal of 0.001 A was obtained after RI correction). At no stage was the signal at the rear reaction boundary zero: an RI signal was always obtained. The fully formed bromine monitorand signal at the front reaction boundary was used as a control signal. Any variation in this signal (from instrumental drift or temperature changes) were used to normalise the response at the rear reaction boundary. Two control signals were therefore monitored on each run; the fully formed monitorand signal and the baseline signal from the carrier as it passed through the flow-cell. The results obtained from a blank injection with no sulphite present gave two fully formed monitorand peaks of different height at each reaction boundary at 393 nm, until the absorbance from the RI components at 550 nm were subtracted. Peaks of equal height were then obtained at each reaction boundary which agrees with our earlier work (see chapter 3).

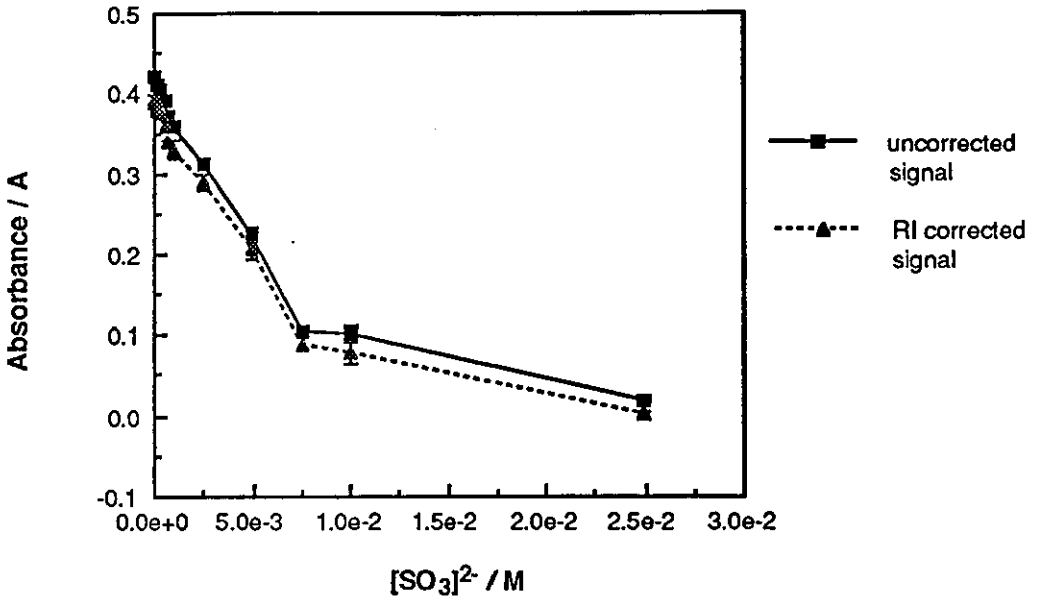

FIGURE 5.3. **Indirect determination of sulphite using bromine as the monitorand by a sandwich technique.**

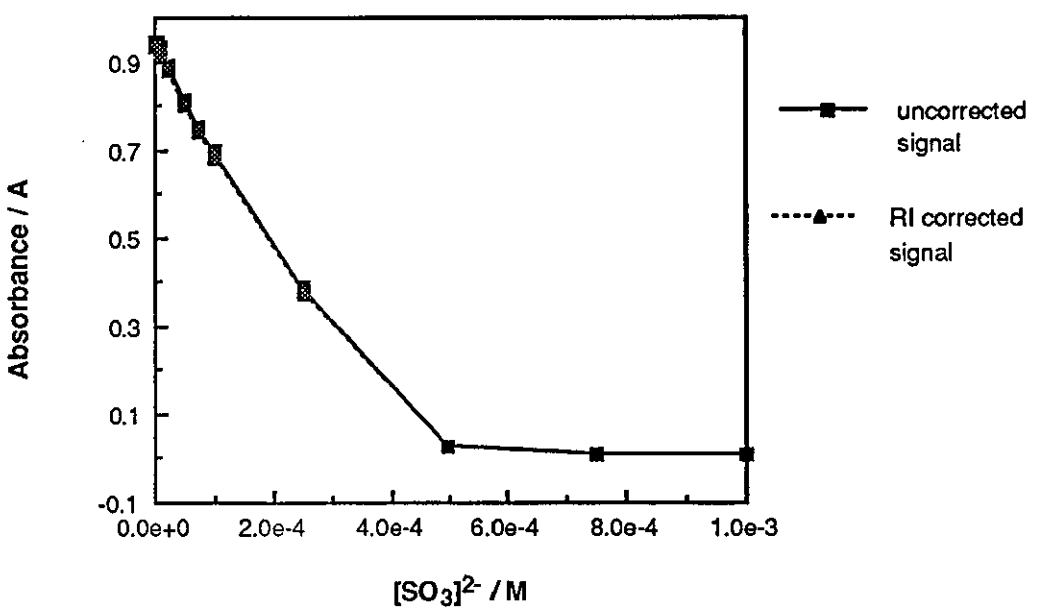

FIGURE 5.4. **Indirect determination of sulphite using iodine as the monitorand by a sandwich technique.**

To increase the sensitivity of the monitorand to lower concentrations of sulphite, the concentration of the bromide/bromate injectate would need to be decreased. This, however, would result in a decrease in the height of the monitorand peak (about 0.4 A at present) which would decrease the precision because of the increase in error associated with the measurement of smaller signals.

An alternative approach was adopted to increase the sensitivity of the technique to lower concentrations of sulphite, the monitorand was changed from bromine to iodine which has a higher molar absorptivity than bromine. As with the bromine system above the fully formed monitorand signal was produced at the front reaction boundary and the reduced signal at the rear. When a blank (reference) solution was run peaks of different height were obtained at each boundary. However, after correcting for the absorbance from the RI components (352 - 500 nm) the peaks at each boundary were still of different height, unlike those obtained above. Factors other than RI must therefore be responsible for the differences in peak heights that were obtained. The front reaction boundary peak could still be used as a control because the ratio of the heights of the two peaks was fixed and any variation could be normalised on that basis.

Figure 5.4. shows the results of the decrease in peak heights (after normalisation) with increasing sulphite concentration, both with and without RI correction. The uncorrected and RI corrected signals are almost identical when iodine is used as the monitorand, but RI correction should be used as its effect will be more pronounced as the signal size decreases particularly at the limit of detection. The range of sulphite standards used were between $1x10^{-6}$ M and $1x10^{-3}$ M SO_3^{2-}. There was no appreciable change in the peak height until the sulphite concentration reached $5x10^{-6}$ M. A rectilinear response to sulphite was obtained over the range $5x10^{-6}$ M to $5x10^{-4}$ M SO_3^{2-}. At $7.5x10^{-4}$ M SO_3^{2-} and above the height of the monitorand signal at the rear reaction boundary reached a minimum which did not alter. The height of the fully formed iodine signal was over twice the size of the bromine signal (1 A in comparison to 0.4 A). This gives a larger leeway to manipulate the concentration of the iodide/iodate injectate to improve the sensitivity of the technique to lower concentrations of sulphite without an appreciable loss in precision.

In Figures 5.3. and 5.4. measurement error bars have been used for three replicate measurements and are shown for a 95 % confidence interval. Because the errors are small they are not clearly shown on either graph for any of the four calibration plots shown.

5.4. Conclusions

The application of the sandwich technique to single boundary measurements in flow injection, involving the use of an indirect method (monitorand/determinand) for the determination of sulphite has been demonstrated. Correction for absorbance due to refractive index effects is recommended in single boundary measurements, whether it is the sole reason for the differences in the peak heights at each boundary or not. This should lead to improved detection limits because as was the case with the bromine system, it will determine whether the signal obtained is due to a refractive index component alone.

A future modification to the manifold would be the inclusion of an eight-port rotary valve used by *Alonso* and co-workers[77,79,191]. This would simplify the manifold because only one valve would be needed to inject a sandwich sample bolus. Reducing the volume of the injected bolus to produce signals similar to those obtained by *Araujo et al.*[191], where the two peaks are not baseline resolved(or alternatively as with the work of *Alonso et al.*[79] one peak with a second peak as a shoulder preceding or following the main peak) would improve sample throughput, which is a major drawback of the current system. It would also be interesting to observe the effect of sample volume on the signals obtained by extending the work of *Araujo et al.*[191] to monitor the total iron and Cr(VI) at their respective λ_{max} as well as the wavelength used over a wider range of sample volumes (0.25 to 3 cm^3).

CHAPTER 6

INFLUENCE OF KINETICS AND REACTION TIME ON THE PEAKS OBTAINED IN SINGLE BOUNDARY MEASUREMENTS

6.1. Introduction

Double peaks are produced in single boundary measurements in flow injection when large volume injections are made. Several workers have utilised this technique for simultaneous determinations of more than one analyte per injection, although they do not refer to the technique as single boundary measurements. *Betteridge and Fields*[202] using a 1.25 cm^3 injection to obtain a pH gradient between the sample and the carrier stream simultaneously determined Pb(II) and V(V) using a colorimetric reagent (4-(2-Pyridylazo)resorcinol). The signal obtained consisted of three peaks the first and third peaks were used for the determination of Pb and the central peak was used for the determination of V. The gradient was formed by injecting an acidic sample into a basic carrier stream; an acidic pH was therefore obtained at the centre of the sample bolus (better condition for V determination). The pH at the interfaces between the sample bolus and carrier stream were less acidic and two peaks were therefore produced either side of the V peak that could be used for the determination Pb.

In an early review on simultaneous determinations in flow injection, *Luque de Castro and Valcarcel Cases*[203] describe several manifolds which can be used to produce more than one signal. These manifolds include those containing more than one detector (both in series and in parallel configurations), multiple injectors and zone splitting/recombination. In the latter the sample is split after the injector and the sub-samples travel through different lengths of tubing before being recombined prior to entering the detector. A manifold using a large injection volume is also described. *Krug et al.*[90] used a commutator (perspex blocks that slide across each other in a linear manner rather than in a rotary movement) to produce multiple peaks by both zone sampling and multiple injections.

Perez Pavon et al.[204] describe a novel injection method for three separate simultaneous determinations, thorium and uranium, Fe(II) and Fe(III) and nitrate and nitrite. A reverse injector loading technique was used, in which the sample was eluted from the sample loop in the opposite direction from which it was loaded. A reduction column was included in the sample loop and experimental parameters were optimised so that the signal obtained consisted of the main peak

preceded or followed by a flatter plateau or shoulder. This technique produces signals similar to those obtained by the sandwich technique described in chapter 5 section 5.1. *Romero-Saldana et al.*[205] describe two designs of manifold for simultaneous kinetic determinations in flow injection in which two signals are produced from one injection by allowing the sample to react with the reagents for two different reaction times. The manifolds are of the zone splitting/recombination configuration, but differ from the conventional design because the valve is used to split the sample (not the manifold itself as described above) so that two signals are obtained because the sample has to travel two different distances from the valve to the detector.

Fernandez et al.[206] describe three manifolds for the simultaneous determination of Ni and Co using differential kinetics: using a single sample injection a double peak was obtained for all three manifold designs. Two of the manifolds employ multidetection (in series and in parallel configurations) to produce the double signal. The third design is a zone splitting/recombination manifold where the sample is split after the injector and recombined at a confluence point before the detector. The group continued the work on zone splitting/recombination, by investigating the two peak output obtained by injecting a dye solution into the manifold: this enabled the evaluation of the geometric and hydrodynamic characteristics of the manifold[41].

In a second paper on the simultaneous determination of Ni and Co using differential kinetics, *Fernandez et al.*[187] modified their procedure by injecting a large sample volume (1 cm^3) into a single-channel manifold. A double peak was obtained and the workers show the position of the double peaks overlaid on the signal obtained from the injection of a preformed metal/complex solution. As the reaction time for the on-line formation of the metal/complex increases the rear peak increases in magnitude and appears partly outside the broad flat topped signal obtained by the injection the preformed complex. In a third paper by *Fernandez et al.*[207] a third option for simultaneously determining Ni and Co by differential kinetics is given. The proposed manifold contains two injection valves arranged in series and use of this manifold also produces a double peak output.

Whitman et al.[76] use double peak formation to determine simultaneously Ni(II) and Fe(II). The Fe(II) was firstly reduced to Fe(III) and this gave a double peak response. Ni gave a large broad peak which could be measured directly by monitoring the signal from the centre of sample bolus. The Fe was monitored at

the second peak and corrections for Ni absorbance were required to obtain the signal from the Fe alone. *Erickson et al.*[108] have used a large volume injection to form double peaks on-line and propose a self-modelling curve resolution method to determine phenolphthalein at the rear boundary peak from a high background signal created by the presence of methyl violet in the mixture. The method is proposed for the resolution of complex spectra in which the matrix has a high background signal that interferes with the determination of the analyte.

The above is a brief review of double peak (single boundary) signals in flow injection. In this chapter the effects of reaction kinetics and the degree of on-line analyte formation on the position of the peaks obtained in relation to those obtained from the injection of preformed analyte complexes are reported.

6.2. Spectrophotometric measurements

6.2.1. Introduction

In their paper on the simultaneous kinetic determination of Ni and Co *Fernandez et al.*[187] introduced a large sample bolus, so that two peaks were obtained from the on-line reactions occurring at the extremities of the bolus, separated by an unmixed zone. When the authors injected a preformed metal complex a large flat topped broad peak was obtained. The authors noted the effect of reaction kinetics on the position of the two peaks formed by the on-line reaction, when compared with the response obtained from the injection of the preformed metal complex. As the reaction rate increased the magnitude and width of the rear boundary peak increased so that it was outside the envelope formed by the injection of the preformed complex. The height and width of the front boundary peak also increased but the peak did not appear outside the envelope formed by the injection of the preformed complex.

In this study on the effect of reaction kinetics on the position of reaction products formed on-line when compared with the response from the injection of a preformed complex at the same component concentration as used for the on-line reaction are reported. The experiment follows the work the of *Fernandez et al.*[187] and the complexes of Ni and Co with 2-hydroxybenzaldehyde thiosemicarbazone (HBAT) were used in this study. The formation of the Ni HBAT complex has a relatively fast rate constant (0.092 s^{-1}) while the reaction rate for formation of the Co HBAT complex is slower (0.221 min^{-1}), because the reaction is preceded by the oxidation of Co(II) to Co(III). Additionally the effects of the degree of on-line

analyte formation were studied by using the results from chapter 4 (section 4.3.) for the experiments with different lengths of coiled reactors. Information for both on-line reactions and the injection of a preformed analyte had been obtained during that experiment.

6.2.2. Experimental

The experimental procedure given in 2.4.1. was again followed using the manifold shown in Figure 2.1. The 8 µl flow-cell was used with forward flow and the signals (at 400 nm) were recorded on the double beam spectrophotometer. Additionally the diode-array spectrophotometer was used to record the signals from the coiled reactor experiments and details of the equipment, solutions and procedures used for that experiment are given in chapter 4, section 4.3. The solutions given in Table 6.1. were prepared by dilution of the stock solutions, for analysis both as on-line reactants and as preformed complexes.

In all of the solutions containing HBAT and acetate buffer, the composition of the solutions were 20% v/v ethanol and 20% v/v buffer. The higher concentrations of HBAT were used by *Fernandez et al.*[187] for the individual determination of Co (0.018% m/v HBAT) and Ni (0.015% m/v HBAT), while the 0.010% m/v HBAT level was used for the simultaneous determination of the two metals. The Co study was made at two pH levels because the rate of reaction was affected by pH. Results were therefore obtained for metal complex formation at three reaction rates.

For the on-line reactions the Ni solution (5) was injected into carriers (2) and (4), and the Co solution (6) was injected into carriers(1), (3) and (4). For the injection of the preformed metal complexes the carrier was chosen to match the pH of the buffer and the concentration of HBAT, i.e. solution (7) was injected into carrier (1) etc.

- (1) Carrier, 0.018% m/v HBAT and acetate buffer pH 5.8
- (2) Carrier, 0.015% m/v HBAT and acetate buffer pH 5.2
- (3) Carrier, 0.010% m/v HBAT and acetate buffer pH 5.8
- (4) Carrier, 0.010% m/v HBAT and acetate buffer pH 5.2

For on-line metal complex formation

- (5) Injectate, 10 mgl^{-1} Ni
- (6) Injectate, 2.5 mgl^{-1} Co

For the preformed metal complexes

- (7) Injectate, 2.5 mgl^{-1} Co, 0.018% m/v HBAT and acetate buffer pH 5.8
- (8) Injectate, 10 mgl^{-1} Ni, 0.015% m/v HBAT and acetate buffer pH 5.2
- (9) Injectate, 10 mgl^{-1} Ni, 0.010% m/v HBAT and acetate buffer pH 5.2
- (10) Injectate, 2.5 mgl^{-1} Co, 0.010% m/v HBAT and acetate buffer pH 5.2
- (11) Injectate, 2.5 mgl^{-1} Co, 0.010% m/v HBAT and acetate buffer pH 5.8

TABLE 6.1. Carrier and injectate solution compositions used for the study of the effects of reaction kinetics on peak positions

6.2.3. Results and discussion

A wavelength of 400 nm was chosen to monitor the metal complexes after obtaining spectra of solutions (1), (7) and (8) and an additional solution where the Ni concentration was lowered to 5 mgl^{-1}. The spectra were obtained on a scanning spectrophotometer over the wavelength range 200 to 800 nm using a 2.0 nm bandpass and Figure 6.1. shows the spectra as overlaid plots. It can be seen that below 360 nm the HBAT/buffer solution (1), absorbs strongly and this would prevent any data being obtained from the metal HBAT complexes at 360 nm or at lower wavelengths.

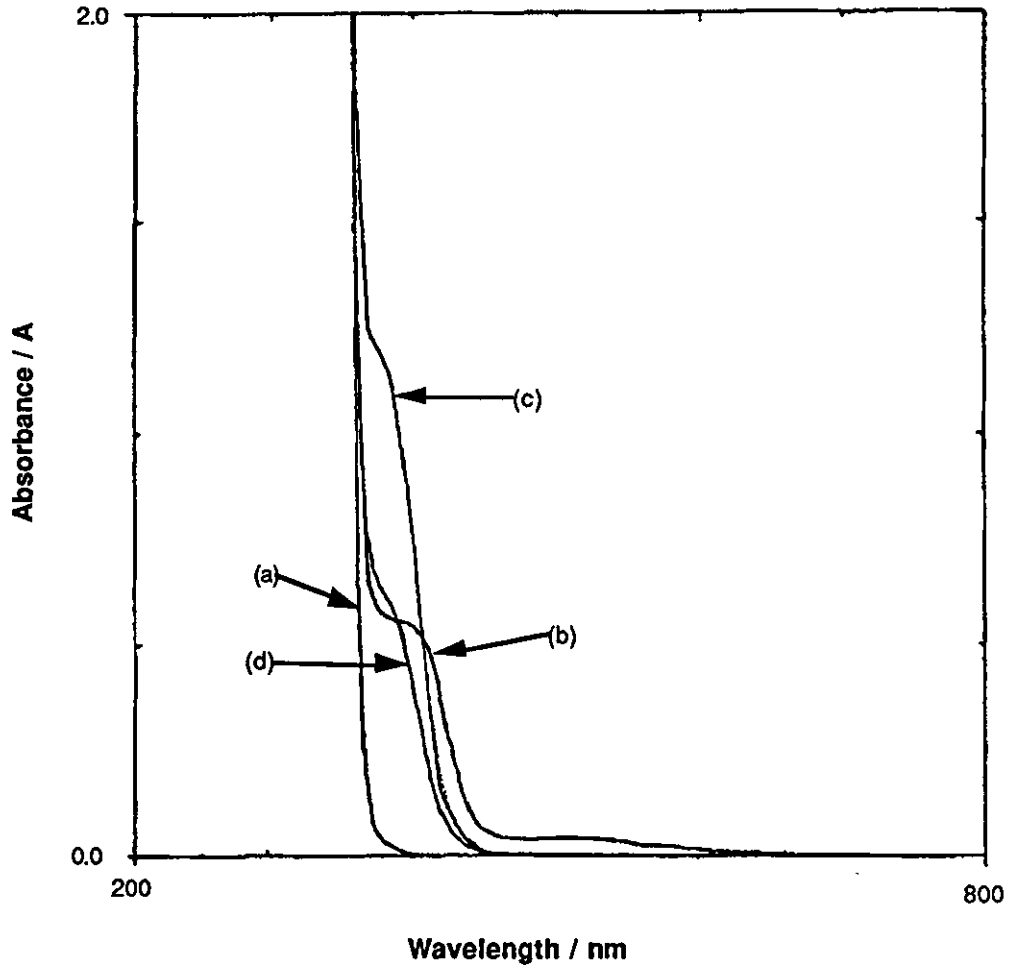

FIGURE 6.1. **UV/vis spectra of HBAT, Ni/HBAT and Co/HBAT; bandpass 2.0 nm, scan rate 2000 $nmmin^{-1}$, using a 1 cm path length quartz cell. (a) 0.18% m/v HBAT in pH 5.8 acetate buffer (blank); (b) blank and 2.5 mgl^{-1} Co ; (c) blank and 10 mgl^{-1} Ni ; (d) blank and 5 mgl^{-1} Ni.**

The results for the injection of the preformed metal complexes and for the on-line formation of the metal complexes are given in the following Table and Figures. The Figures were produced by tracing the chart recorder output for the injection of the preformed metal complexes and for the signals obtained from the metal complexes formed on-line. Tracing the figures was the only method of overlaying the signals for the injection of preformed complexes onto the signals obtained for the same reaction on-line. The results in Table 6.2. are given for t_a (peak appearance time) and t_w (peak washout time) for the preformed complexes, but the t_a values are given for the front boundary peak and the t_w values for the rear boundary peak for the complexes formed on-line. This should determine the position of both boundary peaks formed on-line, in relation to the position of the broad peak formed by the injection of the preformed metal complexes of the same reagent composition as used for the on-line reactions.

In all of the results obtained to date, which repeat the work of *Fernandez et al.*[187], the peaks formed by the on-line reactions did not appear outside the envelope formed by the injection of the preformed metal complexes to the extent shown by the previous workers. In our work the front boundary peak appeared just outside the envelope for the preformed complex for the on-line formation of the Co HBAT complex (see Figures 6.2. and 6.3.). This is the opposite to what has been shown previously, the front boundary peak rise curve is only slightly greater than that of the preformed metal complex containing the same components at the same concentrations and could easily be the result of experimental error (e.g. chart recorder sticking). The results for the Ni HBAT complex which has a faster reaction rate than the Co complexes, show that both boundary peaks from the on-line reaction are formed within the envelope recorded from the injection of the preformed complex (see Figure 6.4.).

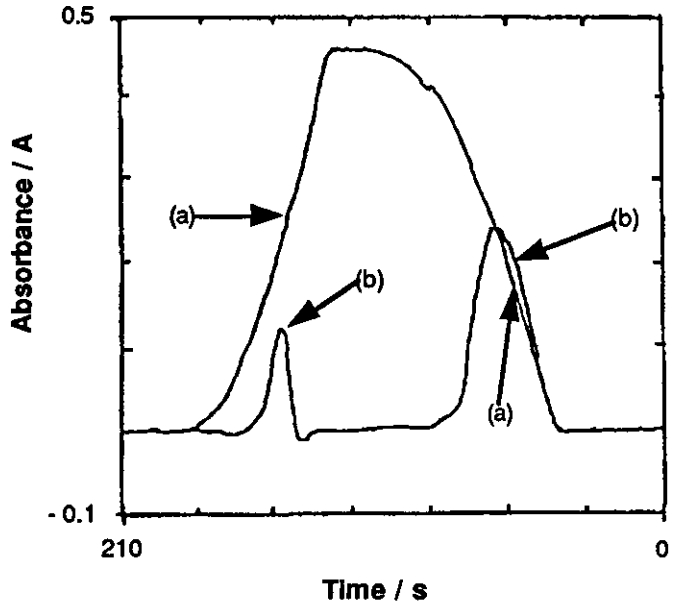

FIGURE 6.2. **Signals obtained at 400 nm for the formation of Co/HBAT as (a) preformed complex and (b) on-line reaction. Carrier 0.010% m/v HBAT in pH 5.2 acetate buffer ; Injectates (a) carrier and 2.5 mgl^{-1} Co ; (b) 2.5 mgl^{-1} Co.**

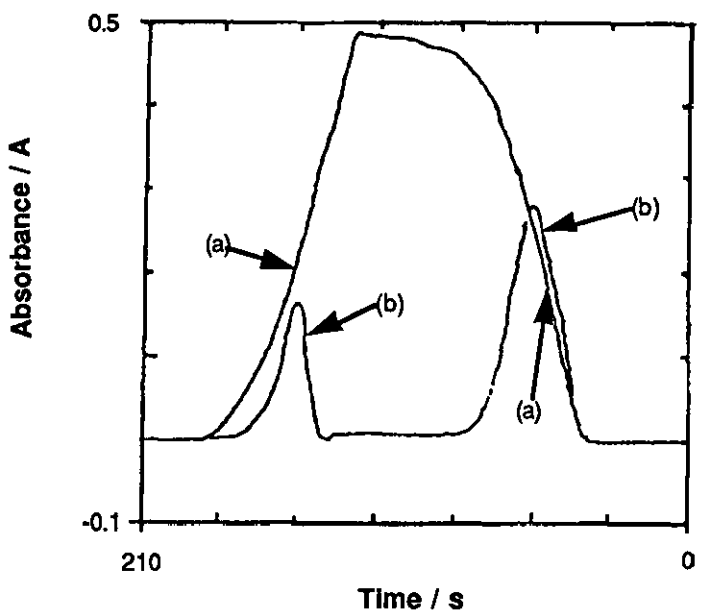

FIGURE 6.3. **Signals obtained at 400 nm for the formation of Co/HBAT as (a) preformed complex and (b) on-line reaction. Carrier 0.010% m/v HBAT in pH 5.8 acetate buffer ; Injectates (a) carrier and 2.5 mgl^{-1} Co ; (b) 2.5 mgl^{-1} Co.**

Carrier*	Injectate*	t_a (s)	t_w (s)	Δt (s)
(1)	(7)	45 ± 0.6	190 ± 2.1	145 ± 2.7
(1)	(6)	41 ± 1.0	171 ± 2.6	130 ± 3.6
(2)	(8)	42 ± 0.7	206 ± 1.5	164 ± 2.2
(2)	(5)	42 ± 0.6	188 ± 1.9	146 ± 2.5
(3)	(11)	43 ± 1.2	191 ± 1.7	148 ± 2.9
(3)	(6)	41 ± 1.0	179 ± 4.4	138 ± 5.4
(4)	(9)	43 ± 1.7	201 ± 2.4	158 ± 4.1
(4)	(5)	42 ± 0.7	169 ± 2.1	127 ± 2.8
(4)	(10)	43 ± 1.2	192 ± 0.7	149 ± 1.9
(4)	(6)	41 ± 0.6	183 ± 1.2	142 ± 1.8

* Carrier and injectate composition as given in Table 6.1. (n = 5 for all injections).

TABLE 6.2. Peak appearance and peak washout times for Co and NI HBAT complexes formed on-line and as preformed complexes.

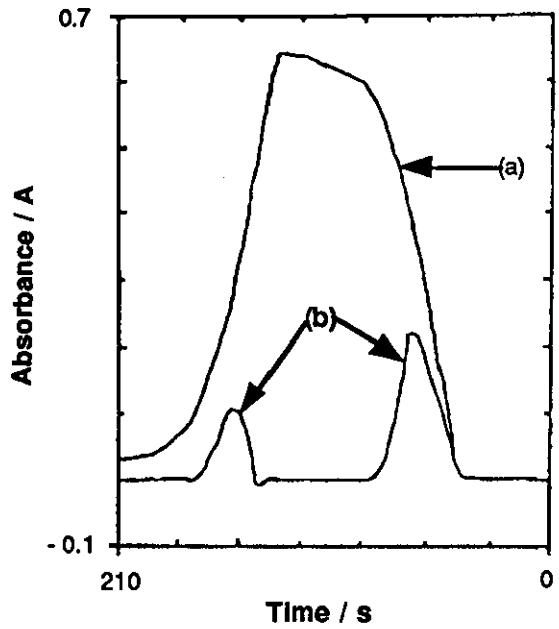

FIGURE 6.4. Signals obtained at 400 nm for the formation of Ni/HBAT as (a) preformed complex and (b) on-line reaction. Carrier 0.010% m/v HBAT in pH 5.8 acetate buffer ; injectates (a) carrier and 10 mgl^{-1} Ni ; (b) 10 mgl^{-1} Ni.

The results for Δt in Table 6.2. and for Figures 6.2. to 6.4. show that the rear boundary peak is formed within the envelope from the injection of the preformed metal complex at all of the conditions used. The Δt values are always less for the on-line reaction than for the injection of the preformed metal complexes. Results for the systems with higher HBAT concentrations are not plotted, but do follow the trend shown in Figures 6.2. to 6.4. The magnitude of the signals are increased by increasing the HBAT level but the position of the peaks formed at each reaction boundary follow those given above for Ni and Co HBAT complexes at 0.010% m/v HBAT.

Reaction kinetics do affect the shape of the signals obtained in flow injection. The front peak obtained for the on-line formation of Ni HBAT complex were much sharper (steeper rise and fall curves) than those obtained for the Co HBAT complexes at both of the concentrations used (compare Figure 6.4. with Figures 6.2. and 6.3.). *Wada et al.*[208] also report that sharper peak profiles were obtained for a Cu 2-(2-thiazolylazol)-4-methyl-5-(sulfomethylamino)benzoic acid (TAMSMB) complex than for a Ni TAMSMB complex. The TAMSMB reacts very

quickly with Cu(II) and much more slowly with Ni(II) and our results agree with their work.

Figure 6.5. shows the response obtained from injecting a preformed Co HBAT complex into a carrier stream of deionised water and an overlaid plot of the response for the injection of the preformed complex into a HBAT/buffer carrier stream. The peak on the plateau before the response begins to decay was found to be due to changes in RI as the ethanol in the injectate mixed with the water carrier stream. A blank injection of HBAT/buffer carrier into deionised water carrier stream produced a double peak response where the rear boundary peak was higher than that obtained at the front (0.115 A and 0.051 A respectively). The need for RI correction if the carrier and injectate streams differ sufficiently in RI is again made apparent. For our measurements in this work, the RI of both streams were matched having the same concentration of both buffer and HBAT. One final anomaly was observed in this work. The preformed Ni HBAT complex tended to coat the inside of the flow-cell and did not return to the original baseline at the end of the injection (see Figure 6.4.). The manifold was therefore flushed with deionised water between injections of the preformed Ni HBAT complexes to overcome this problem with an increase in the time required to perform replicate measurements.

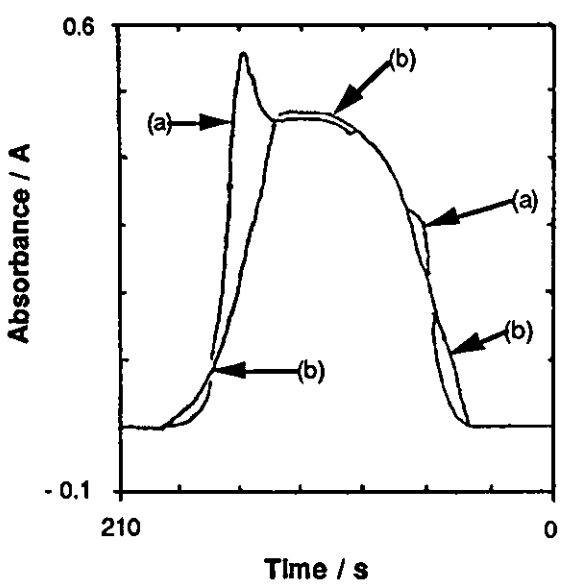

FIGURE 6.5. **Signals obtained at 400 nm for the injection a preformed Co/HBAT complex into different carrier streams. Injectate 2.5 mgl^{-1} Co and 0.010% m/v HBAT in pH 5.2 acetate buffer ; Carriers (a) deionised water ; (b) 0.010% m/v HBAT in pH 5.2 acetate buffer.**

The above section deals with the effects of reaction kinetics on the shape and position of the peaks obtained from on-line reactions. In chapter 4, section 4.3. the range of reaction coils used for the on-line formation of bromine was varied from 10 m to 0.5 m in 0.5 m increments. Results were therefore obtained for different degrees of on-line analyte formation, which would decrease as the length of the coiled reactor was decreased. Figures 6.6. to 6.9. show the response from the on-line formation of bromine overlaid on the response for the injection of preformed bromine at four lengths of coiled reactor. The length of the coiled reactors shown are 1.0, 3.0, 5.0 and 9.0 m for Figures 6.6. to 6.9. respectively. In all of the cases shown neither of the peaks formed during the on-line reaction penetrate the envelope formed by the injection of the preformed bromine. The magnitude of the signals for the products formed on-line increase with increasing reaction coil length but even at 9.0 m there is no penetration of the envelope formed by the injection of the preformed bromine. Only four examples are shown from the experiments for the coiled reactor but the observation was the same for all lengths of coiled reactor used.

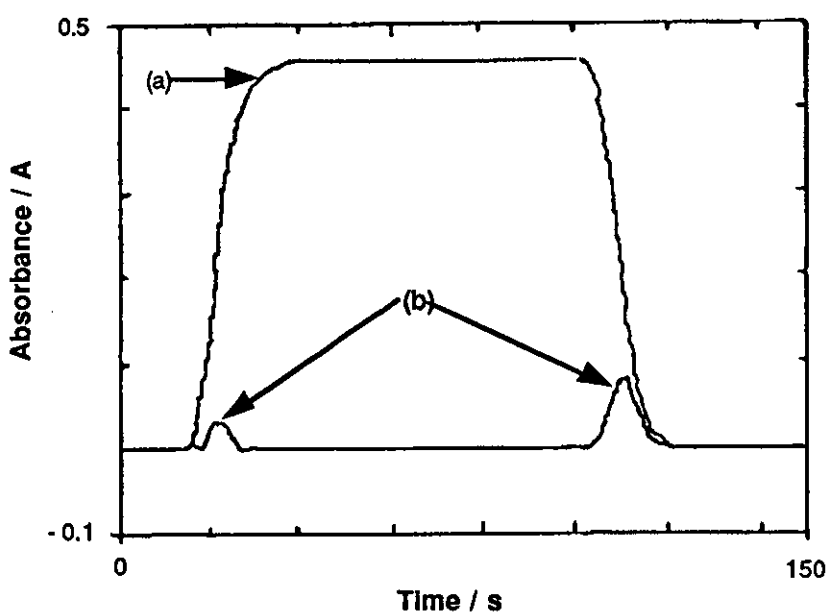

FIGURE 6.6. **Signals obtained at 393 nm for the formation of Br_2 as (a) preformed Br_2 and (b) on-line reaction; using a 1.0 m coiled reactor in the manifold. (a) Carrier deionised water ; injectate $5x10^{-4}$ M BrO_3^- and 0.3 M Br^- ; (b) Carrier 1 M H^+ ; injectate $5x10^{-4}$ M BrO_3^- and 0.3 M Br^-.**

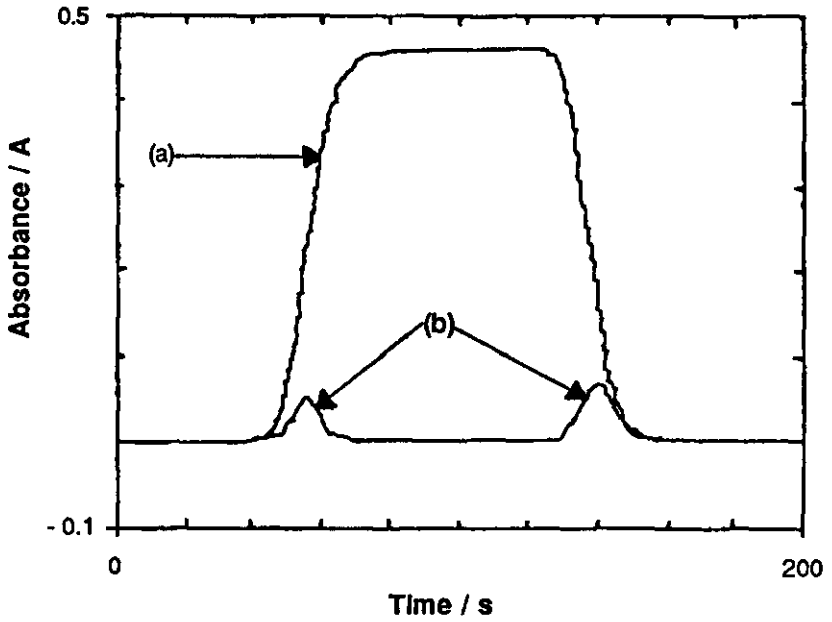

FIGURE 6.7. Signals obtained at 393 nm for the formation of Br_2 as (a) preformed Br_2 and (b) on-line reaction; using a 3.0 m coiled reactor in the manifold. (a) Carrier deionised water ; injectate $5x10^{-4}$ M BrO_3^- and 0.3 M Br^- ; (b) Carrier 1 M H^+ ; injectate $5x10^{-4}$ M BrO_3^- and 0.3 M Br^-.

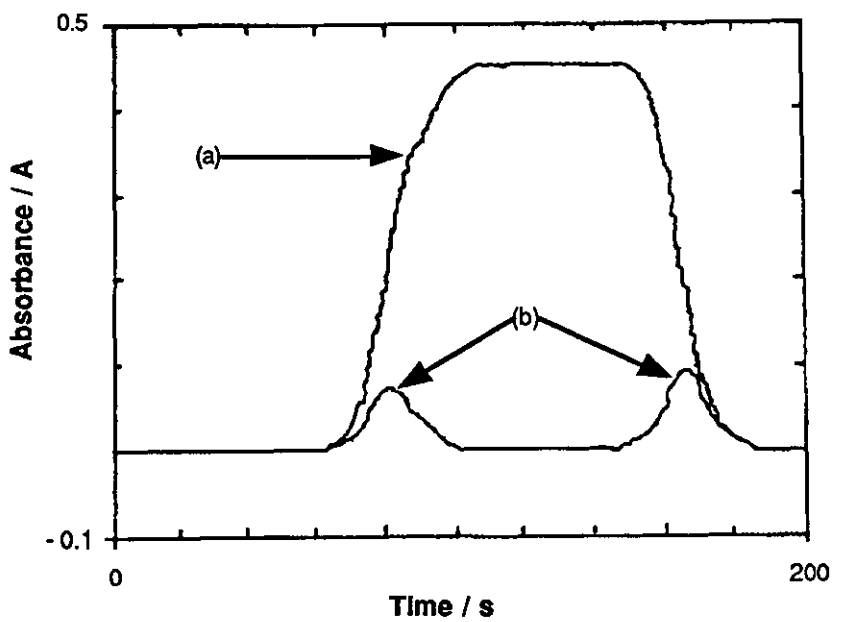

FIGURE 6.8. Signals obtained at 393 nm for the formation of Br_2 as (a) preformed Br_2 and (b) on-line reaction; using a 5.0 m coiled reactor in the manifold. (a) Carrier deionised water ; injectate $5x10^{-4}$ M BrO_3^- and 0.3 M Br^- ; (b) Carrier 1 M H^+ ; injectate $5x10^{-4}$ M BrO_3^- and 0.3 M Br^-.

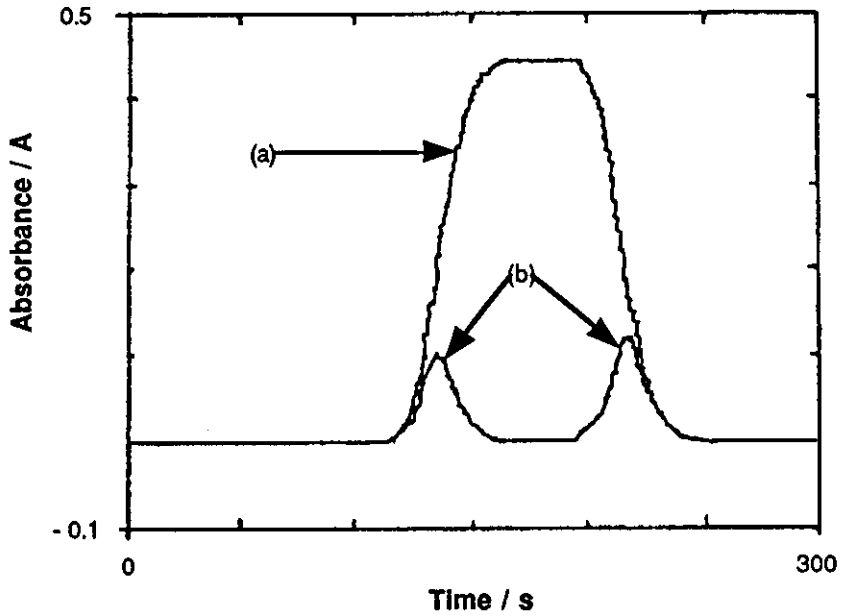

FIGURE 6.9. **Signals obtained at 393 nm for the formation of Br_2 as (a) preformed Br_2 and (b) on-line reaction; using a 9.0 m coiled reactor in the manifold. (a) Carrier deionised water ; injectate $5x10^{-4}$ M BrO_3^- and 0.3 M Br^- ; (b) Carrier 1 M H^+ ; injectate $5x10^{-4}$ M BrO_3^- and 0.3 M Br^-.**

6.3. Electrochemical detection

6.3.1. Introduction

The work in the preceding section dealt with the position of peaks formed by an on-line reaction, relative to the position of a broad single peak formed by the injection of the same analyte as a preformed complex. *Fogg and Zhao*[72] have reported that when monitoring bromine formed on-line using amperometric detection, that the rear boundary peak penetrated the envelope formed by the injection of a preformed bromine solution. Their observation are similar to those of *Fernandez et al.*[187] for the Co HBAT complex, and do not agree with our results for the metal HBAT complexes or for the spectrophotometric detection of bromine. The work of *Fogg and Zhao*[72] was repeated here to find an explanation for the differences in these results and to decide whether electrochemical detection makes any contribution to the position of peaks formed on-line in relation to that formed by the injection of preformed analytes.

6.3.2. Experimental

The experimental procedure given in 2.4.1. was again followed, using the manifold shown in Figure 2.1. The detector was changed from spectrophotometric to electrochemical and details of the cell and associated apparatus are given in 2.2.2. All three solution combinations given in Table 3.1. at the concentrations given in 3.2.2. were again studied and preformed bromine solutions (see 3.2.2.) were also studied. An additional set of solutions where the concentration of bromide was changed from 0.03 M to $3x10^{-3}$ M Br^- were also used.

The glassy carbon working electrode was polished daily using an alumina polishing pad, followed by washing with deionised water and finally drying with a clean piece of tissue paper. A supporting electrolyte solution of 0.1 M KCl was placed in the beaker containing the three electrodes and the effluent from the flow injection manifold entered the beaker through the x-shaped outlets on the lower body of the working electrode holder. Five replicate readings were recorded for each injectate used.

6.3.3. Results and discussion

The hydrodynamic voltammogram of bromine formed on-line (Figure 6.10.) was used to decide the best potential for monitoring bromine in single boundary measurements with electrochemical detection. For both front and rear boundary peaks a potential of 0.00 V was chosen because the separation between the signal from the analyte formed on-line and the background signal was greatest at this potential. The background signal was obtained by measuring the deflection from the null position when the circuit was switched from off, to open with the carrier solution alone flowing over the working electrode.

The rear boundary signal was always higher than that obtained at the front reaction boundary (see Figure 6.10.) for the carrier injectate combination used to obtain the data for the hydrodynamic voltammogram. Refractive index changes will not effect electrochemical measurements, so the differences in the height of the two peaks may be due either to a contribution of the detector cell or to differences in the diffusion of the analyte species formed on-line. Both reaction boundaries have to travel the same distance from the injection valve to the detector and we have as yet been able to satisfactorily explain why the height of the two boundary peaks are different.

Figures 6.11. and 6.12. show the signals obtained for bromine on-line and preformed bromine with solutions containing $3x10^{-3}$ and 0.03 M Br^- respectively. With both Figures the peaks formed at each reaction boundary do not appear outside the envelope formed by the injection of the preformed bromine. Two concentrations of bromide were chosen to give two different degrees of on-line bromine formation; in both instances the bromate was the limiting reagent for the on-line formation of bromine. Our results for the electrochemical detection of bromine agree with our earlier results for spectrophotometric detection. In neither case did the peaks formed on-line appear outside the envelope obtained from the injection of the preformed bromine solutions.

Our results do not agree with those of *Fogg and Zhao*[72]. The previous workers used a measurement potential of 0.38 V, which we found was not the ideal potential for monitoring bromine formed on-line. The choice of detection method (electrochemical or spectrophotometric) does not affect the position of the peaks formed on-line, in relation to those formed by injecting the preformed analyte solution.

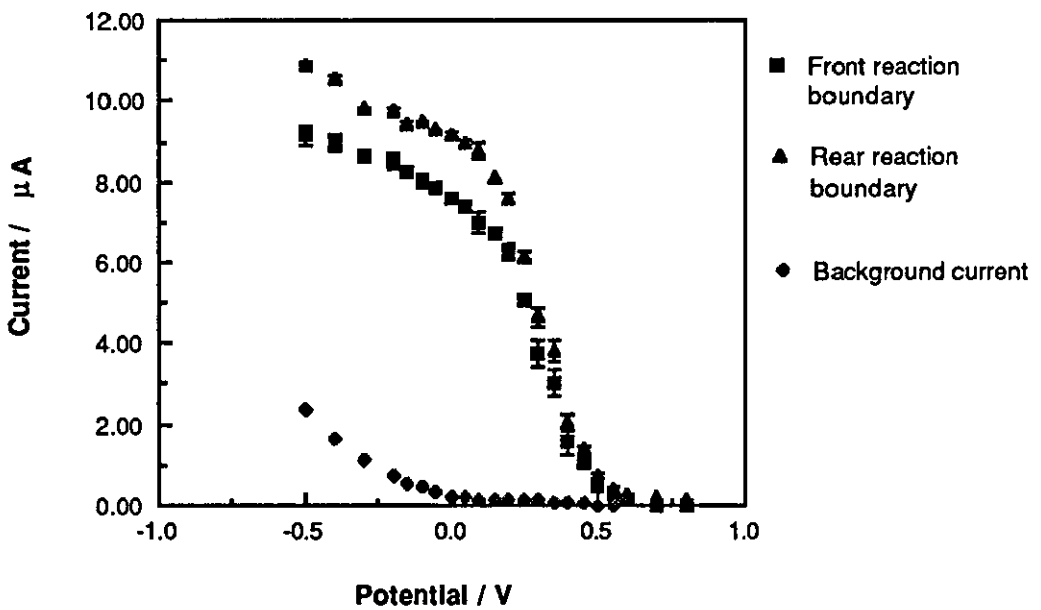

FIGURE 6.10. Hydrodynamic voltammogram of bromine formed on-line using 1 M H^+ and $3x10^{-3}$ M Br^- as the carrier, and $5x10^{-4}$ M BrO_3^- and $3x10^{-3}$ M Br^- as the injectate.

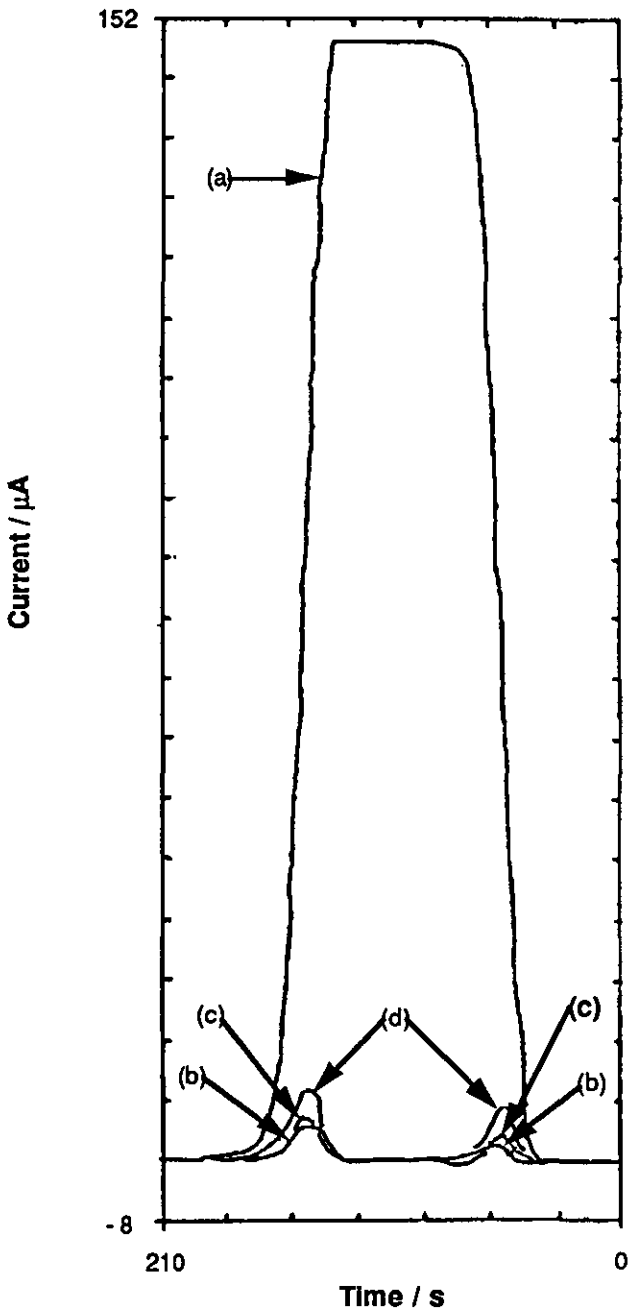

FIGURE 6.11 Signals obtained at 0.0 V for Br_2 as (a) preformed Br_2 and (b) - (d) Br_2 formed on-line. Carrier 1 M H^+ ; Injectates (a) 1 M H^+ and $5x10^{-4}$ M BrO_3^- and $3x10^{-3}$ M Br^- ; (b) $5x10^{-4}$ M BrO_3^- and $3x10^{-3}$ M Br^- ; (c) Carrier 1 M H^+ and $5x10^{-4}$ M BrO_3^- ; Injectate $3x10^{-3}$ M Br^- ; (c) Carrier 1 M H^+ and $3x10^{-3}$ M Br^- ; Injectate $3x10^{-3}$ M Br^- ; (d) Carrier 1 M H^+ and $3x10^{-3}$ M Br^- ; Injectate $5x10^{-4}$ M BrO_3^- and $3x10^{-3}$ M Br^-.

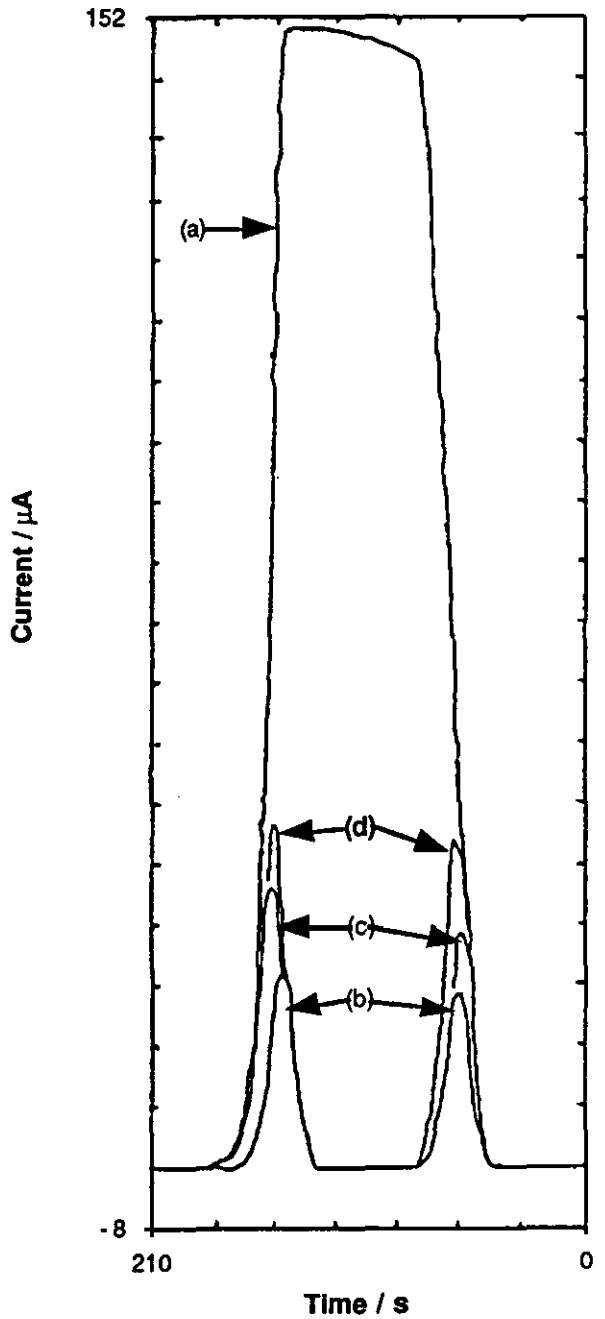

FIGURE 6.12 Signals obtained at 0.0 V for Br_2 as (a) preformed Br_2 and (b) - (d) Br_2 formed on-line. Carrier 1 M H^+ ; Injectates (a) 1 M H^+ and $5x10^{-4}$ M BrO_3^- and 0.03 M Br^- ; (b) $5x10^{-4}$ M BrO_3^- and 0.03 M Br^- ; (c) Carrier 1 M H^+ and $5x10^{-4}$ M BrO_3^- ; Injectate 0.03 M Br^- ; (c) Carrier 1 M H^+ and $3x10^{-3}$ M Br^- ; Injectate $3x10^{-3}$ M Br^- ; (d) Carrier 1 M H^+ and 0.03 M Br^- ; Injectate $5x10^{-4}$ M BrO_3^- and 0.03 M Br^-.

6.4. Electrochemical pretreatment of the working electrode

6.4.1. Introduction

The electrochemical pretreatment of glassy carbon working electrodes has been shown previously to improve electrode performance by producing a less irreversible electrode reaction[126-130,209,210]. *Fogg* and co-workers have shown that pretreatment of the working electrodes are advantageous in the oxidative flow injection determination of sulphite[127], EDTA[130], oxalate[128] and cyanide[126], by increasing the magnitude of the signals obtained and improving the stability of the signals. All of the pretreatment regimes used by *Fogg et al.* above, involved a preanodisation step (hold at > + 1.5 V for 2 to 15 minutes) followed by a precathodisation step (hold at - 0.5 to - 1.0 V for 1 to 2 minutes). The regimes that *Fogg et al.* adopted were based on the work of *Engstrom*[209,210].

Chamsi and Fogg[129] report an improved method for oxidatively determining nitrite by pretreating the electrode using a preanodisation step alone (+ 1.75 V for 5 minutes). The authors studied several pretreatment regimes, including preanodisation/precathodisation and just polishing the electrode in four different solutions. They report that preanodisation in phosphate buffer provided the best conditions for reducing the overpotential and allowing determinations to be made at a less positive potential. *Ghawji and Fogg*[211] have studied the effects of electrode pretreatment on the reductive determination of nitrofurantoin. They report that precathodisation (- 2.7 V for 1 minute) was successful in reducing the background current associated with measurements at high negative potentials, by making the reduction of dissolved molecular oxygen more difficult. This pretreatment regime is useful because it reduces the time spent in sample handling; the samples do not need to be degassed before analysis.

Engstrom[209,210] has suggested that electrochemical pretreatment of the electrodes results in an increase in the number of surface quinone and other groups that may catalyse the oxidation or reduction of the analyte. He has also suggested that contaminants on the electrode surface may be removed by oxidation during preanodisation of the electrode; however, a side effect of pretreatment is an increase in the background current. Precathodisation is needed after a preanodisation step to reduce the oxide layer formed[209,210].

We report the effect of electrochemical pretreatment of a glassy carbon working electrode prior to the determination of bromide formed on-line. This has not been

studied previously, several regimes were used and compared with the response obtained from a freshly polished electrode.

6.4.2. Experimental

The experimental procedure given in 6.3.2. was followed using only one carrier and injectate combination. The carrier was 1 M H^+ and $3x10^{-3}$ M Br^- and the injectate was $5x10^{-4}$ M BrO_3^- and $3x10^{-3}$ M Br^- (the same solution combination that was used to obtain the hydrodynamic voltammogram). The electrode was prepared for use in various ways, firstly it was polished and washed in deionised water then dried on a clean piece of tissue paper. After obtaining the signals from five replicate injections, the electrode was washed with deionised water, dried and used again. Three electrochemical pretreatment regimes were also used after polishing and washing the electrode, with the carrier stream flowing over the electrode:-

- (a) a potential of + 1.75 V was applied for 5 minutes (preanodisation).
- (b) the preanodisation step in (a) was followed by a precathodisation step of - 1.00 V for 1 minute.
- (c) the precathodisation step in (b) was used alone.

Five replicate signals were recorded after each of the electrode treatments used and the results are given in Table 6.3.

6.4.3. Results and discussion

A blank injection of 1 M H^+ into the carrier stream produced no response above the baseline, so the peaks obtained are due to the on-line formation of bromine and not an increase in the acidity.

The results in Table 6.3. show that polishing the electrode alone gave the signals of the highest magnitude at each boundary. The size of the signals was seen to decrease slightly as the replicate injections were made and this response indicates that the electrode surface is changing (being poisoned or passivated) as the number of injections made was increased. The results for washing the electrode indicate that this preparation procedure is not as good as polishing the electrode, because the size of the signals obtained is less. The size of the signals was seen to increase slightly (the opposite effect from the polished electrode) as the

successive injections were made. This suggests that the electrode is being conditioned as the number of runs increases.

Electrochemical pretreatment of the electrode does not improve the response to the bromine formed on-line, nor does it improve the stability of the baseline. The preanodisation (a) treatment gave the worst results for all of the electrode conditioning procedures used. The magnitude of the signals obtained were lower than with any of the other conditioning procedures used and the first signals that were obtained after pretreatment, differed from the subsequent runs and were not included in the Table. The smaller signals that were obtained indicate that whatever functionality has been induced by the pretreatment is inhibiting the detection of the bromine formed on-line (there may be less sites on the electrode surface available for the reduction of the bromine).

Preanodisation followed by precathodisation (b) and precathodisation alone (c) gave similar responses for the on-line formation of bromine, but the signals from the second procedure were lower than those obtained for the first. In both instances the response obtained on the first run after pretreatment contained a small peak before the rear boundary peak and this peak became a shoulder on the rear peak as the number of sequential injections increased. The magnitude of the signals increased slightly during the runs and this again suggest that the electrode is being conditioned on each progressive run. The appearance of a shoulder on the rear boundary peak may indicate that two surface conditions are present on the electrode or that more than one species of analyte is being detected.

		Front Boundary	Rear boundary
Electrode treatment	Duration (minutes)	h_{max} (μA)	h_{max} (μA)
Polished		6.900 ± 0.1141	8.597 ± 0.269
Washed		5.408 ± 0.0516	7.064 ±0.0540
+ 1.75 V	5	3.864 ± 0.1422	5.244 ± 0.0445
+ 1.75 V - 1.00 V	5 1	5.432 ± 0.2188	*1.644 ± 0.1643 7.172 ± 0.2898
- 1.00 V	1	5.076 ± 0.3809	*1.952 ± 0.1424 6.348 ± 0.3123

* a small peak or shoulder was obtained before the rear boundary peak (see text for details) (n = 5).

TABLE 6.3. Peak heights obtained after various electrode conditioning procedures, for the two reaction boundaries formed by injecting $5x10^{-4}$ M BrO_3^- and $3x10^{-3}$ M Br^- into a carrier stream of 1 M H^+ and $3x10^{-3}$ M Br^-.

6.5. Conclusions

In single boundary measurements using a stream switching valve, the degree of on-line analyte formation or the reaction rate of product formation, have no significant influence on the position of the peaks formed on-line when superimposed on the signal obtained from the injection of a preformed analyte. These results do not agree with those of earlier workers[187], and the main difference between our work and theirs was the type of injection used. We believe that they used slug injection and this meant that the peak obtained at the rear reaction boundary would have travelled a longer distance from the valve to the detector and would also have had longer to react and form a complex on-line than that at the front boundary. Allowing a longer reaction time permits a larger degree of on-line analyte formation, which would increase the signal magnitude (h_{max}) and increase dispersion (peak width), the wider an larger signal would then appear outside the envelope formed by the injection of the preformed complex. A further study would be needed with these solutions using slug injection to decide whether this was the reason for the differences in the signals obtained by us and the earlier workers[187].

When using electrochemical detection for bromine formed on-line our results again disagree with those obtained previously[72]. We have not been able to explain the differences in the results. Using a different measurement potential would be expected to give signals of different magnitudes but not to affect the position of the peaks formed on-line.

The electrode conditioning regimes tried offered no advantages over simply polishing the electrode. A wider range of conditions were not investigated because those that were tried did not produce any significant improvement. *Bowers and Yenser*[212] report that cycling the potential between + 0.6 V and much higher positive potentials produced a modified glassy carbon electrode where the redox species were surface confined. Our results indicate that pretreatment at positive potentials (preanodisation) produced the worst response from the electrode. Therefore the approach of *Bowers and Yenser*[212] would be detrimental for this determination.

A more promising approach for electrode pretreatment/conditioning would be the application of a three wave form pulse, of the type used in pulsed amperometric detection (PAD) in liquid chromatography[213-215]. This would be the next area for study and would seem to offer an ideal approach because the pulse could be applied prior to every measurement taken as part of the measurement protocol.

CHAPTER 7

POLY-L-LYSINE MODIFIED ELECTRODES

7.1. Introduction

Modified electrodes are an area of intense research interest in electrochemistry and electroanalytical chemistry. *Merz*[216] has recently reviewed the manufacture of modified electrodes with an emphasis on methods using electrochemical polymerisation and new ion exchanging materials. One of the ion exchanging polymers reviewed was poly-L-lysine which was described as an aminopolymer anion exchanger. Polyelectrolytes may exhibit rather specific properties depending on their morphology; poly-L-lysine appears to have domains filled with solvents where ions can diffuse quite freely. In poly-L-lysine the charge may be propagated by both electron hopping and diffusion of redox sites.

Anson et al.[217] proposed a model for charge transport through the interior of a protonated poly-L-lysine (PLL) coating on a graphite electrode containing $Fe(III)EDTA^-$ and $Fe(II)EDTA^{2-}$ as counterions. The workers state that the coating can be divided conceptually into two regions, "Donnan domains" where counterions are held by electrostatic forces and the remaining volume of the coating is occupied by the supporting electrolyte solution. Experimental data agreed well with the predictions of a two phase model for charge transfer using the reversible $Fe(III)EDTA^-/Fe(II)EDTA^{2-}$ couple. In a second paper *Anson et al.*[218] model the diffusional pathways in the coating by using $Co(III)(C_2O_4)_3^{3-}$ which is irreversibly reduced to $Co(II)(C_2O_4)_3^{4-}$: this Co(II) product is unstable. The use of the irreversible redox counterions prevented electron- or place-exchange reactions occurring within or across the two phases of the coating (these reactions are possible for reversible redox couples). Two diffusional pathways were identified the first where the counterions follow the fixed cationic charges as they move through the coating and the second where the counterions diffuse through the solution contained between the polymer chains of the swollen coating.

PLL has three possible structures, a random coil, an α-helix and a β-sheet. *Yasui and Keiderling*[219] used vibrational circular dichroism (VCD) to study the conformational changes that occur in PLL as the pH is altered. A reversion from α-helix to β-sheet conformation occurred in aqueous solution as the pH is changed from 7 to 12. At the concentrations used for the VCD study the α-helix was unstable and a stable intermediate conformation in the coil/helix

transformation was seen at pH 10.5. The β-sheet conformation is formed from the α-helix when the solution is heated[219,220]. *Shibata et al.*[220] have used circular dichroism and Fourier transform infrared spectroscopy to study the biphasic effects that alcohols have on the transitions of PLL between α-helix and β-sheet conformations. At low alcohol levels α-helix to β-sheet transformations occur but the converse transition occurs at high alcohol levels.

Apart from its use in chemically modifying electrodes, PLL has been used as a model for protein/heparin[221] and protein/drug[222] binding studies. *Ma et al.*[221] immobilised PLL onto a poly(ethylene-vinyl alcohol) (PEVAL) copolymer surface and used it to study the interaction of heparin with polycationic surfaces. Heparin was bound to the PLL by electrostatic forces, but increasing the pH (alkalinity) of the wash solution decreased the charge interaction between the PLL and heparin, and so adsorbed heparin was eluted from the PLL-PEVAL surfaces. *Brown and Wells*[222] used PLL to aggregate and immobilise sodium aurothiomalate as an aid to understanding the mechanism of action of aurothiomalate in rheumatoid arthritis, and its interaction with plasma and tissue proteins. The thiomalate moiety of the aurothiomalate was bound electrostatically to the ε-amino group on PLL; the binding could be weakened (precipitate redissolved) by increasing the ionic strength of the NaCl used and by extremes of pH.

In a recent paper *Munro et al.*[223] have used PLL and ascorbic acid to enhance the response for the surface enhanced resonance Raman scattering (SERRS) analysis of acidic monoazo dyes. The negatively charged dye molecules are attracted to the positively charged, protonated PLL molecules. The protonation of the PLL amino groups is enhanced by the addition of ascorbic acid. The protonated PLL molecules are then bound electrostatically to the citrate layer of the silver sol particles and form and aggregate. This aggregation leads to an intense SERRS response.

The above sections show that PLL is useful as both a binding agent for aggregate formation or as an anion exchanger/preconcentration reagent, in temporarily binding anionic reagents close to the surface of an electrode so that electrochemical detection of an analyte can be enhanced.

7.2. Poly-L-lysine modified solid electrodes

7.2.1. Introduction

Poly-L-lysine has been used previously to chemically modify electrodes. Our work is a continuation of that process and an advance, by trying to use a chemically modified electrode in a flowing solution. The use of a modified electrode in a flow injection system is a continuation of our work with single boundary measurements. *Anson et al.*[217,218] used a PLL modified graphite rotating disk electrode to determine diffusional pathways and charge transport mechanism within the adsorbed film layer using reversible and irreversible redox couples. *Anson et al.*[217,218] report no significant loss in response when the electrodes were rotated in solution. This indicates that the PLL film adhered well to the graphite electrode surface. Two solid electrodes were employed a glassy carbon wall-jet electrode and a platinum rotating disk electrode, both electrodes were initially used in a static mode.

7.2.2. Experimental

Cyclic voltammograms (CV) of the sample solutions were obtained using the experimental procedure given in chapter 2 section 2.4.2. using a Model 174A PAR Polarographic Analyser in conjunction with an X-Y recorder (see 2.2.2.). Two solid working electrodes were used, a 3 mm diameter disk glassy carbon electrode (wall-jet configuration Metrohm EA 286), and a 3 mm diameter disk platinum rotating disk electrode (used in a stationary mode). The three electrode system was completed for both working electrodes, by the addition of a Pt flag counter electrode and a saturated calomel reference electrode. The working electrodes were polished with alumina (0.3 μm), washed to remove any adhering particles and dried on a soft clean tissue before use. The electrodes were also used after a coating of PLL had been applied; the coating was applied after the electrodes had been polished.

A solution of 1 $mgcm^{-3}$ of poly-L-lysine hydrobromide was used to coat the electrodes as they were held upside down. A 5 μl aliquot was placed on the polished electrode surface and 'teased out' to cover the surface, with the tip of the pipette. The inverted electrode was then placed in a drying oven at 80 °C for 2 minutes, to ensure that the coating adhered to the electrode surface and to transform the PLL to the β-sheet conformation. The polished and coated electrodes were used to study a reversible $Fe(CN)_6^{3-}/Fe(CN)_6^{4-}$ and an

irreversible $Co(C_2O_4)^{3-}/Co(C_2O_4)^{4-}$, redox couple. To simulate a flow injection stream the coated electrodes were washed between consecutive CV's with deionised water.

Two solutions were prepared for CV:-

- A 50 cm^3 solution of $1x10^{-3}$ M potassium hexacyanoferrate(III) dissolved in 0.1 M potassium bromide as the supporting electrolyte.
- A 50 cm^3 solution of $1x10^{-3}$ M potassium cobalt(III) oxalate trihydrate (prepared as given in 2.3.1.) dissolved in Britton-Robinson buffer pH 1.7 (see 2.3.3.) as the supporting electrolyte.

The solutions were purged with N_2 for 10 minutes before analysis and purged while the electrodes were being washed.

7.2.3. Results and discussion

The following Figures and Tables show the results of coating the working electrodes with PLL. Results for hexacyanoferrate(III)/(II) are given for both a glassy carbon (GC) and platinum working electrodes. Unfortunately the glassy carbon electrode response decayed during the series of experiments and it was not used to measure the response of the irreversible Co(III)/(II) redox couple. The background signal for the GC electrode increased and became noisy and this was probably due to mechanical failure of the electrode. (Formation of a well between the GC disk and the electrode body that trapped solution would be the most likely explanation).

Figure 7.1. shows the response of a freshly polished and a polished/PLL coated GC electrode to the hexacyanoferrate(III) solution; it can clearly be seen that coating the electrode improves the response to the Fe(III)/(II) redox couple. Figure 7.2. shows the effect of washing the coated GC electrode between consecutive CV's, as the number of washes increases the separation of the cathodic and anodic peaks increase and the response of the electrode becomes less reversible. Table 7.1. gives the cathodic peak currents (i_{pc}), cathodic peak potentials (E_{pc}), anodic peak currents (i_{pa}) and anodic peak potentials (E_{pa}). The peak currents were measured relative to a baseline formed by extending the flat portion of the cathodic wave before the cathodic peak and similarly using the flat portion of the wave before the anodic peak was extended as a baseline for measuring the anodic peak. This method of obtaining a baseline was recommended by *Kissinger and Heinemann*[224] (Figure 2. in that reference) and by

Mabbott[225] (Figure 6B); all the workers were using hexacyanoferrate(III) as their test solution.

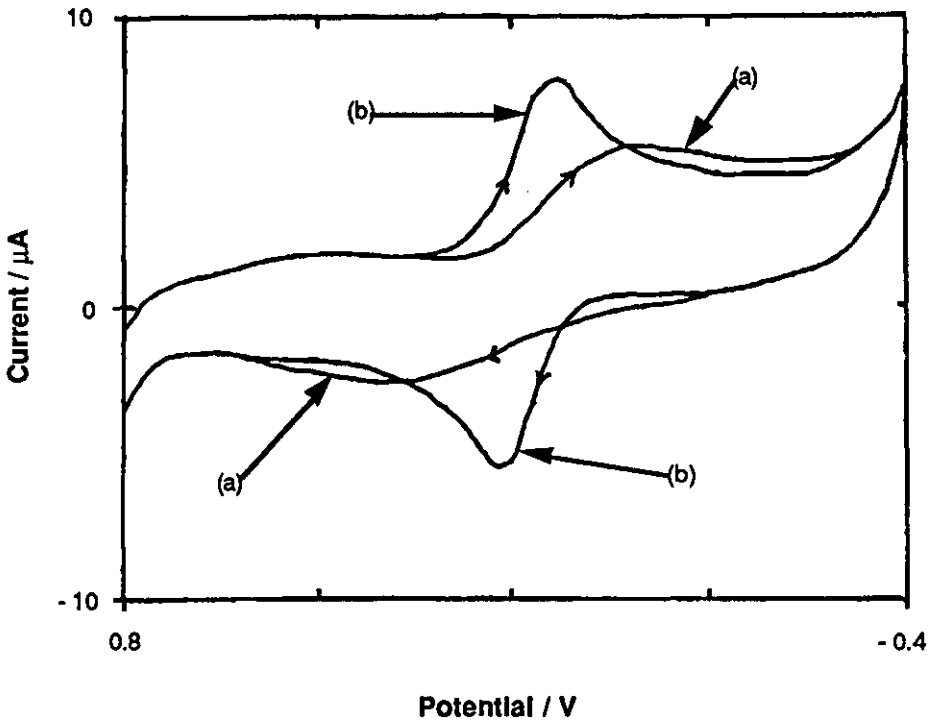

FIGURE 7.1. Cyclic voltammograms of a $1x10^{-3}$ M $K_3Fe(CN)_6$ solution at an uncoated and poly-L-lysine (PLL) coated GC electrode. Scan rate 20 mVs^{-1} (a) polished GC ; (b) PLL coated GC electrode.

The results in Table 7.1. show that the response of a coated PLL electrode is far more enhanced than the polished electrode alone, with an almost ideal peak separation and well defined peaks in the cathodic and anodic part of the voltammogram. The polished electrode's performance is far from ideal; for a reversible redox system with fast kinetics *Nicholson*[226] indicates that a peak separation of

$$\Delta E\left(E_{pa} - E_{pc}\right) = \frac{60}{n} mV \qquad (7)$$

should be obtained, where n is the number of electrons involved in the redox process.

The first three rows of Table 7.1. show what happens when consecutive scans are made without a delay between them. There is no appreciable change in the peak

currents or potentials measured after the electrode has been coated. The lower part of the Table (rows 4 to 8) and Figure 7.2. shows that the electrochemical response to hexacyanoferrate(III) degrades as the number of wash cycles increases. The peak separation is far from the ideal of 60 mV (n = 1), and increases as the number of wash steps increases. The magnitude of both cathodic and anodic peak currents decreases and the potential of the cathodic peak becomes more negative, and the anodic peak potential becomes more positive, as the wash cycles increase. The reversibility of the hexacyanoferrate(III)/(II) redox couple is decreasing as the experiment progressed. When the coated electrode was washed between scans, the sample solution was purged with N_2 for 10 minutes, with the washed electrode immersed in the solution before starting the next scan.

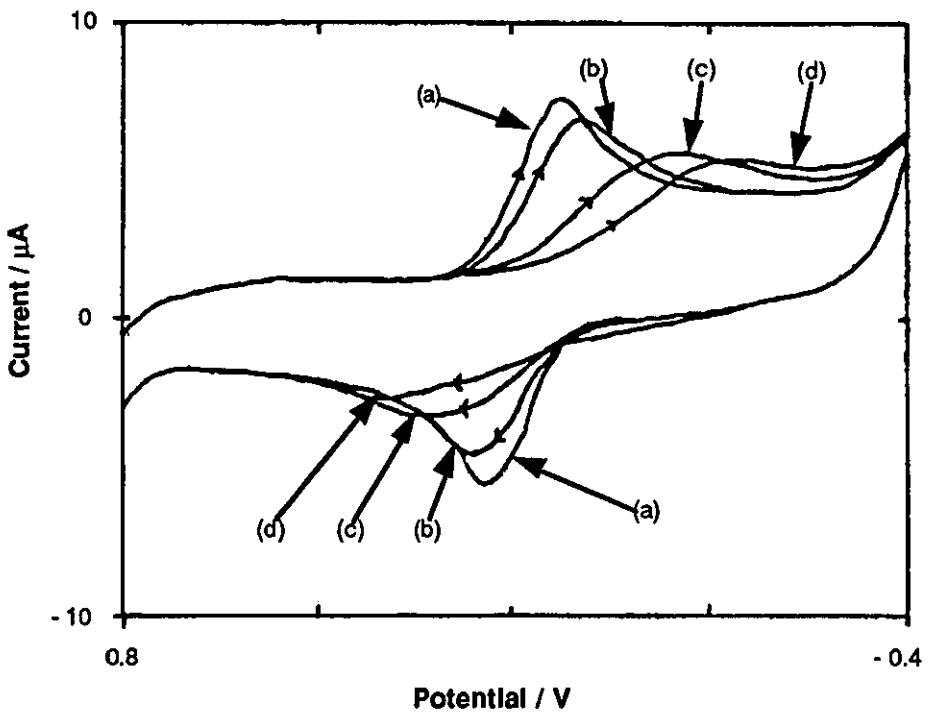

FIGURE 7.2. **Cyclic voltammograms of a $1x10^{-3}$ M $K_3Fe(CN)_6$ solution at a PLL coated GC electrode, showing the effect of successive washing steps. Scan rate 20 mVs^{-1} (a) no wash ; (b) 1st wash ; (c) 2nd wash ; (d) 3rd wash.**

The results in Table 7.1. and Figure 7.2. indicate that the lifetime of the PLL film is limited on a GC surface, the response approaches that of the polished electrode as the film was gradually removed. The degradation in electrode performance was also apparent, when the results from the two experiments are compared (rows 2 and 3, with 4 where a fresh coating of PLL had been applied). Coating the electrode with PLL, may offer a method of regenerating the electrode's response, if the lifetime of the film on the surface could be improved.

Scan	Condition	E_{pc} mV °	i_{pc} µA	E_{pa} mV °	i_{pa} µA	ΔE mV
1	Polished	18 ± 36	3.21	351 ± 30	- 1.54	333 ± 66
1	PLL*	139 ± 9	5.90	218 ± 9	- 5.06	79 ± 18
2 to 5	PLL*	136 ± 9	4.94	218 ± 9	- 5.00	82 ± 18
1	PLL*	130 ± 5	5.83	233 ± 5	- 5.32	103 ± 10
2	PLL*	130 ± 5	4.94	233 ± 5	- 5.32	103 ± 10
3	PLL and washed	103 ± 6	5.13	257 ± 6	- 4.23	154 ± 12
4	PLL and washed	- 39 ± 15	3.85	304 ± 15	- 2.82	343 ± 30
5	PLL and washed	- 151 ± 15	3.46	374 ± 15	- 1.92	525 ± 30

* PLL means that the electrode has been coated with poly-L-lysine, and a wash step is also indicated in the condition column. A scan rate of 20 mVs^{-1} was used for all measurements.

° the error given is the width of the peak at the maximum in potential units.

TABLE 7.1. Peak maximum currents and potentials for hexacyanoferrate(III) solution on a coated and uncoated glassy carbon electrode.

An additional experiment was carried out where 5 µl of the PLL solution was added to the sample solution. When the scans from a freshly polished electrode were compared with those obtained after the addition of the PLL solution, no appreciable enhancement in the electrode's response to the redox couple was seen. This shows that the enhanced response only occurs when the film has been applied directly to the electrode's surface.

The response of the uncoated GC electrode was far from ideal. Further work was therefore carried out using a Pt electrode, with the PLL applied directly to the electrode's surface. Two series of experiments using hexacyanoferrate(III) solution were carried out using an uncoated and PLL coated Pt electrode. The electrode was freshly polished and a CV of the sample solution was obtained after it had been purged with N_2, the electrode was washed with deionised water and the sample was purged with N_2 for the duration of the wash only. A second CV was then obtained and the wash and scan cycle was repeated a further three times. This experiment was repeated again with the polished Pt electrode, but the washed electrode was immersed in the sample solution for 10 minutes while it was being purged with N_2 between runs. Five scans were obtained. The second to fifth scans were obtained after a wash step. The above two experiments were repeated with a PLL coated Pt electrode. The results are given in Tables 7.2. and 7.3. for the uncoated and PLL coated electrode respectively.

The response of the freshly polished Pt electrode was much better than that of the GC electrode, as can be seen in Table 7.2. A ΔE value of 86 mV was obtained. While the value is not ideal for a reversible reaction, it is far closer to it than those previously obtained with the GC electrode. (The larger ΔE value may be due to the formation of an oxide layer on the freshly polished electrodes surface). The effect of washing the polished electrode was a degradation in its response to the hexacyanoferrate(III)/(II) couple, and this degradation was decreased when the electrode was immersed in the solution for an equilibration time before the next scan (compare the difference in response between the polished electrode when a 10 minute immersion period between scans was used Table 7.2.).

In Table 7.3. the results of coating the electrode with PLL are given; the effect of washing the electrode with deionised water was a degradation in the response to the redox couple in solution. The lifetime of the PLL film at the electrode surface was limited; the drop off in response would indicate that the PLL was being removed by the wash solution. These results are similar to those obtained with the GC electrode and indicate that the lifetime of the film at the electrode surface

was finite with the preparation method used. The results in Table 7.3. are similar to those obtained in Table 7.2.. When the electrode was immersed in the sample solution during a 10 minute N_2 purge, the decay in the electrode's response was slower, than when a scan was obtained without an equilibration period. This would indicate that an equilibrium period was required for the hexacyanoferrate(III) solution to diffuse towards the electrode's surface. Our observation that an equilibrium period is required are in agreement with the recent work of *Bianco et al.*[227] The workers continuously recorded the response of a PLL coated pyrolytic graphite electrode immersed in a sample solution of hexacyanoferrate(III) for over 30 minutes using CV. They report that both cathodic and anodic peaks increased in magnitude up to 30 minutes (steady state signal) but there was no appreciable increase in signal size after that time. *Bianco et al.*[227] used a higher molecular weight PLL (M_r 271,000 compared to 9,800 in our work) and they may have observed that less time was required to attain the steady state signal with a lower molecular weight PLL.

Coating the electrode with PLL improved the response to the redox couple, the slowest decay in the electrode's performance was obtained when the PLL coated electrode was immersed in the sample solution for 10 minutes after the wash step. When the coated electrode was not immersed in the sample solution for 10 minutes after the wash step, the response was similar to that obtained for the polished electrode with the 10 minute immersion period (compare the results for the lower part of Table 7.2. with those in the upper part of Table 7.3.). The results indicate that coating the electrode may retard the formation of an oxide layer or the passivation of the electrode surface. In all of the results obtained (Table 7.1. to 7.3.) the reversibility of the redox couple decreased as the number of wash steps increased.

The results given in Table 7.3. show that when consecutive scans (scans 2 to 4) of the sample solution are made, without washing the electrode, the CV's obtained are superimposed upon each other. The response for these consecutive scans indicates that with a reversible redox couple, there is no appreciable change in peak current or potential, when the redox couple has been confined to the electrode's surface.

In the following Figures and Tables the response of an uncoated and PLL coated Pt electrode to the irreversible $Co(C_2O_4)_3^{3-}/Co(C_2O_4)_3^{4-}$ redox couple are given. Figure 7.3. shows the response of an uncoated and coated electrode to the irreversible redox couple; the response was improved when the electrode had

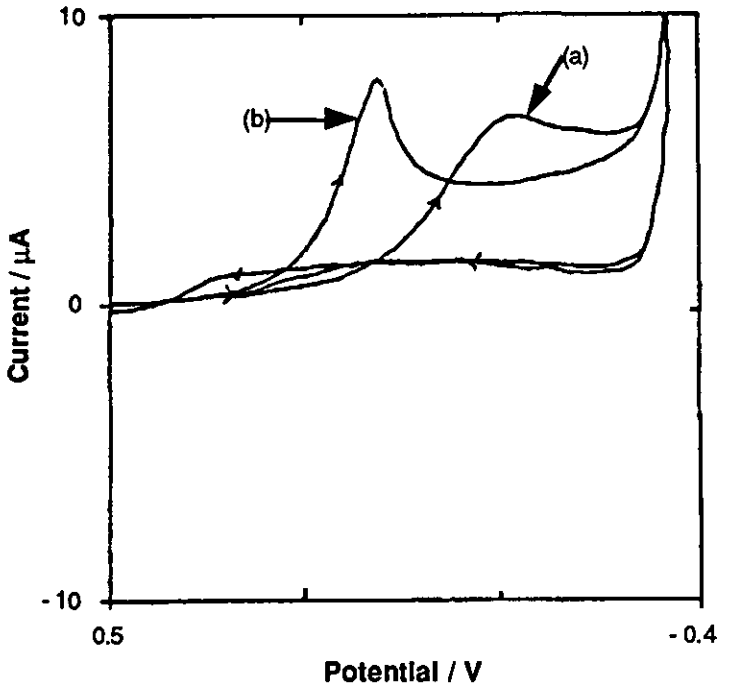

FIGURE 7.3. **Cyclic voltammograms of a $1x10^{-3}$ M $K_3Co(C_2O_4)_3$ solution in pH 1.7 buffer at an uncoated and PLL coated Pt electrode. Scan rate 20 mVs^{-1} (a) polished Pt ; (b) PLL coated Pt electrode.**

Scan	Condition	E_{pc} mV °	i_{pc} µA	E_{pa} mV °	i_{pa} µA	ΔE mV
1	Polished	115 ± 9	5.71	225 ± 9	- 4.74	110 ±18
2	Washed	89 ± 9	4.87	254 ± 18	- 2.69	165 ± 27
3	Washed	47 ± 18	4.17	287 ± 30	- 1.92	240 ± 48
4	Washed	0 ± 23	3.85	334 ± 30	- 1.28	334 ± 53
5	Washed	- 18 ± 17	3.78	375 ± 35	- 0.64	393 ± 52
1	Polished	127 ± 9	6.15	213 ± 9	- 5.32	86 ± 18
2	*washed 10 min eq	118 ± 9	5.90	216 ± 12	- 5.06	98 ± 21
3	*washed 10 min eq	106 ±9	5.13	239 ± 15	- 4.16	133 ± 24
4	*washed 10 min eq	86 ± 12	4.62	274 ± 15	- 2.37	188 ± 27
5	*washed 10 min eq	39 ± 24	3.85	307 ± 17	- 1.80	268 ± 41

* 10 minutes equilibrating time in the purging solution after washing the electrode.

° definition as given with Table 7.1.

TABLE 7.2. Peak maximum currents and potentials for a hexacyanoferrate(III) solution using a polished Pt electrode.

Scan	Condition	E_{pc} mV °	i_{pc} µA	E_{pa} mV °	i_{pa} µA	ΔE mV
1	PLL	124 ± 9	6.67	192 ± 9	- 6.41	68 ± 18
2	Washed	121 ± 9	6.41	204 ± 9	- 5.64	83 ± 18
3	Washed	109 ± 9	5.90	228 ± 9	- 3.72	119 ± 18
4	Washed	77 ± 12	4.87	263 ± 18	- 2.82	186 ± 30
5	Washed	21 ± 30	3.97	313 ± 30	- 1.80	292 ± 60
1	PLL	133 ± 9	6.60	204 ± 9	- 6.22	71 ± 18
2 to 4	PLL	133 ± 9	6.60	204 ± 9	- 6.15	71 ± 18
5	*washed 10 min eq	121 ± 9	6.35	210 ± 9	- 5.19	89 ± 18
6	*washed 10 min eq	118 ± 9	5.96	222 ± 12	- 4.87	104 ± 21
7	*washed 10 min eq	118 ± 9	5.51	239 ± 12	- 4.36	121 ± 21
8	*washed 10 min eq	98 ± 12	5.06	242 ± 12	- 4.10	144 ± 24

* definition as given with Table 7.2.

° definition as given with Table 7.1.

TABLE 7.3. Peak maximum currents and potentials for a hexacyanoferrate(III) solution using a poly-L-lysine coated Pt electrode.

been coated with PLL. The cathodic peak was more positive and was better defined on the coated electrode in comparison to the response obtained on an uncoated polished Pt electrode. In Figure 7.4. and Table 7.4. the effect of washing the coated electrode with deionised water, on the response to the irreversible redox couple are shown. The electrode was washed after the initial scan and immersed in the sample solution for 10 minutes while it was purged with N_2. The second scan was then obtained and two further wash/scan steps were recorded. The results are similar to those obtained with the reversible redox couple. As the number of wash steps increased, the decay in the response of the electrode increased. The cathodic peak becomes less reversible (a negative shift in potential) and the magnitude of the signals decreased as the number of washes increased. Coating the electrode with PLL did not make the oxidation of Co(II) to Co(III) possible and no anodic peak was recorded on the reverse scan. However, the cathodic peak became more reversible, a positive shift in the potential of the peak was observed with the coated electrode when compared with the CV obtained from the polished electrode alone.

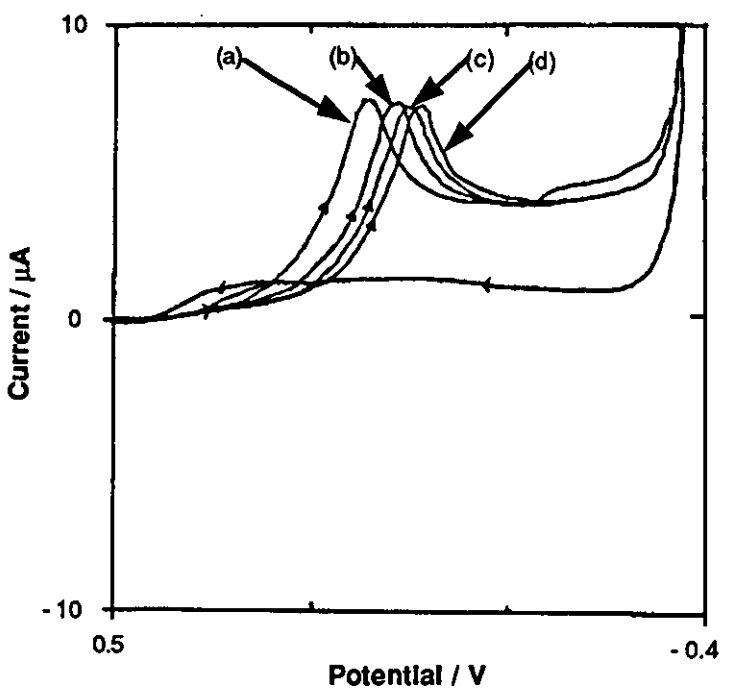

FIGURE 7.4. **Cyclic voltammograms of a $1x10^{-3}$ M $K_3Co(C_2O_4)_3$ solution in pH 1.7 buffer at a PLL coated Pt electrode, showing the effect of successive washing steps. Scan rate 20 mVs^{-1} (a) no wash ; (b) 1st wash ; (c) 2nd wash ; (d) 3rd wash.**

We have stated above that the lifetime of a PLL film is finite at both a GC and Pt electrode. This observation has been made when our work was compared with that of another member of the group (Pirzad) on PLL coated screen printed carbon ink electrodes. This electrode had a larger surface area (116 mm^2) and a rougher surface finish than either of the solid electrodes used in our work. Figure 7.5. shows the response obtained at a PLL coated screen printed electrode for the CV of a hexacyanoferrate(III) solution. When this device was washed between consecutive scans there was no appreciable change in the response to the redox couple. After the first scan the device was washed with deionised water and after the second scan the device was washed with a 1 M NaCl solution, followed by a deionised water rinse before the third scan was obtained. Washing with a NaCl solution should desorb any loosely bound PLL.[222,227] Pirzad also observed that the response of a PLL coated electrode was better than that obtained at an uncoated electrode. The lifetime of the film at our electrodes needs to be improved and further studies will be needed to achieve this objective.

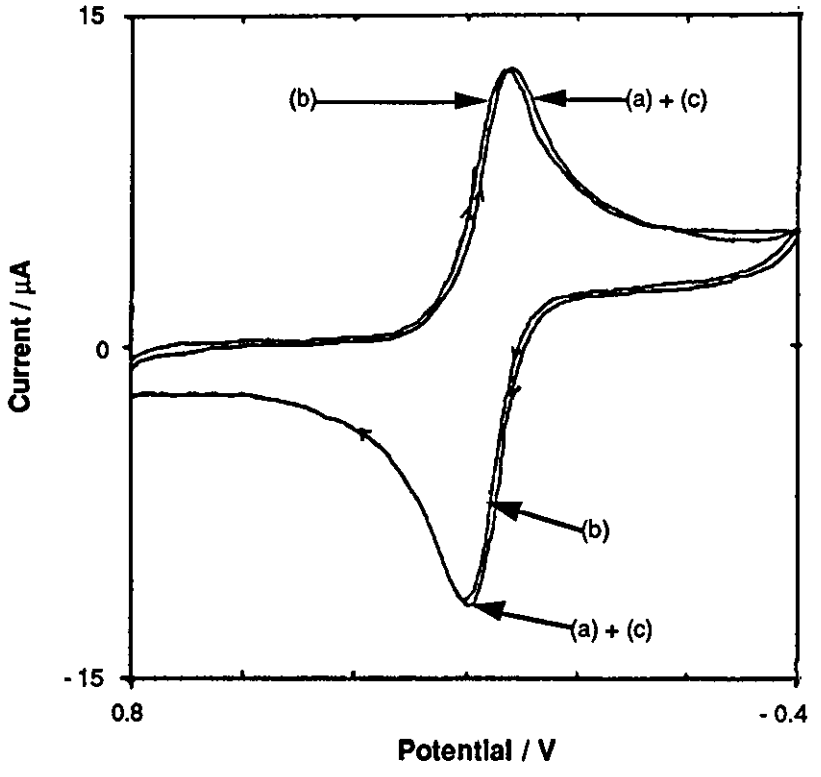

FIGURE 7.5. **Cyclic voltammograms of a $1x10^{-4}$ M $K_3Fe(CN)_6$ solution in pH 6.0 Britton-Robinson buffer, at a PLL coated C-ink screen printed electrode, showing the effects of successive washing steps. Scan rate 20 mVs^{-1} (a) no wash ; (b) deionised water wash ; (c) 1 M NaCl wash followed by a deionised water wash. (Reproduced by permission of Ramin Pirzad).**

The effect of the rate of voltage scan on the signals obtained at a PLL modified Pt electrode was studied. Scan rates of 5, 20, 50, 100, and 200 mVs^{-1} were used and four CV's were recorded at each scan rate. The sample solution was purged for 10 minutes with N_2 before the first scan and three consecutive CV's were then recorded. The solution was then purged for a further 10 minutes with N_2 before a fourth CV was recorded. Figure 7.6. shows the CV's obtained at a scan rate of 20 mVs^{-1}. The first and fourth CV's are almost identical, but the second and third scans give poorly defined cathodic peaks. This pattern was repeated at all of the scan rates used. These results differ slightly from those obtained previously with a reversible redox couple. The consecutive scans for the Co(III)/Co(II) couple show that the reduced species formed, Co(II), inhibits the further reduction of Co(III) at the electrode's surface. With the reversible redox couple, this effect was not seen because any reduced Fe(II) at the electrode surface could readily be reoxidised to Fe(III).

Scan	Condition	E_{pc} mV °	i_{pc} µA
1	PLL	116 ± 6	7.44
2	*washed 10 min eq	72 ± 9	7.37
3	*washed 10 min eq	51 ± 9	7.18
4	*washed 10 min eq	33 ± 9	7.08

* definition as given with Table 7.2.

° definition as given with Table 7.1.

TABLE 7.4. Peak maximum currents and potentials, for a cobalt(III) oxalate trihydrate solution using a poly-L-lysine coated Pt electrode.

The effect of allowing an equilibrium period were exactly the same as reported for the reversible redox couple previously. The reversibility of the reaction decreased (cathodic potential became more negative) and the magnitude of the

current i_{pc} decreased slightly. (A larger decrease would be expected if the electrode had been removed from the solution and washed before the fourth scan). The results indicate that an equilibrium period is required to allow fresh analyte species to diffuse to the electrodes surface, and this is also in agreement with the work of *Bianco et al.*[227] In the case of this reaction, time was also required for the Co(II) to diffuse away from the electrode's surface, and with the reversible redox couple the water of the wash solution would need to be replaced by fresh analyte solution.

Figure 7.7. shows a plot of peak current against the square root of the scan rate, a linear plot was obtained for the first and fourth scans, but not for the second and third. The first and fourth scans were almost superimposed on each other, their correlation coefficients were 0.998 and 0.999 respectively. A linear increase in cathodic current with the square root of scan rate indicates that mass transport to the electrode surface is by diffusion[228] through the film and *Murray*[229] has reported similar behaviour for polymer film electrodes.

The response of the electrode to the irreversible redox couple decayed after the experiments with the variation in the scan rates had been completed. If the response obtained in Figures 7.3. and 7.4. are compared with those obtained in Figure 7.6. the degradation in the electrodes performance becomes apparent. The CV's obtained in Figure 7.6. have a wider separation between the start of the forward scan and the end of the reverse scan than was previously the case. The pattern of the response of the Pt electrode was similar to that of the GC electrode, and a high background signal was obtained. This would indicate the presence of a 'well' between the electrode and the PTFE body, and this well would allow solution to be trapped between the electrode and its inert body, giving rise to erratic background signals. It has been said that PLL acts as an anion exchanger[216,227].

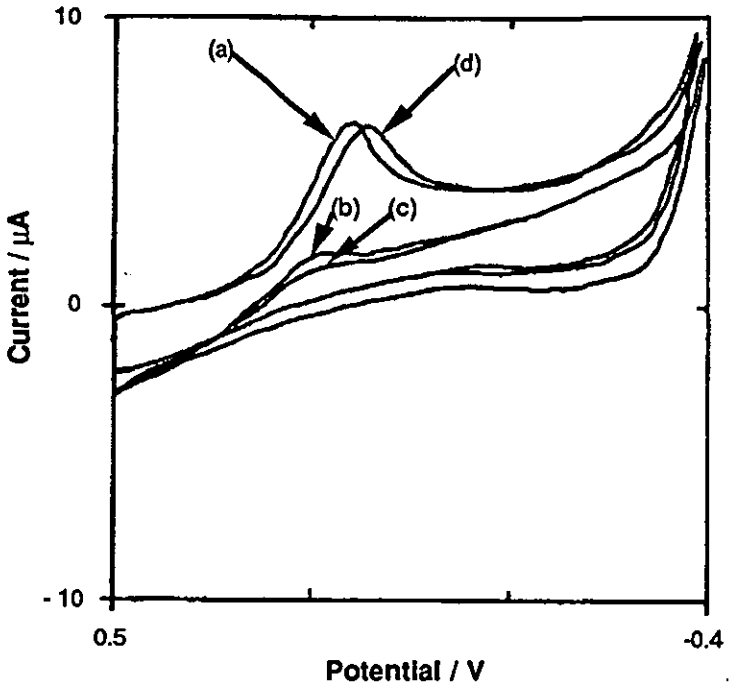

FIGURE 7.6. Cyclic voltammograms of a $1x10^{-3}$ M $K_3Co(C_2O_4)_3$ solution in pH 1.7 buffer at a PLL coated Pt electrode, with 3 consecutive scans followed by a fourth scan after a 10 minute delay. Scan rate 20 mVs^{-1} (a) 1st scan ; (b) 2nd scan ; (c) 3rd scan ; (d) 10 minute delay then 4th scan.

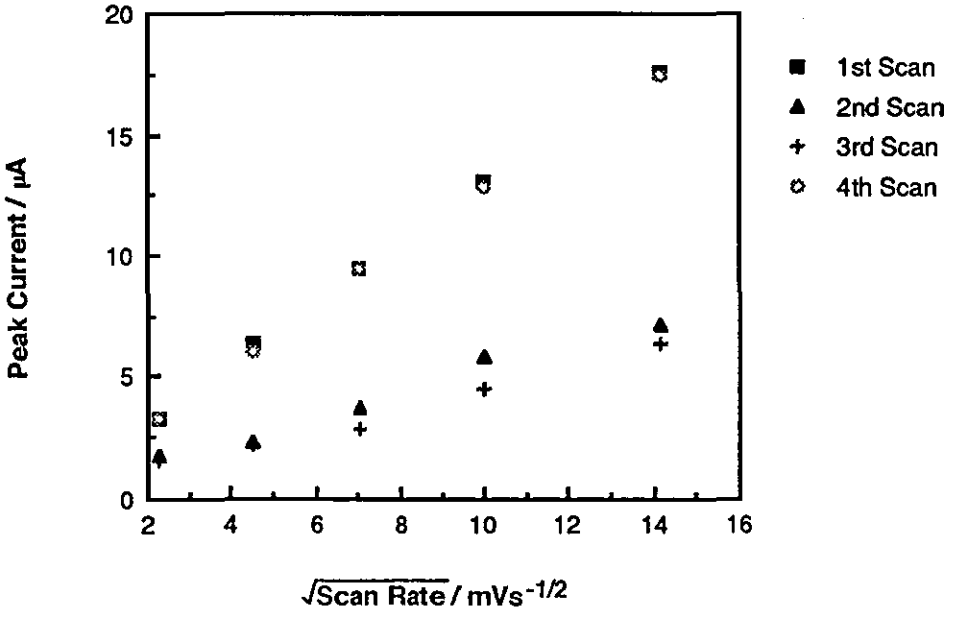

FIGURE 7.7. Cathodic peak currents plotted against the square root of the scan rate for a solution of cobalt(III) oxalate trihydrate using a poly-L-lysine modified Pt electrode.

Using propriety software (SYBIL) in the department, molecular modelling of PLL has been used to support this supposition and the results are shown in Figures 7.8. and 7.9. Figure 7.8 shows the structure of PLL in a β-sheet conformation for a nominal ten monomer chain length. The molecule has a flat structure with the side-chains pointing outwards, as can best be seen in the end view. Figure 7.9. shows the calculation of charge densities based on the Gasteiger-Huckel equation for a five monomer PLL chain. The molecule is negatively charged at the C-terminal and positively charged at the amine groups of the side-chains pointing out into the solution. These positively charged side-chains would attract any anions in solution and temporarily bind them to the electrode so that electrochemistry could be carried out on the bound analyte species.

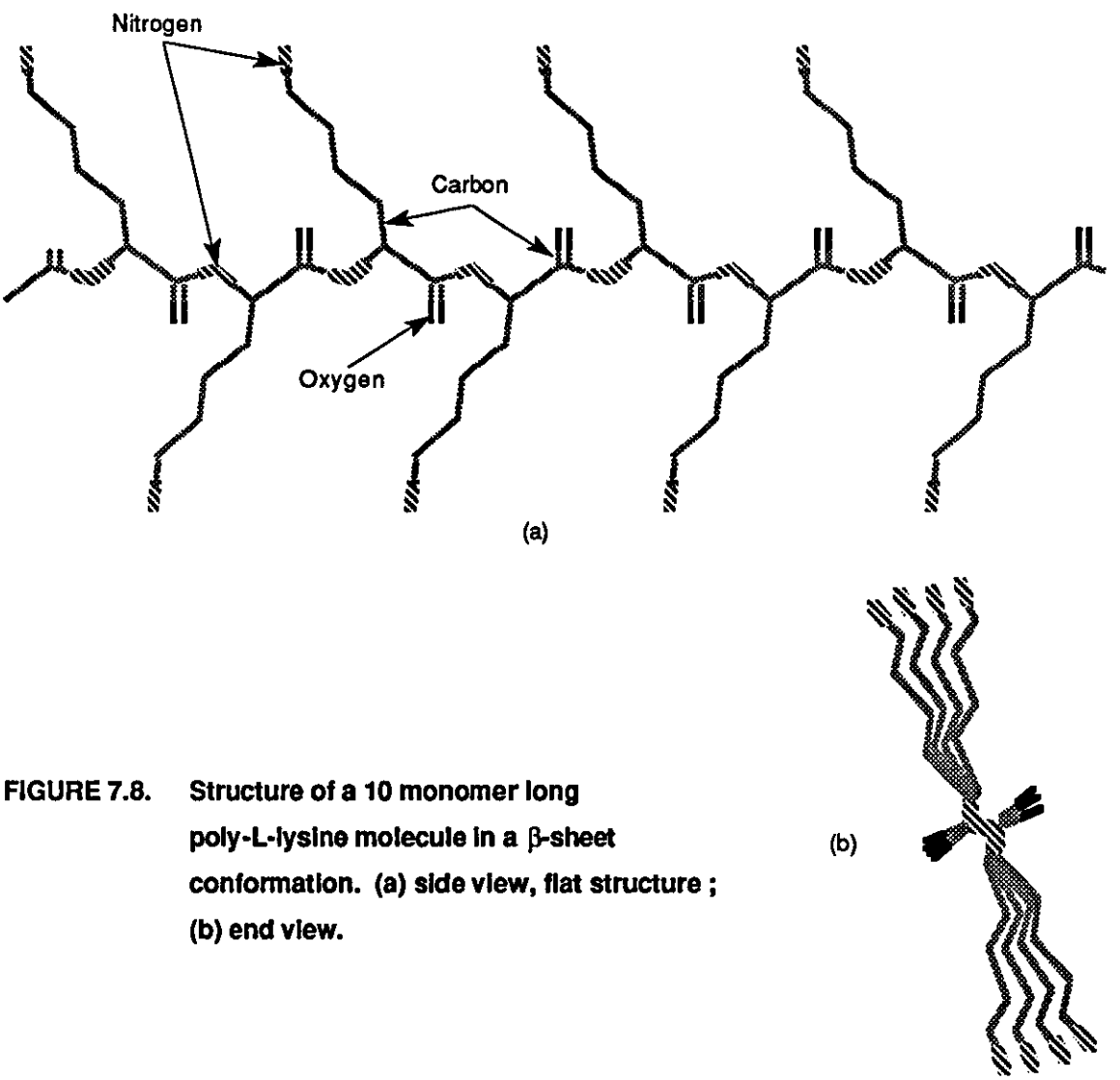

FIGURE 7.8. **Structure of a 10 monomer long poly-L-lysine molecule in a β-sheet conformation. (a) side view, flat structure ; (b) end view.**

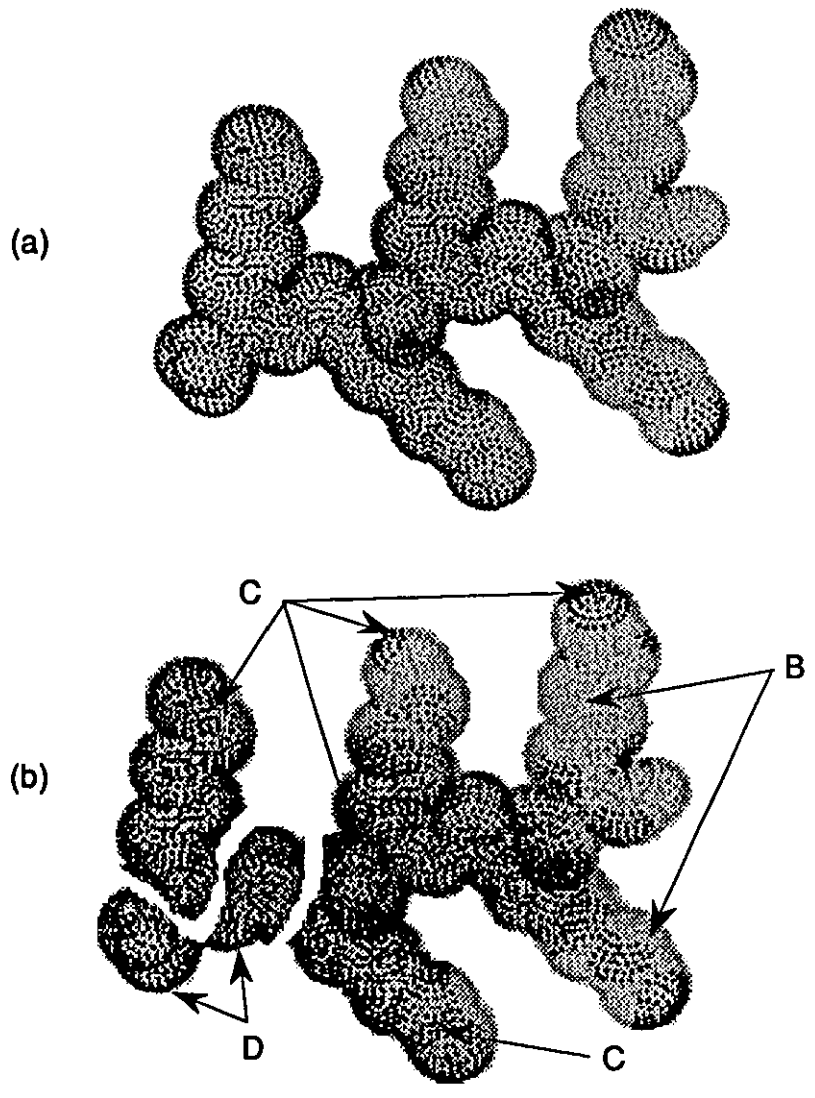

Cluster	Gasteiger-Huckel Charge Density Kcal mole^{-1}*	Number of Dots
A	8.74e+01 to 1.29e+02	47
B	4.57e+01 to 8.74e+01	2457
C	4.02e+00 to 4.57e+01	2648
D	- 3.77e+00 to 4.02e+00	1003
E	- 7.94e+01 to - 3.77e+01	368
F	- 1.21e+02 to - 7.94e+01	30

*Nominal charges used in the equation C = 0, N = +1 and O = -1.

FIGURE 7.9. Charge distribution based on the Gasteiger-Huckel equation for a 5 monomer long poly-L-lysine molecule. (a) Cluster map, (b) exploded view of cluster map.

7.3. Adsorptive stripping voltammetry at a poly-L-lysine modified hanging mercury drop electrode.

7.3.1. Introduction

Modification of hanging mercury drop electrodes (HMDE's) with polyelectrolytes have been carried out previously in this laboratory[230,231]. *Moreira and Fogg*[230] accumulated copper(II) from tap water at a HMDE modified by the adsorption of a film of poly-L-histidine. The poly-L-histidine film was reported as being an effective accumulation agent for Cu(II), and at a pH of 4.5 it was capable of removing Cu(II) from its EDTA complex. The same workers used a poly-L-lysine modified HMDE to determine potassium hexacyanoferrate(III) as its Cu(II) complex[231].

With the difficulties encountered in the mechanical failure of our two solid electrodes (GC and Pt) and the delay in replacing the electrodes, work was transferred to a PLL modified HMDE. Several reactions were studied and our preliminary results are reported below. If a successful reaction was found it was our intention to transfer the reaction to a flow injection manifold with PLL modified solid electrode.

7.3.2. Experimental

The apparatus used for adsorptive stripping voltammetry has been described previously in 2.2.3., and the procedure used for stripping analysis was as given in 2.4.3. Three different reactions were studied, the reduction of perrhenate, the accumulation of an Fe(III)/EDTA complex and the accumulation of a Cr(III)/DTPA complex. The experimental procedure used for each determination is given below.

Reduction of perrhenate

The voltammetric response of potassium perrhenate $KReO_4$, was studied in five supporting electrolytes including, sodium acetate pH 5.4, KH_2PO_4 buffer pH 7.0 (see 2.3.2 for details of preparation), 0.2 M and 2 M HCl (prepared by dilution of concentrated AnalaR acid) and 2 M KCl. The concentration of ReO_4^- used in all of the experiments was $1x10^{-5}$ M. Three accumulation potentials of 0, - 0.2 and - 0.6 V, and three accumulation times of 30, 60 and 120 seconds, were used to record the response in each of the supporting electrolytes. Signals were obtained with and without the addition of a 2 $\mu g cm^{-3}$ solution of PLL.

Determination of chromium(III)

The response of a $1x10^{-4}$ M solution of Cr(III) in a supporting electrolyte of pH 6.2 sodium acetate buffer/0.5 M $NaNO_3$ containing, $1x10^{-5}$ M DTPA was recorded using an accumulation potential of - 0.9 V. Two accumulation times were used, 60 and 120 seconds and the effect of the addition of 1, 2 and 4 μgcm^{-3} PLL solution were recorded. An additional experiment was carried out, by varying the concentration of $NaNO_3$, using 0.1 M and 1 M solutions in addition to the 0.5 M solution, a PLL concentration of 1 μgcm^{-3} was used with each of the nitrate solutions. A PLL/DTPA (1 $mgcm^{-3}$, $1x10^{-3}$ M respectively) solution in 0.5 M $NaHCO_3$ buffer was also prepared and results from the addition of this solution were recorded.

Determination of iron(III)

The response of a $1x10^{-5}$ M solution of Fe(III) in a supporting electrolyte of pH 5.2 sodium acetate buffer containing, $1x10^{-5}$ M EDTA was recorded using accumulation potentials of 0.2 and 0 V. Two accumulation times of 60 and 120 s, were used and signals were recorded with and without the addition of a 2 μgcm^{-3} PLL solution.

7.3.3. Results and discussion

The results obtained from the preliminary work for the analysis of ReO_4^-, Cr(III) and Fe(III), with and without the addition of PLL (using differential pulse voltammetry) were far from encouraging. Only a small length of time was spent studying the three analytes. A more detailed examination would be required before the approach of using PLL to enhance the adsorption of metals and metal/ligand complexes on a HMDE could be abandoned as being unsatisfactory.

The results for ReO_4^- in 0.2 M HCl and the two buffer solutions were similar for all of the conditions used. No response was obtained for Re and only a H_2 evolution wave at - 1.6 V was recorded. When a 2 M HCl solution was used an additional signal at - 0.4 V was recorded, which corresponds to a reduction from Re(VII) to Re(IV)[232-235]. Workers have reported an 8 electron reduction from Re(VII) to the rhenide ion Re^- in 2 M KCl[232-235]. A shoulder was recorded on the H_2 wave but it could not be used to determine Re. The addition of PLL did not improve the response of the HMDE to Re and no further work with perrhenate was carried out. *Brown and Wells*[222], and *Bianco et al.*[227] have reported that the

binding of analytes to PLL is weakened by increasing the ionic strength of Cl^- in solution. The strength of the Cl^- solutions used for Re analysis is probably inhibiting the binding of perrhenate to the PLL film which would explain why our results show no improvement from the addition of PLL to the analyte solution.

The method used for the analysis of Cr(III) was based on the procedure described by *Golimowski et al.*[236] A peak due to Cr(III) was obtained at - 1.25 V when the stripping analysis was carried out in the presence of the buffer and DTPA. Figure 7.10. shows that the addition of a 1 $\mu g cm^{-3}$ PLL solution to the sample was detrimental, because the peak at - 1.25 V disappeared and a signal was obtained at - 1.5 V followed by a H_2 evolution wave at - 1.55 V. When the PLL concentration was raised to 2 $\mu g cm^{-3}$ the position of the peak shifted in the positive direction to - 1.4 V and the H_2 wave also became more positive (- 1.53 V). Increasing the PLL concentration further to 4 $\mu g cm^{-3}$ moved the peak to - 1.3 V and the H_2 wave to -1.5 V, and although the peak increased in magnitude from - 2.6 μA at - 1.5 V to - 3.6 μA at - 1.3 V, addition of further Cr(III) did not change the magnitude of the signal.

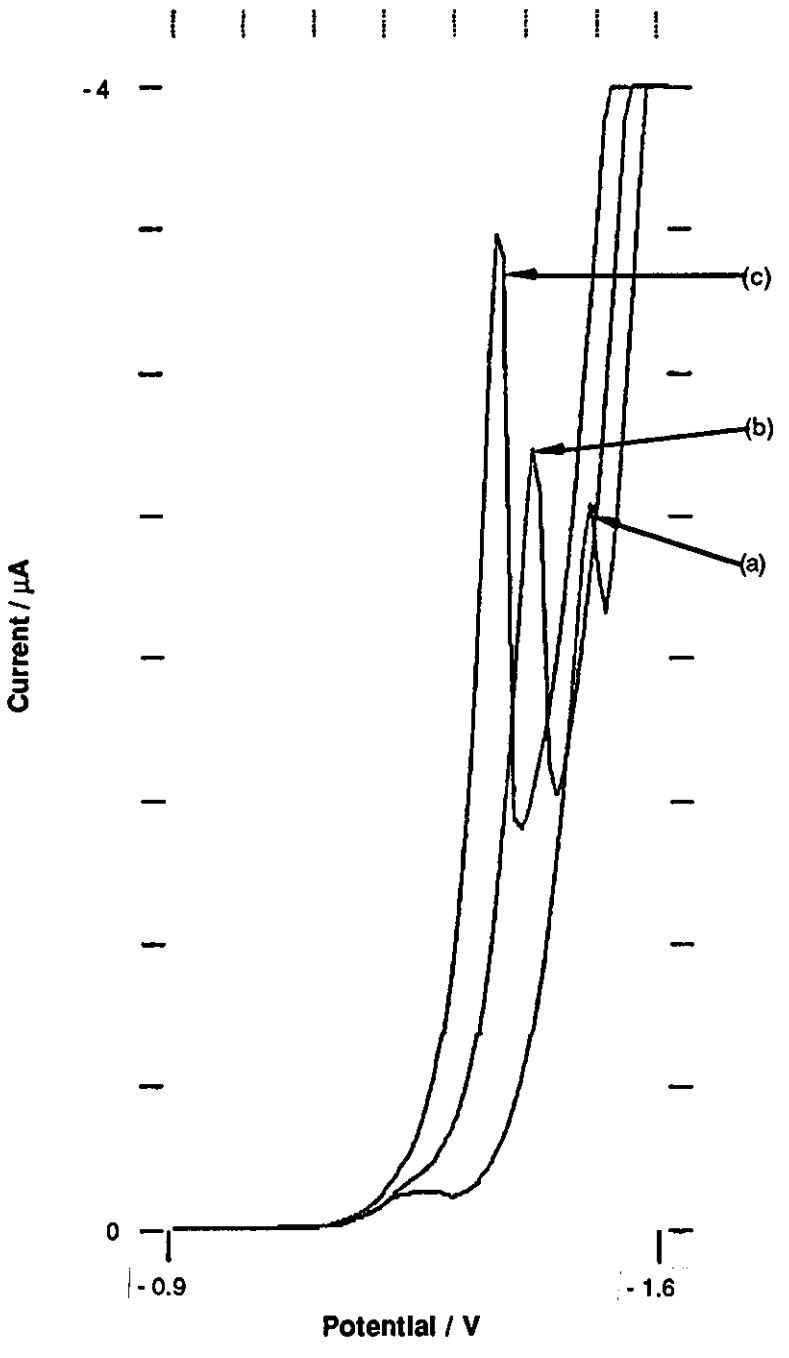

FIGURE 7.10. Differential pulse voltammograms of Cr(III)/DTPA complex at a PLL modified HMDE. Scan rate 10 mVs^{-1}, sample, $1x10^{-4}$ M Cr(III) and $1x10^{-5}$ M DTPA in pH 6.2 acetate buffer/0.5 M $NaNO_3$. (a) 1 μgcm^{-3} PLL ; (b) 2 μgcm^{-3} PLL ; (c) 4 μgcm^{-3} PLL.

The peak obtained at - 1.5 V was found to be due to nitrate, as the concentration of NO_3^- was changed from 0.1 M to 1 M, and a PLL concentration of 1 μgcm^{-3} was maintained, the peak increased in height and became more positive in potential. Increasing the accumulation time had no appreciable effect on the signal, probably because the surface of the HMDE was saturated with NO_3^- at the concentrations used. This was not a satisfactory method for the determination of Cr(III), because the Cr(III)/DTPA peak was masked by NO_3^- and the method could not be used to determine NO_3^- since the response occurred at very high NO_3^- levels. *Hnatowich et al.*[237] and *Krejcarek and Tucker*[238] report on a simple and efficient method of binding DTPA to proteins and using the latter method a PLL/DTPA complex was formed. Addition of a PLL/DTPA solution to Cr(III) in pH 6.2 buffer did not produce a signal at - 1.2 V nor was any signal produced before H_2 evolution at - 1.6 V.

Anson et al.[217] used Fe(III)EDTA$^-$ to study charge transport mechanisms in a protonated PLL film. Solid Fe(III)EDTA$^-$ was prepared by the method given by *Sawyer and McKinnie*[239]. Our work was an adaptation of the method given by *Sawyer and McKinnie*[239] so that an Fe(III)EDTA$^-$ complex would be formed in solution. The results for the determination of Fe(III) were again negative. When an accumulation potential of 0.2 V was used a peak - 225 nA was obtained at 0.15 V and this was due to the $1x10^{-5}$ M EDTA solution added to the buffer (see Figure 7.11.). Addition of an equal concentration of Fe(III) gave a - 176 nA peak and the peak was shifted to 0.12 V. An additional peak of - 24 nA was obtained at - 0.13 V. Addition of 2 μgcm^{-3} PLL solution caused a further decrease in the magnitude of the EDTA peak to- 155 nA and also shifted the peak maximum to 1.0 V, there was no change in the potential or magnitude of the smaller peak at - 0.13 V. Further additions of Fe(III) and PLL caused no further change in either peak, and changing the accumulation time gave no appreciable enhancement in the signal. Changing the accumulation potential to 0 V gave no response at all. If an Fe(III)EDTA complex was being formed the complex was not being adsorbed and the signals obtained due to the high concentration of reagents in solution. Addition of PLL gave no improvement to the signals obtained.

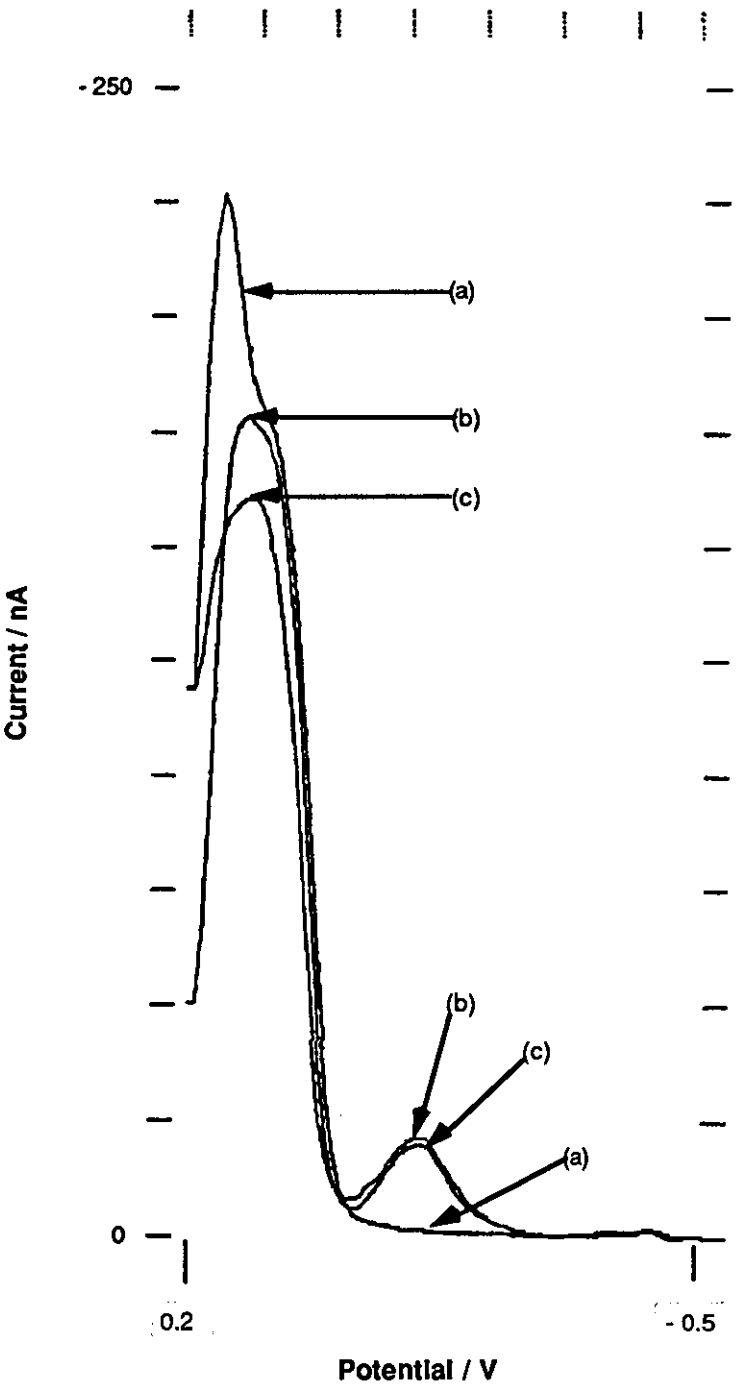

FIGURE 7.11. Differential pulse voltammograms of Fe(III)/EDTA complex at a PLL modified HMDE. Scan rate 10 mVs^{-1} ; (a) $1x10^{-5}$ M EDTA ; (b) (a) and $1x10^{-5}$ M Fe(III) ; (c) (b) and 2 μgcm^{-3} PLL.

7.4 Conclusions

Addition of poly-L-lysine to solid electrodes improves the response to negatively charged electroactive species. The film at the electrode surface acts as an anion exchanger and *Bianco et al.*[227] have shown that it inhibits the electrochemistry of positively charged species (see the CV for $Ru(NH_3)_6^{3+}$ at a coated and uncoated pyrolytic graphite electrode). The workers[227] have also indicated that the binding of anions to a protonated PLL film is weakened by high ionic strength of the supporting electrolyte and by high pH values (the amount of incorporated species was halved by increasing the pH from 1.6 to 8.4).

The lifetime of the PLL film was finite at the GC and Pt electrodes for the coating method used and this area needs to be improved if PLL modified electrodes are to be successfully employed in flowing solutions. *Frenzel*[240] has recently reported on an improved method of coating a GC electrode with a mercury film. The elemental mercury did not adhere well to the highly polished GC surface; the adsorption of the mercury film on the electrode's surface was improved by preparing a rougher surface than was obtained by the normal polishing method. A homogenous, mechanically stable mercury film was obtained by this preparation method that gave excellent electrochemical response (improved sensitivity, decrease in background currents, improved lifetime for hydrogen overvoltage and improved peak resolution). The next stage of our work would be to try the electrode preparation method of *Frenzel*[240] to see if the lifetime of the PLL film at the electrodes surface could be improved. Other methods of preparing a dry film of PLL on the electrode's surface would also need to be studied.

The metal complexes chosen for adsorptive stripping voltammetry at a PLL modified HMDE did not produce any encouraging results. *Paneli and Voulgaropoulos*[241] have recently reviewed the applications of adsorptive stripping voltammetry for the determination of trace and ultratrace metals. Several metal/ligand complexes are described and some of these systems may benefit from adsorptive stripping voltammetry at a PLL modified HMDE. Molecular modelling may prove useful in selecting suitable metal/ligand complexes where the ligand is anionic; the success of molecular modelling in choosing suitable systems could then be assessed. PLL is only one polyelectrolyte and our experience with this could be used to select other polyelectrolytes (e.g. poly-L-arginine) for film formation and it would be interesting to see what happens if a cationic exchanging film (e.g. polyglutamate) is bound to the electrode's surface.

CHAPTER 8

CONCLUSIONS AND FURTHER WORK

8.1. General considerations

The work with single boundary measurements has covered several aspects of flow analysis and this chapter will be used to unite all of the ideas into a single theme and to indicate which areas will yield the most promising results and where future work should be concentrated.

A stream switching valve was used in the experimental work to produce the double peak output that is commonly obtained with single boundary measurements in flow analysis. For large volume injections the advantage of a stream switching method of injection over a conventional injection method, is that the volume of the loop of the injection valve makes no contribution to the signals obtained at each of the two boundaries produced. The advantages of stream switching for smaller injection volumes are not as great, because usually a higher degree of mixing between the sample and reagents occurs than in single boundary measurements. Both reaction boundaries formed in single boundary measurements should experience the same conditions when entering the FI manifold. They should both travel the same distance from the injection valve to the detector and allow the same degree of on-line analyte conversion to occur at each boundary. Both signals obtained at each of the two boundaries experience the same degree of dispersion.

With loop injection the rear boundary has a longer distance to travel between the injection valve and the detector than the front reaction boundary, and this means that it has a longer period for on-line analyte formation because of its increased residence time in the flow manifold. The longer residence time also means that the dispersion of the rear boundary peak produced by loop injection will be higher than the front boundary peak. The different conditions encountered by the double signal output produced by loop injection for single boundary measurements means that an additional factor needs to be considered in any calculation of the processes that occur at each of the two reaction boundaries produced. To avoid this additional complication stream switching was used as stated above. The advantage of using loop injection is that a different degree of on-line analyte formation can be obtained at each of the 2 reaction boundaries produced. This can then be used to produce 2 ranges of calibration curve. Alternatively for simultaneous kinetic determinations, the rear boundary peak

can be used to monitor the formation of the product with the slowest reaction rate and corrections made for any contribution from a product with a faster reaction rate. This would be done initially by determining the analyte components individually (recording the signals at each boundary) and then using the front boundary signal, (where the signal is mainly due to the analyte with the faster reaction rate) to correct for the contribution of the faster formed analyte to the rear boundary signal.

8.2. Refractive index correction

The first part of this study concentrated on refractive index (RI) correction of signals obtained in single boundary measurements. The observations made are equally valid for any injection method, where two wavelengths can be monitored simultaneously and where the second wavelength chosen can be used to monitor non-specific absorbance that is due to changes in RI alone. I have shown that a diode-array spectrophotometer can be used to monitor an analyte signal and its RI component at two different wavelengths, and that correction for RI was possible by subtracting the signals obtained at the second wavelength (non-specific absorbance) from the signal obtained at the first wavelength (analyte absorbance). Signals of equal height were obtained at the two reaction boundaries produced in single boundary measurements, after RI correction had been used.

This was achieved without the need for RI matching that had been previously employed. This method offers an improvement in contamination control by removing the need to add another reagent and the inherent risks that are associated with this. RI correction was made by manually subtracting the signals obtained at the second wavelength away from the signals obtained at the first wavelength; it would be possible with more recent versions of the diode-array spectrophotometer to make the RI corrections automatically.

I have stated above that a diode-array spectrophotometer can be used for RI correction, but other designs of spectrophotometer were also evaluated. A single beam visible and a double beam ultraviolet/visible spectrophotometers were also used. The former design (single beam) could not successfully be use for RI correction because it did not respond in a consistent manner and the results obtained indicated that overcompensation sometimes occurred. The double beam instrument was successfully employed for RI correction. A simple diagnostic test was devised to evaluate the suitability of a spectrophotometer design for RI

correction. Sample solutions that produced only non-specific absorbance (no analytical signal in the visible region of the spectrum in this case) were injected into the flow manifold and their responses were recorded. When the instrument being studied responded in a consistent manner to the injected solutions I found that it could successfully be used for RI correction. Conversely, when the instrument being studied did not respond in a consistent manner I found that it could not successfully be used for RI correction. The instrumental response obtained consisted of, two positive absorbance signals with the diode-array, a negative absorbance signal followed by a positive absorbance signal with the double beam instrument and a mixture of the two responses for the single beam instrument. This inconsistent response to the injected solutions when the single beam instrument was used is why I recommend that it should not be used for RI correction. Any extension of this work might involve modification in the design of the instrument so that several instrumental parameters could be evaluated (aperture size, focal length, field stop and other optical parameters).

The influence of the length of the coiled reactor used in the manifold on the signals obtained in single boundary measurements was studied and it was found that longer reactors were beneficial in reducing the contribution of RI to the main analytical signal. Reactors over 5.0 m are not recommended because RI correction becomes difficult as the contribution of other factors, such as the diffusion of more than one analyte species. It is possible that tribromide (Br_3^-) is being formed in addition to bromine (Br_2) and the equilibrium between the two species will change as a the reaction time is increased in the longer reactors. The differences in the heights of the peaks obtained at the two reaction boundaries will then be due to factors other than a difference in RI. It is suggested that further work will be needed to decide which species is present and, if both are, what influence do they have on the diffusion of each other. At longer reactor dimensions signal distortion from high back pressure may occur and these cannot be compensated for easily. (The distortion of the signal profiles obtained are not always consistent).

The influence of the volume of the flow-cell and the direction of flow through the flow-cell on the signals obtained in single boundary measurements have also been studied. Their direct influence on RI correction is limited, but small volume flow-cells are recommended to reduce the contribution of the cell to the dispersion of the sample bolus. The influence of the direction of flow through a flow-cell was greater for the larger volume flow-cells, but it had an equal effect on both analyte and RI signals. With the flow-cells where the manufacturer had

clearly indicated a direction of flow, this flow direction should be followed if problems with signal distortion are to be avoided. In the case of the 8 µl flow-cell where no flow direction through the cell was indicated, I found that either flow direction could be used with no detrimental effect on the signals produced.

It has been shown that RI correction is possible without RI matching, but when should it be used and where is its influence greatest? RI effects are most noticeable on small signals close to the limit of detection for most optical methods and correction should be used to decide if the signal obtained is truly from the analyte alone or just a response to apparent absorbance (RI). I have also assumed that the on-line formation of bromine was a relatively simple process but this may not be true. It is not certain that bromine was being monitored, it is possible that tribromide was being monitored. Further work will be needed to decide which species is present or if both are, and what influence they have on the diffusion of each other. The differences in RI observed for the on-line formation of bromine were mainly due to the presence of a high concentration of acid (1 M HNO_3). When the acid was present in both carrier and injectate lines, signals of equal height were obtained at each reaction boundary with and without RI correction and the non-specific absorbance signals were small ($\leq$ 0.001 A).

When the concentration of the acid was decreased, as was the case for on-line triiodide formation (0.1 M HNO_3) the contributions of RI to the heights of the signals obtained were small, but still present. In this instance subtraction of the RI signals did not account for the differences in the height of the signals obtained at each reaction boundary and the explanation for the differences lies elsewhere. The influence of the diffusion of triiodide on the diffusion and formation of iodine has not yet been assessed. I suggest that further work on triiodide/iodine, and tribromide/bromine formation will be needed to decide what influence they have on the diffusion of each other. If two analyte species are being formed on-line, at which point in the reaction is the equilibrium between the two species changed in favour of one species over the other.

8.3. Sandwich techniques as a modification of single boundary measurements

The next logical step for developing single boundary measurements in FI, is to obtain more data from the double peak output that is normally produced by this method. Single boundary methodology was altered by using a class of techniques known as "sandwich techniques" and it is in this area that I recommend any

future effort should be concentrated. The sandwich technique was applied to the indirect determination of sulphite using bromine and iodine as the monitorand species. The experimental manifold was simple: a more sophisticated device could be developed later. A three-way valve was used in conjunction with the stream switching valve to produce a sandwich sample bolus. The front boundary signal was due to the monitorand alone (fully formed control signal) and the rear boundary signal was due to the presence of sulphite (peak height decreased as the concentration of sulphite increased). The three-way valve was manually operated and the stream switching valve was under computer control. The results produced by this method were encouraging. RI correction of the signals produced is still recommended to decide if the signals obtained are just due to non-specific absorbance or not.

A modification of the manifold would be the inclusion of an eight-port rotary valve to produce the sandwich sample bolus and this would simplify the manifold (only one valve would be needed). The useful aspect of the sandwich techniques is that more than one species can be monitored per injection, by using mixed reagents or by including a catalyst (or reducing) column in one of the loops on the valve. It is also possible to construct dual calibration curves by ensuring a different degree of dilution occurs at each of the two boundaries produced by this injection methodology. An extension of this work might involve studying the effect of varying the volumes of sample injected on the shape of the signals produced. If a mixed reagent was used to simultaneously determine 2 analyte species, at a common wavelength where both analyte species absorbed and the analytes react at a different rate with the mixed reagent. Then the influence of injection volume on simultaneous determinations could be assessed. If these analyte species also had a unique λ_{max} for each analyte species, then the influence of injection volume on single component determinations could be assessed. If all three wavelengths could be monitored simultaneously then the influence of the injected volume on single component and multicomponent determinations could be assessed at the same time. In the hypothetical cases given above it would be advisable to work in a concentration range well above the limit of detection so that sensitivity and RI effects can be neglected.

8.4. Other factors that affect single boundary measurements

It has been shown that using a single bead string reactor (SBSR) in single boundary measurements leads to a decrease in dispersion that manifests itself as a decrease in the width of the peaks obtained. In single boundary measurements

this is shown as a decrease in the width of the peaks measured from the start of the front boundary peak to the tail of the rear boundary peak. If SBSRs are used as mixing devices in single boundary measurements they should be placed before or after the main reaction coil, to decrease the dispersion of the sample bolus while still permitting sufficient time for a high enough degree of on-line analyte formation. I have found that SBSRs would be more usefully employed at lower flow rates than were used in our experiments if problems with high back pressure are to be avoided. A suggestion for further work with SBSRs in single boundary manifolds would include assessing their influence on the signals obtained as the injection volume is decreased and comparing the results obtained with other designs of reactors (which are matched in volume with the SBSR).

In single boundary measurements using a stream switching valve, I have found, under the conditions used, that the degree and rate of on-line analyte formation had no influence on the position of the peaks obtained from the on-line reaction. This was shown by superimposing the peaks obtained from the on-line reaction on the signal obtained from the injection of preformed analyte. Under the experimental conditions used the signals obtained from the analyte formed on-line did not appear outside the large, broad flat topped signals that were obtained when the preformed analyte was injected to any appreciable degree.

The results obtained for studying the influence of the rate and degree of on-line analyte formation on the position of the peaks of an on-line reaction when compared with the signal obtained for the injection of the same analyte as a preformed complex were different from those obtained by previous workers. It is possible that they used a slug injection method and not a time based stream switching method which I used. (The method of injection used and the concentration of some of the complexes used is not clearly stated in the work of Valcarcel which was used to design my experiment). The differences arise because the rear reaction boundary formed by slug injection has to travel through the sample loop on the injection valve and therefore has a longer residence time in the flow manifold than the front reaction boundary. This means that a higher degree of analyte formation occurs at the rear reaction boundary than occurs at the front reaction boundary.

I suggest that further work would clarify if the difference in the results obtained are due to the injection methods used. A direct comparison should be made by using the same solutions and observing the influence of the type of injection method used (stream switching and slug injection) . The chemistries used should

have different rates of product formation to prove if the rate of product formation influences the shape and position of the peaks formed by an on-line reaction, when compared with the signals obtained from the injection of the same analyte as a preformed complex.

Electrochemical detection was also used to investigate the influence of the degree of on-line analyte formation on the position of the peaks obtained when compared with the signals obtained from the injection of the same analyte as a preformed complex. The findings were identical to those obtained above using spectrophotometric detection; the signals obtained from an on-line reaction did not appear outside the envelope formed by the injection of a preformed complex. The method of detection makes no significant contribution to the position of the peaks obtained from on-line reactions, provided it has a sufficiently fast response. While using electrochemical detection various electrode conditioning regimes were used to enhance the response to the analyte; none of these methods produced an enhanced response. An extension of this study would be the application of a three wave pulse to the working electrode. The apparatus for generating this type is not available in this laboratory but I recommend that a study is made using a three wave pulse. The three wave pulse is more commonly used in pulsed amperometric detection in liquid chromatography, but it has the advantage of being readily applied before each measurement is taken as part of the measurement cycle.

8.5. Chemically modified electrodes for flow analysis

Addition of poly-L-lysine (PLL) to solid electrodes (glassy carbon, CG and Pt) improves the response to negatively charged electroactive species. The film on the electrode surface acts as an anion exchanger and it has been shown to inhibit the electrochemistry of positively charged species. The binding of anions to a protonated PLL film is weakened by high pH and by high ionic strength of the supporting electrolyte. I have found that the lifetime of the PLL film at the electrode surface is finite and that the film is relatively easily removed by washing the electrode with deionised water. This means that at present the coated electrodes are not suitable for use in flow analysis. A suggestion for further work would involve investigating methods of improving the binding of the PLL film to surface of the solid electrode.

The method of drying the film and converting it into the β-sheet conformation was also found to be detrimental to the solid electrode. A 'well' effect was

observed due to the heating where the Teflon supporting material came away from the working electrode cylinder and this allowed solution to enter between the support and the working electrode. This effect became apparent because the magnitude of the background signals increased with the increasing number of preparation stages used. A possible approach for coating the electrodes would be the dissolution of PLL in a high concentration of alcohol (β-sheet conformation obtained) and evaporation of the alcohol from the electrodes surface under a nitrogen stream.

There are several areas where an extension of the study of polyelectrolyte modified electrodes may prove to be beneficial. The film has not yet been fully characterised and I suggest that the effect of different molecular mass PLL films on the electrochemistry at modified solid electrodes should be studied. The information gained from this study could then be used for other polyelectrolyte films such as a film that binds cations to the electrodes surface i.e. the opposite charged species from those that have already been studied. The use of molecular modelling to select suitable target metal/ligand complexes and other charged species of interest has not yet been fully exploited. The electroactive species selected by the molecular modelling package could then be studied and this would also enable researchers to evaluate the suitability of a molecular modelling package for selecting target analyte complexes.

Other types of electrodes may also benefit from modification with PLL and similar polyelectrolytes. These would include the hanging mercury drop electrode (HMDE) and screen printed electrodes using a C-ink substrate. The latter devices could be used to produce sensor based technology (capillary fill devices mainly).

The research work reported in this thesis has indicated several areas where further work is warranted. It was only a lack of time that stopped me from pursuing some of the above suggestions, while a lack of suitable equipment prevented me from studying others. The last chapter (7) dealt with modified electrodes and the shortest period of my research was spent investigating the use and application of modified electrodes. At present these modified electrodes are not suitable for FI, because of the limited lifetime of the PLL film at the electrode surface. If the adhesion of the film can be improved, the modified electrodes may be used in FI systems. The electroanalytical group is continuing to investigate the use of these modified electrodes and the results that they are reporting indicate that this area of research may prove to be very fruitful.

REFERENCES

1. Ruzicka, J., and Hansen, E. H., *Anal. Chim. Acta*, 1975, **78**, 145.

2. Stewart, K. K., Beecher, G. R., and Hare, P. E., *Anal. Biochem.*, 1976, **70**, 167.

3. Skeggs, L. T., Jr., *Am. J. Clin. Pathol.*, 1957, **28**, 311.

4. Stewart, K. K., *Talanta*, 1981, **28**, 789.

5. Mottola, H. A., *Anal. Chem.*, 1981, **53**, 1312.

6. Nagy, G., Feher, Z., and Pungor, E., *Anal. Chim. Acta*, 1970, **52**, 47.

7. Ruzicka, J., and Stewart, J. W. B., *Anal. Chim. Acta*, 1975, **79**, 79.

8. Stewart, J. W. B., Ruzicka, J., Bergamin Filho, H., and Zagatto, E. A. G., *Anal. Chim. Acta*, 1976, **81**, 371.

9. Ruzicka, J., Stewart, J. W. B., and Zagatto, E. A., *Anal. Chim. Acta*, 1976, **81**, 387.

10. Stewart, J. W. B., and Ruzicka, J., *Anal. Chim. Acta*, 1976, **82**, 137.

11. Hansen, E. H., and Ruzicka, J., *Anal. Chim. Acta*, 1976, **87**, 353.

12. Ruzicka, J., Hansen, E. H., and Zagatto, E. A., *Anal. Chim. Acta*, 1977, **88**, 1.

13. Hansen, E. H., Ruzicka, J., and Reitz, B., *Anal. Chim. Acta*, 1977, **89**, 241.

14. Ruzicka, J., Hansen, E. H., and Mosbaek, H., *Anal. Chim. Acta*, 1977, **92**, 235.

15. Ruzicka, J., and Hansen, E. H., *Anal. Chim. Acta*, 1978, **99**, 37.

16. Betteridge, D., *Anal. Chem.*, 1978, **50**, 832.

17. Ruzicka, J., and Hansen, E. H., *Anal. Chim. Acta*, 1980, **114**, 19.

18. Ruzicka, J., and Hansen, E. H., *Anal. Chim. Acta*, 1986, **179**, 1.

19. Ruzicka, J., and Hansen, E. H., *"Flow Injection Analysis"*, 2nd Edition, Wiley, New York, 1988.

20. Valcarcel, M., and Luque de Castro, M. D., *"Flow Injection Analysis. Principles and Applications"*, Ellis Horwood, Chichester, 1987).

21. Miller, J. N., *Anal. Proc.*, 1984, **21**, 372.

22. Pacey, G. E., and Bubnis, B. P., *Trends Anal. Chem.*, 1987, **6**, 165.

23. Masoom, M., and Townshend, A., *J. Chem. Soc. Pak.*, 1988, **10**, 269.

24. Ruzicka, J., and Christian, G. D., *Analyst*, 1990, **115**, 475.

25. Puchades, R., Maquieira, A., Atienza, J., and Herrero, M. A., *J. Autom. Chem.*, 1990, **12**, 163.

26. Chen, D., Luque de Castro, M. D., and Valcarcel, M., *Analyst*, 1991, **116**, 1095.

27. Ruzicka, J., *Anal. Chim. Acta*, 1992, **261**, 3.

28. Tyson, J. F., *Analyst*, 1984, **109**, 319.

29. Snyder, L. R., *Anal. Chim. Acta*, 1980, **114**, 3.

30. Ruzicka, J., *Anal. Proc.*, 1981, **18**, 267.

31. Patton, C. J., and Crouch, S. R., *Anal. Chim. Acta*, 1986, **179**, 189.

32. Knox, J. H., *"High Performance Liquid Chromatography"*, Edinburgh University Press, Edinburgh, 1980.

33. Ranger, C. B., *Anal. Chem.*, 1981, **53**, 20.

34. Burke, E. M., Suares, F. X., Hillman, D. C., and Heithmar, E. M., *Wat. Res.*, 1989, **23**, 519.

35. Tyson, J. F., *Fresenius Z. Anal. Chem.*, 1988, **329**, 675.

36. Ruzicka, J., and Hansen, E. H., *Talanta*, 1982, **29**, 157.

37. Stone, D. C., and Tyson, J. F., *Analyst*, 1987, **112**, 515.

38. Tijssen, R., *Anal. Chim. Acta*, 1980, **114**, 71.

39. van den Berg, J. H. M., Deedler, R. S., and Egberink, H. G. M., *Anal. Chim. Acta*, 1980, **114**, 91.

40. Brooks, S. H., and Dorsey, J. G., *Anal. Chim. Acta*, 1990, **229**, 35.

41. Fernandez, A., Gomez-Nieto, M. A., Luque de Castro, M. D., and Valcarcel, M., *Anal. Chim. Acta*, 1984, **165**, 217.

42. Betteridge, D., Marczewski, C. Z., and Wade, A. P., *Anal. Chim. Acta*, 1984, **165**, 227.

43. Stults, C. L. M., Wade, A. P., and Crouch, S. R., *Anal. Chim. Acta*, 1987, **192**, 301.

44. Crowe, C. D., Levin, H. W., Betteridge, D., and Wade, A. P., *Anal. Chim. Acta*, 1987, **194**, 49.

45. Hung, T.-C., Chuang, A., and Meng, P.-J., *Bull. Inst. Chem. Acad. Sin.*, 1987, **34**, 1.

46. Kolev, S. D., and Pungor, E., *Anal. Chim. Acta*, 1988, **208**, 133.

47. Tyson, J. F., *Quim. Anal.*, 1989, **8**, 171.

48. Tyson, J. F., Fogg, A. G., and Wang, X., *Quim. Anal.*, 1989, **8**, 179.

49. Tyson, J. F., *Analyst*, 1990, **115**, 587.

50. Clark, G. D., Hungerford, J. M., and Christian, G. D., *Anal. Chem.*, 1989, **61**, 973.

51. Tyson, J. F., and Marsden, A. B., *Anal. Chim. Acta*, 1988, **214**, 447.

52. Wada, H., Sawa, Y., Morimoto, M., Ishizuchi, T., and Nakagawa, G., *Anal. Chim. Acta*, 1989, **220**, 293.

53. Hansen, E. H., *Anal. Proc.*, 1981, **18**, 261.

54. Tyson, J. F., *Analyst*, 1985, **110**, 419.

55. Hull, R. D., Malick, R. E., and Dorsey, J. G., *Anal. Chim. Acta*, 1992, **267**, 1.

56. Taylor, G. I., *Proc. Roy. Soc.*, 1953, **A219**, 186.

57. Tyson, J. F., and Idris, A. B., *Analyst*, 1981, **106**, 1125.

58. Stone, D. C., and Tyson, J. F., *Analyst*, 1989, **114**, 1453.

59. Stulik, K., and Pacakova, V., *"Electroanalytical Measurements in Flowing Liquids"*, Ellis Horwood, Chichester, 1987.

60. Reijn, J. M., van der Linden, W. E., and Poppe, H., *Anal. Chim. Acta*, 1981, **123**, 229.

61. Brooks, S. H., Leff, D. V., Hernandez Torres, M. A., and Dorsey, J. G., *Anal. Chem.*, 1988, **60**, 2737.

62. van Nugteren-Osinga, I. C., Bos, M., and van der Linden, W. E., *Anal. Chim. Acta*, 1988, **214**, 77.

63. van Nugteren-Osinga, I. C., Hoogendam, E., Bos, M., and van der Linden, W. E., *Anal. Chim. Acta*, 1990, **239**, 245.

64. Kolev, S. D., and Pungor, E., *Anal. Chem.*, 1988, **60**, 1700.

65. Kolev, S. D., *Anal. Chim. Acta*, 1990, **229**, 183.

66. Johnson, K. S., and Petty, R. L., *Anal. Chem.*, 1982, **54**, 1185.

67. Fogg, A. G., *Analyst*, 1986, **111**, 859.

68. Fogg, A. G., Guta, C. W., and Chamsi, A. Y., *Analyst*, 1987, **112**, 253.

69. Fogg, A. G., Wang, X., and Tyson, J. F., *Analyst*, 1989, **114**, 1119.

70. Fogg, A. G., Cipko, E., Farabella, L., and Tyson, J. F., *Analyst*, 1990, **115**, 593.

71. Fogg, A. G., Wang, X., and Tyson, J. F., *Analyst*, 1990, **115**, 305.

72. Fogg, A. G., and Zhao, R., *Electroanalysis*, 1991, **3**, 273.

73. Frenzel, W., *Fresenius Z. Anal. Chem.*, 1988, **329**, 668.

74. Israel, Y., and Barnes, R. M., *Analyst*, 1989, **114**, 843.

75. Kamson, O. F., *Anal. Chim. Acta*, 1986, **179**, 475.

76. Whitman, D. A., Christian, G. D., and Ruzicka, J., *Anal. Chim. Acta*, 1988, **214**, 197.

77. Alonso, J., Bartroli, J., Del Valle, M., Escalada, M., and Barber, R., *Anal. Chim. Acta*, 1987, **199**, 191.

78. Rios, A., Luque de Castro, M. D., and Valcarcel, M., *Talanta*, 1989, **36**, 612.

79. Alonso, J., Bartroli, J., Del Valle, M., and Barber, R., *Anal. Chim. Acta*, 1989, **219**, 345.

80. Stewart, K. K., *Anal. Chim. Acta*, 1986, **179**, 59.

81. Turner, D. R., Knox, S., Whitfield, M., and Correira dos Santos, M., *Anal. Proc.*, 1987, **24**, 360.

82. Tyson, J. F., *Anal. Chim. Acta*, 1986, **179**, 131.

83. Tyson, J. F., *Anal. Proc.*, 1987, **24**, 362.

84. Tyson, J. F., *Fresenius Z. Anal. Chem.*, 1988, **329**, 663.

85. Clark, G. D., Zable, J., Ruzicka, J., and Christian, G. D., *Talanta*, 1991, **38**, 119.

86. Carroll, M. K., and Tyson, J. F., *J. Chem. Educ.*, 1993, **70**, A210.

87. Ruzicka, J., and Hansen, E. H., *Anal. Chim. Acta*, 1983, **145**, 1.

88. Tyson, J. F., *Anal. Proc.*, 1989, **26**, 318.

89. Joergensen, S. S., Petersen, K. M., and Hansen, L. A., *Anal. Chim. Acta*, 1985, **169**, 51.

90. Krug, F. J., Bergamin Filho, H., and Zagatto, E. A. G., *Anal. Chim. Acta*, 1986, **179**, 103.

91. Poppe, H., *Anal. Chim. Acta*, 1983, **145**, 17.

92. Krull, I. S., in Ahuja, S., (Ed.), *ACS Symposium Series*, 1986, **297**, 137.

93. Kuban, V., *Crit. Rev. Anal. Chem.*, 1992, **23**, 15.

94. Burguera, J. L. *"Flow Injection Atomic Spectroscopy"*, Marcel Dekker, New York, 1989.

95. Tyson, J. F., *Anal. Chim. Acta*, 1990, **234**, 3.

96. Valcarcel, M., and Luque de Castro, M. D., *Anal. Chim. Acta*, 1991, **250**, 157.

97. Trojanowicz, M., Worsfold, P. J., and Clinch, J. R., *Trends Anal. Chem.*, 1988, **7**, 301.

98. Abbott, S. R., and Kelderman, H. H., in Ahuja, S., (Ed.), *ACS Symposium Series*, 1986, **297**, 107.

99. Lobinski, R., and Marczenko, Z., *Crit. Rev. Anal. Chem.*, 1992, **23**, 55.

100. Lazaro, F., Rios, A., Luque de Castro, M. D., and Valcarcel, M., *Anal. Chim. Acta*, 1986, **179**, 279.

101. Blanco, M., Gene, J., Iturriaga, H., Maspoch, S., and Riba, J., *Talanta*, 1987, **34**, 987.

102. Rios, A., Lazaro, F., Luque de Castro, M. D., and Valcarcel, M., *Anal. Chim. Acta*, 1987, **199**, 15.

103. Lukkari, I., and Lindberg, W., *Anal. Chim. Acta*, 1988, **211**, 1.

104. Kuban, V., Gladilovich, D. B., Sommer, L., and Popov, P., *Talanta*, 1989, **36**, 463.

105. Lindberg, W., Clark, G. D., Hanna, C. P., Whitman, D. A., Christian, G. D., and Ruzicka, J., *Anal. Chem.*, 1990, **62**, 849.

106. Blanco, M., Coello, J., Gene, J., Iturriaga, H., and Maspoch, S., *Fresenius J. Anal. Chem.*, 1990, **338**, 831.

107. Vithanage, R. S., and Dasgupta, P. K., *Anal. Chem.*, 1986, **58**, 326.

108. Erickson, B. C., Ruzicka, J., and Kowalski, B. R., *Anal. Chim. Acta*, 1989, **218**, 303.

109. Zagatto, E. A. G., Arruda, M. A. Z., Jacintho, A. O., and Mattos, I. L., *Anal. Chim. Acta*, 1990, **234**, 153.

110. Valcarcel, M., and Luque de Castro, M. D., *Anal. Proc.*, 1989, **26**, 313.

111. Valcarcel, M., and Luque de Castro, M. D., *Analyst*, 1993, **118**, 593.

112. Pungor, E., Feher, Z., and Varadi, M., *CRC, Crit. Rev. Anal. Chem.*, 1980, **9**, 97.

113. Gunasingham, H., and Fleet, B., in Bard, A. J., (Ed.), *Electroanalytical Chemistry*, 1990, **16**, 89.

114. Fleischmann, M., Pons, S., Rolison, D. R., and Schmidt, P. P., *"Ultramicroelectrodes"*, Datatech Systems, Inc., Morganton, NC, 1987.

115. Kauffmann, J.-M., and Vire, J.-C., *Anal. Chim. Acta*, 1993, **273**, 329.

116. Zittel, H. E., and Miller, F. J., *Anal. Chem.*, 1965, **37**, 200.

117. Wang, J., Golden, T., and Li, R., *Anal. Chem.*, 1988, **60**, 1642.

118. Cosgrove, M., Moody, G. J., and Thomas, J. D. R., *Analyst*, 1988, **113**, 1811.

119. Moody, G. J., Sanghera, G. S., and Thomas, J. D. R., *Analyst*, 1986, **111**, 1235.

120. Fogg, A. G., Scullion, S. P., and Edmonds, T. E., *Analyst*, 1989, **114**, 579.

121. Fogg, A. G., Ali, M. A., and Abdalla, M. A., *Analyst*, 1983, **108**, 840.

122. Fogg, A. G., Chamsi, A. Y., Barros, A. A., and Cabral, J. O., *Analyst*, 1984, **109**, 901.

123. Chamsi, A. Y., and Fogg, A. G., *Analyst*, 1986, **111**, 879.

124. Fogg, A. G., and Bsebsu, N. K., *Analyst*, 1984, **109**, 19.

125. Fogg, A. G., Fernandez-Arciniega, M. A., and Alonso, R. M., *Analyst*, 1985, **110**, 345.

126. Fogg, A. G., and Alonso, R. M., *Analyst*, 1987, **112**, 1071.

127. Fogg, A. G., Fernandez-Arciniega, M. A., and Alonso, R. M., *Analyst*, 1985, **110**, 851.

128. Fogg, A. G., Alonso, R. M., and Fernandez-Arciniega, M. A., *Analyst*, 1986, **111**, 249.

129. Chamsi, A. Y., and Fogg, A. G., *Analyst*, 1988, **113**, 1723.

130. Fogg, A. G., Fernandez-Arciniega, M. A., and Alonso, R. M., *Analyst*, 1985, **110**, 1201.

131. Levich, V. G. *"Physicochemical Hydrodynamics"*, Prentice-Hall, Englewood Cliffs, NJ., 1962.

132. Yamada, J., and Matsuda, H., *J. Electroanal. Chem.*, 1973, **44**, 189.

133. Compton, R. G., Fisher, A. C., and Tyley, G. P., *J. Appl. Electrochem.*, 1991, **21**, 295.

134. Compton, R. G., Fisher, A. C., Latham, M. H., Wellington, R. G., Brett, C. M. A., and Olivera Brett, A. M. C. F., *J. Appl. Electrochem.*, 1993, **23**, 98.

135. Powell, F. E., and Fogg, A. G., *Analyst*, 1988, **113**, 483.

136. Powell, F. E., and Fogg, A. G., *Analyst*, 1989, **114**, 799.

137. Powell, F. E., and Fogg, A. G., *Electroanalysis*, 1990, **2**, 463.

138. Compton, R. G., and Unwin, P. R., *J. Electroanal. Chem.*, 1986, **205**, 1.

139. Weber, S. G., *J. Electroanal. Chem.*, 1983, **145**, 1.

140. Matsuda, H., *J. Electroanal. Chem.*, 1967, **15**, 325.

141. Wang, J., and Chen, L., *Anal. Chem.*, 1991, **63**, 1499.

142. Fogg, A. G., and Summan, A. M., *Analyst*, 1984, **109**, 1029.

143. Sah, P. P. T., and Daniels, T. C., *Rec. Trav. Chim. Pay-Bas*, 1950, **69**, 1545.

144. Newell, L. C., and Maxson, R. N., *Inorg. Synth.*, 1939, **I**, 45.

145. Bailar, J. C., Jr., and Jones, E. M., *Inorg. Synth.*, 1939, **I**, 35.

146. Miller, J. C., and Miller, J. N., *"Statistics for Analytical Chemistry"*, 2nd Edition,Ellis Horwood, Chichester, 1988.

147. Betteridge, D., Dagless, E. L., Fields, B., and Graves, N. F., *Analyst*, 1978, **103**, 897.

148. Krug, F. J., Bergamin Filho, H., Zagatto, E. A. G., and Jorgensen, S. S., *Analyst*, 1977, **102**, 503.

149. Fields, B., *Anal. Proc.*, 1979, **16**, 4.

150. Ham, G., *Anal. Proc.*, 1981, **18**, 69.

151. Betteridge, D., Cheng, W. C., Dagless, E. L., David, P., Goad, T. B., Deans, D. R., Newton, D. A., and Pierce, T. B., *Analyst*, 1983, **108**, 1.

152. Leach, R. A., Ruzicka, J., and Harris, J. M., *Anal. Chem.*, 1983, **55**, 1669.

153. Little, J. N., and Fallick, G. J., *J. Chromatogr.*, 1975, **112**, 389.

154. Stewart, J. E., *Appl. Opt.*, 1979, **18**, 5.

155. Stewart, J. E., *Appl. Opt.*, 1981, **20**, 654.

156. Stewart, J. E., *Anal. Chem.*, 1981, **53**, 1125.

157. Lyons, J. W., and Faulkner, L. R., *Anal. Chem.*, 1982, **54**, 1960.

158. Synovec, R. E., *Anal. Chem.*, 1987, **59**, 2877.

159. Evans, C. E., Shabushnig, J. G., and McGuffin, V. L., *J. Chromatogr.*, 1988, **459**, 119.

160. Evans, C. E., and McGuffin, V. L., *J. Chromatogr.*, 1990, **503**, 127.

161. Leach, R. A., and Harris, J. M., *J. Chromatogr.*, 1981, **218**, 15.

162. Pelletier, M. J., Thorsheilm, H. R., and Harris, J. M., *Anal. Chem.*, 1982, **54**, 239.

163. Bornhop, D. J., and Dovichi, N. J., *Anal. Chem.*, 1986, **58**, 504.

164. Pawliszyn, J., *Anal. Chem.*, 1986, **58**, 3207.

165. Pawliszyn, J., *Anal. Chem.*, 1986, **58**, 243.

166. Cheng, Y.-F., and Dovichi, N. J., *Mikrochim. Acta [Wien]*, 1986, **III**, 351.

167. Hancock, D. O., and Synovec, R. E., *Anal. Chem.*, 1988, **60**, 1915.

168. Lima, L. R., III., and Synovec, R. E., *Anal. Chem.*, 1993, **65**, 128.

169. Fogg, A. G., Bsebsu, N. K., and Abdalla, M. A., *Analyst*, 1982, **107**, 1462.

170. Ishii, D., Asai, K., Hibi, K., Jonokuchi, T., and Nagaya, M., *J. Chromatogr.*, 1977, **144**, 157.

171. Tsuda, T., Tsuboi, K., and Nakagawa, G., *J. Chromatogr.*, 1981, **214**, 283.

172. Yang, F. J., *J. Chromatogr. Sci.*, 1982, **20**, 241.

173. Larkins, L. A., and Westcott, S. G., *Anal. Proc.*, 1986, **23**, 258.

174. Reijn, J. M., van der Linden, W. E., and Poppe, H., *Anal. Chim. Acta*, 1980, **114**, 105.

175. Poppe, H., *Anal. Chim. Acta*, 1980, **114**, 59.

176. Stone, D. C., and Tyson, J. F., *Anal. Proc.*, 1986, **23**, 23.

177. Stone, D. C., and Tyson, J. F., *Anal. Chim. Acta*, 1986, **179**, 427.

178. Burgess, C., and Mielenz, K. D., (Ed.). *"Advances in Standards and Methodology in Spectrophotometry"*, Elsevier, Amsterdam, 1987.

179. Blanco, M., Coello, J., Iturriaga, H., Maspoch, S., and Riba, J., *Anal. Chim. Acta*, 1990, **234**, 395.

180. Stewart, J. E., *J. Chromatogr.*, 1979, **174**, 283.

181. Reijn, J. M., van der Linden, W. E., and Poppe, H., *Anal. Chim. Acta*, 1981, **126**, 1.

182. Reijn, J. M., Poppe, H., and van der Linden, W. E., *Anal. Chim. Acta*, 1983, **145**, 59.

183. van Veen, J. I. F., van Opstal, M. A. J., Reijn, J. M., van Bennekom, W. P., and Bult, A., *Anal. Chim. Acta*, 1988, **204**, 29.

184. Reijn, J. M., Poppe, H., and van der Linden, W. E., *Anal. Chem.*, 1984, **56**, 943.

185. Yoshizawa, D., Shimizu, K., Sato, G. P., Kumakura, K., and Aoki, K., *Anal. Sci.*, 1989, **5**, 567.

186. Fogg, A. G., Scullion, S. P., and Edmonds, T. E., *Analyst*, 1990, **115**, 599.

187. Fernandez, A., Luque de Castro, M. D., and Valcarcel, M., *Anal. Chim. Acta*, 1987, **193**, 107.

188. Rios, A., Luque de Castro, M. D., and Valcarcel, M., *Anal. Chim. Acta*, 1986, **187**, 139.

189. Rios, A., Luque de Castro, M. D., and Valcarcel, M., *Anal. Chem.*, 1986, **58**, 663.

190. Bermudez, B., Rios, A., Luque de Castro, M. D., and Valcarcel, M., *Talanta*, 1988, **35**, 810.

191. Araujo, A. N., Lima, J. L. F. C., Rangel, A. O. S. S., Alonso, J., Bartroli, J., and Barber, R., *Analyst*, 1989, **114**, 1465.

192. Dasgupta, P. K., and Hwang, H., *Anal. Chem.*, 1985, **57**, 1009.

193. Betteridge, D., Dagless, E. L., Fields, B., Sweet, P., and Deans, D. R., *Anal. Proc.*, 1981, **18**, 26.

194. Betteridge, D., and Fields, B. F., *Anal. Chim. Acta*, 1981, **132**, 139.

195. Perez Pavon, J. L., Moreno Codero, B., Hernandez Mendez, J., and Agudo, R. M. I., *Anal. Chem.*, 1989, **61**, 1789.

196. Erickson, B. C., Kowalski, B. R., and Ruzicka, J., *Anal. Chem.*, 1987, **59**, 1246.

197. Montesinos, J. L., Bartroli, J., del Valle, M., Lima, J. L. F. C., and Araujo, A. N., *Anal. Chim. Acta*, 1990, **234**, 67.

198. Araujo, A. N., Lima, J. L. F. C., Rangel, A. O. S. S., and Teixeira, M. T. M., *J. Flow Injection Anal.*, 1992, **9**, 69.

199. Alonso-Chamarro, J., Bartroli, J., and Barber, R., *Anal. Chim. Acta*, 1992, **261**, 219.

200. Luque de Castro, M. D., *Talanta*, 1989, **36**, 591.

201. Monks, C. D., Nacapricha, D., and Taylor, C. G., *Analyst*, 1993, **118**, 623.

202. Betteridge, D., and Fields, B., *Anal. Chem.*, 1978, **50**, 654.

203. Luque de Castro, M. D., and Valcarcel Cases, M., *Analyst*, 1984, **109**, 413.

204. Perez Pavon, J. L., Garcia Pinto, C., Moreno Cordero, B., and Hernandez Mendez, J., *Anal. Chem.*, 1990, **62**, 2405.

205. Romero-Saldana, M., Rios, A., Luque de Castro, M. D., and Valcarcel, M., *Talanta*, 1991, **38**, 291.

206. Fernandez, A., Luque de Castro, M. D., and Valcarcel, M., *Anal. Chem.*, 1984, **56**, 1146.

207. Fernandez, A., Luque de Castro, M. D., and Valcarcel, M., *Analyst*, 1987, **112**, 803.

208. Wada, H., Hiraoka, S., Yuchi, A., and Nakagawa, G., *Anal. Chim. Acta*, 1986, **179**, 181.

209. Engstrom, R. C., *Anal. Chem.*, 1982, **54**, 2310.

210. Engstrom, R. C., and Strasser, V. A., *Anal. Chem.*, 1984, **56**, 136.

211. Ghawji, A. B., and Fogg, A. G., *Analyst*, 1986, **111**, 157.

212. Bowers, M. L., and Yenser B.A., *Anal. Chim. Acta*, 1991, **243**, 43.

213. Goldstein, E. L., and van de Mark, M. R., *Electrochim. Acta*, 1982, **27**, 1079.

214. Johnson, D. C., Polta, J. A., Polta, T. Z., Neuburger, G. G., Johnson, J., Tang, A. P.-C., Yeo, I.-H., and Baur, J., *J. Chem. Soc. Faraday Trans. 1.*, 1986, **82**, 1081.

215. Neuberger, G. G., and Johnson, D. C., *Anal. Chem.*, 1987, **59**, 203.

216. Merz, A., in Steckhan, E., (Ed.), *Current Topics in Chemistry*, 1990, **152**, 49.

217. Anson, F. C., Saveant, J.-M., and Shigehara, K., *J. Am. Chem. Soc.*, 1983, **105**, 1096.

218. Anson, F. C., Osaka, T., and Saveant, J.-M., *J. Phys. Chem.*, 1983, **87**, 640.

219. Yasui, S. C., and Keiderling, T. A., *J. Am. Chem. Soc.*, 1986, **108**, 5576.

220. Shibata, A., Yamamoto, M., Yamashita, T., Chiou, J.-S., Kamaya, H., and Ueda, I., *Biochem.*, 1992, **31**, 5728.

221. Ma, X., Mohammad, S. F., and Kim, S. W., *J. Colloid Interface Sci.*, 1991, **147**, 251.

222. Brown, R. A., and Wells, T. M., *J. Pharm. Pharmacol.*, 1992, **44**, 467.

223. Munro, C. H., Smith, W. E., and White, P. C., *Analyst*, 1993, **118**, 731.

224. Kissinger, P. T., and Heineman, W. R., *J. Chem. Educ.*, 1983, **60**, 702.

225. Mabbott, G. A., *J. Chem. Educ.*, 1983, **60**, 697.

226. Nicholson, R. S., *Anal. Chem.*, 1965, **37**, 1351.

227. Bianco, P., Haladjian, J., and Giannandrea-Derocles, S., *Electroanalysis*, 1994, **6**, 67.

228. Pletcher, D., *"A First Course in Electrode Processes"*, The Electrochemical Consultancy, Romsey, 1991.

229. Murray, R. W., in Bard, A. J., (Ed.), *Electroanalytical Chemistry*, 1984, **13**, 191.

230. Moreira, J. C., Zhao, R., and Fogg, A. G., *Analyst*, 1990, **115**, 1561.

231. Moreira, J. C., and Fogg, A. G., *Analyst*, 1990, **115**, 1565.

232. Lingane, J. J., *J. Amer. Chem. Soc.*, 1942, **64**, 1001.

233. Rulfs, C. L., and Elving, P. J., *J. Amer. Chem. Soc.*, 1951, **73**, 3284.

234. Magee, R. J., Scott, I. A. P., and Wilson, C. L., *Talanta*, 1959, **2**, 376.

235. Colton, R., Dalziel, J., Griffith, W. P., and Wilkinson, G., *J. Chem. Soc.*, 1960, 71.

236. Golimowski, J., Valenta, P., and Nurnberg, H. W., *Fresenius Z. Anal. Chem.*, 1985, **322**, 315.

237. Hnatowich, D. J., Layne, W. W., Childs, R. L., Lanteigne, D., Davis, M. A., Griffin, T. W., and Doherty, P. W., *Science*, 1983, **220**, 613.

238. Krejcarek, G. E., and Tucker, K. L., *Biochem. Biophys. Research Comm.*, 1977, **77**, 581.

239. Sawyer, D. T., and McKinnie, J. M., *J. Amer. Chem. Soc.*, 1960, **82**, 4191.

240. Frenzel, W., *Anal. Chim. Acta*, 1993, **273**, 123.

241. Paneli, M. G., and Voulgaropoulos, A., *Electroanalysis*, 1993, **5**, 355.